

NORTHWESTERN UNIVERSITY

A Platform for Ribosome Engineering in Living *Escherichia coli*

A DISSERTATION

SUBMITTED TO THE GRADUATE SCHOOL
IN PARTIAL FULFILLMENT OF THE REQUIREMENTS

for the degree

DOCTOR OF PHILOSOPHY

Field of Chemical Engineering

By
Erik Daniel Carlson

EVANSTON, ILLINOIS

September 2017

ABSTRACT

A Platform for Ribosome Engineering in Living *Escherichia coli*

Erik Daniel Carlson

The *Escherichia coli* ribosome is a 2.4 MDa molecular machine that consists of a large subunit and a small subunit, and is the key catalyst in gene expression, responsible for synthesizing proteins from amino acids in a sequence-defined fashion with impressive speed and accuracy. Expanding the repertoire of ribosome substrates and functions would be greatly beneficial for the advancement of systems and synthetic biology. However, as with any biological system, engineering objectives are often completely opposed to the growth and reproduction objectives of the organism. This problem can be solved using a specialized orthogonal ribosome that translates only a specific type of engineered messenger RNAs (mRNAs) and avoids translation of native cellular mRNAs. Before this work, efforts to construct such orthogonal ribosomes focused on modifying the small subunit alone, as orthogonality is endowed by modifying the Shine-Dalgarno sequence of an mRNA and the complementary sequence in the 16S ribosomal RNA (rRNA) of the small subunit. Unfortunately, free exchange between the subunits meant the large subunit, which is responsible for peptide bond formation and protein excretion, could not be extensively engineered.

Here we develop an engineered ribosome with tethered subunits (termed Ribo-T), which contains a single core hybrid rRNA composed of small and large subunit rRNA sequences, and is capable of protein synthesis *in vitro* and *in vivo*. Considering that the ribosome is one of nature's most evolved, fine-tuned and conserved structures, it is especially surprising that Ribo-T can even fully support cell growth in *E. coli* strains lacking wild-type untethered ribosomes. One of the exciting

implications of Ribo-T with an orthogonal small subunit (oRibo-T) is the possibility of introducing mutations in large ribosomal subunits that would be deleterious if introduced in an untethered wild-type ribosome, all in living *E. coli*. We show the ability to evolve oRibo-T by selecting otherwise dominantly lethal rRNA mutations in the large ribosomal subunit that facilitate translation of challenging protein sequences. The Ribo-T and orthogonal Ribo-T system was then improved significantly by tether and orthogonal pair optimization, expanding the utility of this system. Importantly, towards the goal of enabling non-canonical amino acid (ncAA) incorporation, the Ribo-T system was shown to work with established orthogonal translation systems to incorporate the ncAA pAzF into *sf-gfp*. We then outline work creating engineering strains towards genomic integration of Ribo-T into ribosomal operons, to enable ribosome engineering towards development of novel drugs that kill bacteria resistant to common antibiotics, designer therapeutics, and new classes of sequence-defined polymers with tunable properties such as shape memory and self-healing.

Acknowledgements

Firstly, thank you to my advisor Dr. Mike Jewett for taking a risk on a first year with very little biology know-how. You fostered such a special lab environment, I am so thankful to have been a part of it. I fear all future work experiences will pale in comparison. Thanks to my committee Dr. Bill Miller, Dr. Josh Leonard and Dr. Shura Mankin for their support. Special thanks to Shura, you have been like a second PI to me and I am forever grateful. My PhD would have been far less happy without the UIC crew. Dr. Cedric Orelle, you are a gem and I miss you dearly, I wish France were a little closer. Thank you to Dr. Nora Vazquez-Laslop, Teresa Szal, Tajna Florin, Kolya Aleksashin and Dorota Klepacki. Teresa, thank you for introducing me to real perogies.

My lab family is full of wonderful human beings and scientists. Thank you to Eric Hodgman, Brian Fritz and Laura Timmerman for starting it all out, it takes a special kind of crazy to join a fresh lab and I love it. Adam Hockenberry, thank you for staying it this long with me and thanks Mike for not making us leave sooner. Thank you to Lauren for introducing me to games and pie. If you weren't in lab I'd have gone crazy. My best lab job ever, thank you Party Planning Committee: co-founder Laura, Jessica Perez, Jennifer Kay, Ashty Karim, and Anne D'Aquino. Gan, thank you for all you taught me, and for being such a solid desk-mate, bench-mate, and friend. I had the privilege of working with amazing undergrads, thank you Kirsten Swonger, Christina Burghard and Emm Fulk. Thank you to Anne D'Aquino and Do Soon Kim, I enjoyed working with you, these projects are in great hands. Thank you to all my lab mates, you people are what make the Jewett lab so special. Thank you to the fantastic Chemical and Biological Engineering department office staff who enable us to do what we do.

Life is also beautiful outside lab. Thank you to the Pot Shop friends for pottery therapy. Thanks to Dr. John Samuel Austin III, Sister Margaret Allard, Aunt Barbie Markay, the ever-lovely Louisa Savereide, Brooks, my Bloomfield friends, and my wonderful 2010 class who made my grad school years the best so far. Teresa Deluca and Emily Leitch, I love you always, very few people know me like you two. Seriously next-level favourites. Thank you to Paul, Danica & Rye Carlson and Patrick Donahue who have made this last year so surprisingly special.

Finally, I am here today because of an amazingly supportive and loving family. Thank you all. Mom and Dad, thank you for the example you set in work, life and family. Thank you to Mormor and Grandpa Bruce for providing the Wisconsin retreat. Steven, you are my muse and I am in constant awe of the human you have become and your incredible abilities across the board. I wish your lab got poached. Paul, I'm so glad yours did. You are my everything. I love sharing degrees, schools, research areas, and hopefully a future lab. Thanks for bringing three more amazing Carlson kids into the mega-sibling mix. Danica, you are the best sister-in-law, I'm so thankful someone is looking after our precious Paul.

Dedication

To my Grandpa Bruce.

Table of contents

ABSTRACT	2
Acknowledgements	4
Dedication	6
Table of contents.....	7
List of Figures	11
List of Tables	20
1. Introduction.....	21
1.1 Non-standard amino acid incorporation.....	21
1.2 The <i>Escherichia coli</i> ribosome.....	25
1.3 Ribosome engineering.....	26
1.3.1 <i>In vitro</i> ribosome engineering.....	26
1.3.2 <i>In vivo</i> ribosome engineering.....	26
1.4 Creating Ribo-T: (Design, Build, Test) ⁿ	29
1.4.1 First tries to tie: An infinite loop.....	30
1.4.2 Breaking the infinite loop.....	35
1.4.3 Acknowledgements	37
1.4.4 Publication.....	37

2. Protein synthesis by ribosomes with tethered subunits	38
2.1 Abstract	38
2.2 First tries to tie	39
2.3 Circular permutations of 23S rRNA	44
2.3.1 Introduction	44
2.3.2 Methods	45
2.3.3 Results and discussion	52
2.4 A ribosome with tethered subunits, Ribo-T	55
2.4.1 Introduction	56
2.4.2 Methods	59
2.4.3 Results and discussion	67
2.5 An expanded mutation space <i>in vivo</i>	77
2.5.1 Introduction	77
2.5.2 Methods	77
2.5.3 Results and discussion	84
2.6 Conclusions and future directions	92
2.7 Additional information	93
2.7.1 Acknowledgements	93
2.7.2 Author Contributions	94
2.7.3 Publishing and Patent information	94
2.8 Tables	95

3.	Improvements to a ribosome with tethered subunits for <i>in vivo</i> ribosome engineering.....	101
3.1	Introduction.....	102
3.2	Materials and Methods.....	105
3.2.1	Construction of the tether libraries.....	105
3.2.2	Replacement of the wild-type ribosome by Ribo-T v2.0.....	106
3.2.3	Selecting mutants, evaluating growth rate and analyzing tethers	106
3.2.4	Total RNA analysis of tethered Ribo-T v2.0.	107
3.2.5	Selection of new orthogonal pairs.....	108
3.2.6	Evaluation of new orthogonal pairs	115
3.2.7	Non-canonical amino acid incorporation with Ribo-T	116
3.3	Tether optimization improves growth with Ribo-T	120
3.4	Improved orthogonal function	124
3.3.1	Evaluation of evolved orthogonal pairs.....	126
3.5	Non-canonical amino acid incorporation by a ribosome with tethered subunits	130
3.6	Discussion.....	132
3.7	Acknowledgements, contributions and publishing information.....	133
3.8	Supplementary figures and tables	134
4.	Conclusions and future outlook	142
	References.....	145

	10
Appendices.....	152
A. Comparison to a stapled ribosome	152
A.1 Introduction.....	152
A.2 Materials and methods	153
A.2.1 A stapled ribosome with a wild-type anti-Shine-Dalgarno site.....	153
A.2.2 A stapled ribosome with orthogonal anti-Shine-Dalgarno site	154
A.3 Results and discussion.....	155
A.3.1 Testing a stapled ribosome in the cell growth assay.....	155
A.3.2 Testing a stapled ribosome in the orthogonal assay.....	157
A.4 Conclusions.....	158
A.5 Acknowledgements.....	158
B. Designer strains for ribosome engineering	159
B.1 Introduction	159
B.2 Materials and methods.....	162
B.3 Results and discussion	164
B.4 Future works	164
B.5 Primers, gBlocks and tables.....	166
Recipes.....	170

List of Figures

- Figure 1.1 Non-canonical amino acid incorporation.** Simplified cartoon of non-canonical amino acid incorporation process with UAG amber suppression. Producing proteins and peptides with non- canonical amino acids requires an expanded genetic code with multiple biological parts. These parts include (i) an open coding channel reassigned to a non-canonical monomer, (ii) monomer-transfer RNA (tRNA) substrates that can decode the open codon (that are typically produced by an orthogonal aminoacyl-tRNA synthetase (o- aaRS) specifically charging a non-canonical monomer to its orthogonal tRNA), (iii) delivery of monomer-tRNA substrates to the ribosome by elongation factor Tu (EF-Tu), and (iv) compatible ribosomes. To ensure efficient operation of a re-engineered translation apparatus, many parts must be reconfigured.23
- Figure 1.2 *E. coli* ribosome components, structure and function.** Ribosomal proteins (rProteins) are shown in white, 16S rRNA in tan, 23S and 5S rRNA in grey. Messenger RNA is in green, tRNA in forest green, and nascent polypeptide chain in red. Crystal structures adapted from PDB 2WWL and 2WWQ.....25
- Figure 1.3 Ribosome engineering in living *E. coli*.** a. Wild-type Shine-Dalgarno (SD) mediated mechanism for translation initiation. b. Mutating SD/antiSD pair creates orthogonal small subunits. The large 50S subunit works with both wild-type and orthogonal 30S subunits. c. 23S rRNA is fused with orthogonal 16S rRNA to create a ribosome with tethered subunits (Ribo-T).28
- Figure 1.4 Timeline in creating Ribo-T.** A) Wildtype ribosome and rRNA operon. B) First generation Ribo-T design. Circularly permuted 23S at helix 34 or 63, connected to a 16S with an orthogonal (o) mRNA recognition site (*). HH-hammerhead ribozyme, HDV-hepatitis delta virus ribozyme. C) 23S rRNA circular permutation study. D) Design, build and test of new Ribo-T structure. E) Successful Ribo-T with tether connection at large subunit 23S helix 101 and small subunit 16S helix 44. F) Sucrose gradient with fractionation experiment demonstrating stable Ribo-T tether in intact ribosomes. Crystal structures: PDB 3R8T & 4GD2.....32
- Figure 2.1.** a. DNA operons of wild-type *rnmB* operon (top) and rearranged Ribo-T initial tries ribosomes with a tether connecting a circularly permuted 23S gene and orthogonal 16S rRNA. XhoI and XbaI sites allow for tether incorporation. b. Ribosome crystal structure with initial tether sites chosen at 23S helix 34 (H34) and 23S helix 63 (H63). An RNA tether will connect either H34 or H63 to the 16S 5' end. c. Testing hammerhead (HH) and hepatitis delta virus (HDV) efficiencies using *in vitro* transcription reactions and denaturing RNA electrophoresis gel.41

Figure 2.2. Tether library generation. a. Agarose gel showing individual primers (7 left lanes) and PCR assembled into a library of tethers (rightmost lane). b. Library and Ribo-T plasmid are digested with *XhoI* and *XbaI* restriction enzymes. c. Digested tether library and plasmid backbone are ligated to form a plasmid with Ribo-T. d. Plasmids are extracted from cells. Undigested (left) and *XhoI/XbaI* digested plasmids (right) run on an agarose gel to confirm library integration. 43

Figure 2.3. The general scheme of constructing rRNA operon in which the mature 23S rRNA gene sequence is replaced with the circularly permuted gene.44

Figure 2.4. The experimental scheme of preparing and testing circularly permuted 23S rRNA gene library. a, CP23S template is generated from pCP23S-EagI plasmid by EagI digestion and ligation. Each CP23S variant is generated by PCR using circularized 23S rRNA gene as a template and a unique primer pair, with added sequences overlapping the destination plasmid backbone. b, Plasmid backbone is prepared by digestion of pAM552- Δ 23S-AflIII with AflIII restriction enzyme, which linearizes the backbone at the 23S processing stem site. c, Gibson assembly is used to incorporate each CP23S variant into the plasmid backbone to generate the 91 target circular permutants. d, The pAM-CP23S plasmids are transformed into Δ 7 *rrn* SQ171 strain carrying pCSacB plasmid with wt rRNA operon and transformants resistant to ampicillin, erythromycin and sucrose are selected. e, a complete replacement of pCSacB with pAM-CP23S is verified by a three-primer diagnostic PCR.46

Figure 2.5. Key plasmids. a, pAM552 plasmid is a derivative of pLK35⁵³ from which the unessential segments of the pBR322 cloning vector have been removed. pAM552 contains the entire *rrnB* operon of *E. coli* under the control of the phage lambda P_L promoter which is constitutively active in the conventional *E. coli* strains but is silent at 30° in the strain POP2136 (30°C) carrying the *cI857* gene of the temperature-sensitive lambda repressor⁵⁴. The 16S rRNA gene is shown in orange with the 16S rRNA processing stem sequences indicated in yellow. The 23S rRNA gene is blue and the corresponding processing stem sequences are light blue. The intergenic tRNA^{Glu} gene is shown in dark grey. b, The map of the pRibo-T8/9 plasmid derived from pAM552. The native 5' and 3' ends of the 23S rRNA were linked via a tetranucleotide sequence GAGA (connector C shown in green), and circularly permuted 23 rRNA gene, 'opened' in the apex loop of H101, was inserted in the apex loop of 16S rRNA helix h44 via an A₈ linker T1 and an A₉ linker T2 (red bars). c, The map of the backbone plasmid pT7wtK and the reporter plasmids pT7oGFP and pLpp5oGFP, expressing *sf-gfp* controlled by an orthogonal SD sequence (orange semi-circle) under T7 or *lpp5* promoters (black triangles). d, The map of the pACYC177-derived plasmid containing *secM/lacZ α* reporter gene controlled by the T7 promoter (black triangle) and alternative SD sequence (orange semi-circle). The sequence of the *secM-lacZ α* reporter matches that in the originally described plasmid pNH122⁵⁵.47

Figure 2.6. Global screening of circularly permuted 23S rRNAs identifies variants capable of replacing the natural 23S rRNA in a functional ribosome. Secondary structure diagram of 23S rRNA⁵⁶ showing the spectrum of the CP constructs tested for their ability to support cell growth in the absence of wild type ribosomes. The new ends of the CP variants of 23S rRNA were introduced in the apex or internal loops of the rRNA hairpins. The corresponding constructs are named per the position of the new 5' end in the structure of the wt mature 23S rRNA (e.g., CP104). The names of the constructs (and the corresponding rRNA hairpin loops) that can support cell growth are shown in green and those that failed to produce sufficiently active ribosomes are shown in red. To assess viability, two independent biological replicates for each CP were carried out. For all viable CP constructs the lack of wt rRNA genes was verified by PCR as shown in the Extended Data Fig. 2 and the identity of CP constructs in the resulting clones was verified by plasmid sequencing.53

Figure 2.7. Circularly permuted 23S rRNA mutation mapped to ribosome crystal structure. (Top) The location of the new ends of CP variants of the 23S rRNA in the crystallographic structure of the *E. coli* 70S ribosome⁵⁷ (PDB 3R8T and 4GD2). Spheres represent the atoms of the nucleotides corresponding to the new 5' and 3' ends. The ends of the viable CP variants are green and those of the non-viable versions are red. The loops of helices h44 and H101 in the small and large subunit rRNA, respectively, used for subsequent experiments, are indicated by arrows. (Bottom) Same as above, but after removal of the small subunit. Two views represent the interface and solvent sides of the large ribosomal subunit.54

Figure 2.8. Ribo-T design. **a**, Wild type (left) and Ribo-T (right) rRNA genes. In the bacterial wild type rRNA operon (e.g., *E. coli* *rrnB* operon shown in the figure), small and large subunit rRNAs are excised from the primary transcript and processed to form mature individual 16S, 23S and 5S rRNA. In Ribo-T, the circularly permuted 23S rRNA gene, 'closed' at its native ends with a 4 nt long connector **C** and 'opened' in the loop of H101, is inserted via short tethers **T1** and **T2** into the apex loop of h44 in the 16S rRNA gene. The resulting hybrid rRNA gene is transcribed as a single chimeric 16S/23S rRNA with its 5' and 3' ends likely processed by the enzymes of 16S rRNA maturation. **b**, Secondary structure of the mature wild type (left) and Ribo-T (right) rRNAs. The red dots in wild type 16S and 23S rRNA indicate the apex loops of h44 and H101, which in Ribo-T are connected by tethers **T1** and **T2**. The arrows at the 16S rRNA ends and the tethers in the Ribo-T map indicate the direction of transcription of the chimeric 16S/23S rRNA. **c**, The locations of the **T1** and **T2** tethers in the three-dimensional model of Ribo-T (based on the structure of *E. coli* ribosome in the unrotated state⁵⁷ (PDB 3R8T and 4GD2)). In the small subunit, 16S rRNA and small subunit proteins are colored yellow and orange, respectively; in the large subunit 23S rRNA and 5S rRNA are colored blue and proteins are cyan; the P site-bound tRNA is olive; the connector **C** linking native 5' and 3' ends of the 23S rRNA is green and the tethers **T1** and **T2** linking 16S and 23S rRNA are red. On the right, the ribosome has been opened as a book exposing the subunit interface sides. Helices h44 (16S) and H101 (23S) are highlighted in orange and blue, respectively. Ribosomal proteins are removed for clarity.57

Figure 2.9. The Ribo-T tethers allow for the ribosome ratcheting. Distance changes (Å) between the 16S rRNA and 23S rRNA residues h44 and H101 connected by the oligo(A) linkers in Ribo-T when the ribosome undergoes the transition from the classic to the rotated state. The distances between the 5' phosphorus atoms of the corresponding nucleotides are shown. 16S and 23S rRNAs in the non-rotated state are tan and pale blue, and in the rotated state are gold and blue, respectively. The structures of the *E. coli* ribosomes used for measuring the distances and generating the figure have PDB accession numbers 3R8T and 4GD2 (non-rotated state) and 3R8S and 4GD1 (rotated state).....58

Figure 2.10. Ribo-T supporting cell growth and actively translating a, Agarose gel electrophoresis of total RNA prepared from SQ171 cells expressing wt ribosomes ("WT") or Ribo-T. The gel is representative of 5 independent biological replicates. A faint band in the Ribo-T sample migrating slightly faster than 16S rRNA likely represents a small fraction of Ribo-T with a cleaved linker seen in some preparations. **b,** (left) Sucrose gradient fractionation of polysomes prepared from cells expressing wt ribosomes (upper panel) or Ribo-T (lower panel). The position of the peaks corresponding to monosomes (70S), disomes (P2), trisomes (P3) and tetrasomes (P4) are indicated by arrows. (right) The agarose electrophoresis analysis of RNA extracted from the corresponding sucrose gradient peaks is shown.....67

Figure 2.11. Chromosomal mutations enhance growth of SQ171 cells in which Ribo-T completely replace wt ribosomes. a, Growth curves of the parental SQ171 cells transformed with the pAM552(G2058) plasmid (black curve) or pRibo-T8/9 plasmid (blue curve) or selected fast growing mutant (SQ171fg) transformed with pRibo-T8/9 (green curve). The cells express homogeneous populations of ribosomes (wt for pAM552 transformants or Ribo-T for the pRibo-T8/9 transformants, see panels b and c). b, PCR analysis of rDNA in the SQ171fg strain transformed with pRibo-T8/9 (the SQ110 strain that carries a single chromosomal copy of *rnn* allele served as a wt control). The PCR primers amplify the 302 bp 23S rRNA gene segment 'across' the H101 hairpin in wild type rDNA. In pRibo-T, the primer annealing sites are more than 4.8 kb apart (black dashed line), which prevents formation of the PCR product. Two additional primers designed to amplify a 467 bp fragment from the *lacZ* gene were included in the same PCR reaction as an internal control. The gel is representative of 2 independent biological experiments. c, Primer extension analysis of rRNA expressed in the SQ171fg cells transformed with pAM552 (WT), pAM552 with the A2058G mutation, or pRibo-T8/9 which carries the A2058G mutation. Primer extension was carried out in the presence of dTTP and ddCTP. Because Ribo-T contains the A2058G mutation in the 23S rRNA sequence, the generated cDNA is one nucleotide shorter than the one generated on the wild type 23S rRNA template. The lack of the 20 nt cDNA band in the Ribo-T sample demonstrates the absence of wt 23S rRNA in the SQ171fg cells transformed with pRibo-T8/9. The gel is representative of 3 independent biological experiments. d, e, Chromosomal mutations in SQ171fg: d, a nonsense mutation in the Leu codon 22 of the *ybeX* gene encoding protein similar to Mg²⁺/Co²⁺ efflux transporter; e, a missense mutation in the codon 549 of the *rpsA* gene encoding ribosomal protein S1.....69

Figure 2.12. Ribo-T composition and integrity of the linkers. a, b, Analysis of rRNA extracted from the isolated wild-type ribosomes or Ribo-T in a denaturing 4% (a) or 8% (b) polyacrylamide gel. a, Ribo-T(1) and Ribo-T(2) represent two individual preparations with Ribo-T(2) isolated following the standard procedure (see Methods), and Ribo-T(1) isolated by immediate pelleting through the sucrose cushion after the cell lysis. The faint bands in the Ribo-T2 preparation indicated by the asterisks could be occasionally seen in some preparations; they probably represent rRNA fragments generated by cleavage of the linkers in a small fraction of Ribo-T either in the cell or during Ribo-T preparation. b, 5S rRNAs present in Ribo-T. c, The relative abundance of small and large subunit proteins in Ribo-T in comparison with wild-type ribosome as determined by mass spectrometry (protein L26 could not be reliably quantified in Ribo-T and wild-type ribosomes). The data represent the average of three technical replicates, and error bars indicate the s.d. d, Analysis of the integrity of the T1 and T2 linkers in a Ribo-T preparation by primer extension. The 22-nucleotide-long primer was extended across the T1 linker in the presence of ddCTP terminator and the 23S-nucleotide-long primer was extended across the T2 linker in the presence of ddGTP terminator. Control samples (2) represent the unextended primers. The gels are representative of two independent experiments.71

Figure 2.13. Ribo-T can successfully translate most cellular polypeptides. a, Protein synthesis rate in SQ171fg cells expressing wild-type ribosomes or Ribo-T. Protein synthesis was measured by quantifying the incorporation of [³⁵S] L-methionine into TCA-insoluble protein fraction during a 45-s incubation at 37 °C in minimal medium. The bar graphs represent the average values of experiments performed in two biological replicates each done in two technical duplicates. Error bars denote s.d. b, c, 2D gel electrophoresis analysis of the proteins expressed in exponentially growing SQ171fg transformed with pAM552 (A2058G) (b) or pRibo-T (c).72

Figure 2.14. Chemical probing of the structure of the Ribo-T linkers. Ribo-T or wt ribosomes were modified by dimethylsulfate and extracted rRNA was subjected to primer extension analysis. In each gel, the left two lanes ('C' and 'A') represent sequencing reactions followed by dimethylsulfate-modified sample and control (unmodified) RNA. The diagrams on the right represent the secondary structures of helices H101 and h44 in wild type ribosomes (left) and Ribo-T (right) with the nucleotide residues modified strongly, moderately and weakly indicated by black, gray and white circles, respectively. The shown gels are representative of two independent experiments.74

Figure 2.15. Functional characterization of Ribo-T. a, Sucrose gradient analysis of wild-type ribosomes (top) and Ribo-T (bottom) under 15mM MgCl₂ (solid line) or 1.5mM MgCl₂ subunit dissociating conditions (dotted line). The peak marked with grey arrow and 'X' may represent Ribo-T dimers. The result was qualitatively verified in an independent experiment performed at Mg²⁺ concentrations 1.5mM and 10mM. b, In vitro translation of proteins by isolated Ribo-T. Top, SDS-PAGE analysis of the dihydrofolate reductase (DHFR) protein synthesized in the Dribosome PURExpress system supplemented with purified wild-type ribosomes or Ribo-T (T); wild-type ribosomes provided with the kit (WT*) were used as a control. The transcription-translation reaction was carried out in the presence of [35S]L-methionine in the absence or presence of 50 mM erythromycin (ERY). The A2058G mutation in Ribo-T renders the Ribo-T-driven translation resistant to the antibiotic. The 'no erythromycin' samples are a representative result of two independent biological experiments. Bottom, time course of sfGFP protein expression in the Δribosome PURExpress system supplemented with purified wild-type (black) or Ribo-T (grey) ribosomes. The kobs rates (385 ± 13 relative fluorescent units (RFU) min⁻¹ (mean ± s.d.) for wild-type, 177 ± 6 RFU min⁻¹ for RiboT) were determined from the initial slopes. The activity of both ribosomes was fully inhibited by 50 mg ml⁻¹ chloramphenicol (time points indicated by x). Each curve is an average of two independent biological replicates, with error bars indicating the s.d. c, Toeprinting analysis of translation of a 20-codon synthetic gene RST1⁷⁰ by wild-type ribosomes or Ribo-T. The antibiotic thiostrepton (THS), present at 50 mM, arrests the initiating ribosome at the start codon⁷¹ (black arrowhead). The threonyl-tRNA synthetase inhibitor borrelidin (BOR) arrests translation at the fourth codon of RST1 mRNA (grey arrowhead)⁷⁰. The position of a toeprint band that would correspond to the ribosome that has reached the RST1 stop codon is shown by an open arrowhead. A more pronounced toeprint band at the start codon in the samples lacking thiostrepton indicates that Ribo-T departs from the initiation codon slower than wild-type ribosomes. A weaker borrelidin-specific band observed in the Ribo-T sample suggests that under our experimental conditions, fewer Ribo-T compared to wild-type ribosomes were able to reach the fifth codon, apparently owing to slower initiation.....75

Figure 2.16. Translation of the orthogonal *sf-gfp* gene by oRibo-T *in vivo* and *in vitro*. a, Expression of an orthogonal *sf-gfp* reporter in the *E. coli* POP2136 cells transformed with pAM552 plasmid encoding wt rRNA (wt Rbs), pAM552 with an orthogonal SD sequence in 16S rRNA of a non-tethered ribosome (oRbs) or poRibo-T1 expressing an orthogonal Ribo-T (green bar). Cells lacking *gfp* reporter (wt Rbs Δ*gfp*) were used as a background fluorescence control. The data represent the average value of six biological replicates in technical triplicates with the error bars indicating the standard deviation. b, *In vitro* translation of the orthogonal *sf-gfp* reporter by non-tethered non-orthogonal wt ribosomes (pink lines), or oRibo-T(A2058G) (which also contained cellular wt ribosomes) (green lines). The dotted lines correspond to the translation reactions without antibiotic and solid lines represent reactions supplemented with 50 μM clindamycin (Cld). c, same as b, but oRibo-T contained a G693A mutation instead of A2058G and clindamycin was replaced with 100 μM pactamycin (Pct). The red star in the cartoons indicate the ribosomal subunit carrying the antibiotic resistance mutation. Graphs in b and c are each representative of two biological replicates each done in technical triplicates with the error bars indicating the standard deviation in the shown experiment.....85

Figure 2.17. Promoter mutation in oRibo-T improves transformation of the *E. coli* cells.

Transformation of BL21 cells with the original poRibo-T1 construct and with poRibo-T2 construct carrying a point mutation in the '-10' box of the P_L promoter controlling oRibo-T transcription. The plates show representative results of three independent biological experiments.

.....87

Figure 2.18. Evolving Ribo-T to identify gain-of-function PTC mutations that facilitate synthesis of problematic amino acid sequences.

a, The SecM-LacZa reporter with an orthogonal Shine-Dalgarno (o-SD) sequence is translated in the cell by oRibo-T. SecM-dependent ribosome stalling prevents expression of the lacZa gene unless a ribosomal mutation allows for bypass of the SecM arrest site. b, The placement of Phe-tRNAs bound in the P-site (orange) and A-site (yellow) of the PTC⁶¹. The conserved 23S rRNA residues A2451 and C2452 (blue) form the amino acid side-chain binding pocket in the A-site. c, Top, colonies formed on X-gal/isopropyl β-D-1- thiogalactopyranoside (IPTG) plates by the *E. coli* C41 cells transformed with the *secM-lacZa* reporter plasmid and a library of poRibo-T2 plasmids with the PTC mutations at positions 2451 and 2452. Bottom, identity of 2451 and 2452 residues in poRibo-T2 plasmids isolated from randomly picked 16 white colonies and 15 blue colonies. d, The *E. coli* C41 cells transformed with the *secM-lacZa* reporter and individual poRibo-T2 plasmids with different nucleotide combinations at positions 2451 and 2452. The transformed cells were initially plated on LB agar antibiotic plate without X-gal or IPTG (all colonies pale), and three randomly picked transformants were then streaked on the shown indicator plate containing X-gal and IPTG. The poRibo-T2 mutant with the A2058G mutation, which is known to enhance the bypass of the SecM arrest sequence⁵⁵, was used as a positive control. A mutation of another essential PTC nucleotide (U2585G), which has been proposed to be implicated in some translation arrest scenarios⁷⁹, showed no effect on SecM arrest. The photographs of the agar plates in c and d have been contrast-enhanced for better colour separation. e, The A2451C mutation enhances bypass of the SecM stalling sequence by oRibo-T in vitro. The orthogonal construct containing secM stalling sequence fused in frame to the truncated *lacZa* gene was translated in the Δribosome PURExpress cell-free translation system supplemented with wild-type non-tethered ribosomes or preparations of oRibo-T (A2451 or C2451). The Ribo-T constructs carried the pactamycin-resistance mutation G693A in 16S rRNA, and the reactions were carried out in the presence of pactamycin, which, in addition to the presence of an orthogonal Shine-Dalgarno sequence, ensured that the reporter is translated exclusively by oRibo-T (see the control wild-type lane with no translation products). Numbers on the left indicate the size (kDa) of molecular mass markers. The bar graph at the bottom shows the efficiency of bypass (ratio between the full-size and SecM-arrested translation products). A representative gel of two independent experiments is shown, with error bars indicating the s.d.89

Figure 3.1. Ribo-T system improvement strategies.

a. Schematic of Ribo-T showing tether (red) and orthogonal ribosome binding site (yellow). b. The tether is optimized in cells growing exclusively from the Ribo-T plasmid. c. Previously published Ribo-T tether sequence. d. Orthogonal function evolved for Ribo-T. e. Previously published orthogonal mRNA (o-mRNA) Shine-Dalgarno (SD) sequence and orthogonal 16S rRNA anti-SD sequence shown..... 103

Figure 3.2. Optimizing tether sequence improves performance. a. Wild-type 23S rRNA Helix 101 and 16S rRNA helix44 are connected to create Ribo-T with 9A for 5' tether, T1, and 8A for 3' tether, T2. b. Library 1: paired 5' tether T1 poly A from 7-20 nucleotides, with 3' tether T2 poly T from 7-20 nucleotides. Library 2: unpaired polyA on both T1 and T2, ranging in 7-20 nucleotides long. Library 3: randomized T1 (8N) and T2 (9N) keeping residues of opened H101 and h44 apex loops. Library 4: randomized apex-to-apex T1 (15N) and T2 (10N) of tether. c. Selection scheme for improved tethers. Strains lacking genomic copies of rRNA operons ($\Delta 7rrn$) are transformed with plasmid-based Ribo-T tether libraries, and the wild-type pCSacB plasmid is removed. d. Doubling time rank and tether sequences of selected library 4 colonies. 121

Figure 3.3. Optimizing tether sequence improves performance. a. Ribo-T: previously published tether sequence. Ribo-T-v2: fastest growing and most frequent selected tether sequence. b. Growth rate and max OD₆₀₀ of SQ171 slow growing (sg) and SQ171 and fast growing (fg) cells growing with pAM552 (wild-type *rnb* operon), pRibo-T and pRibo-T-v2. c. Spot plated SQ171 and SQ171fg cells growing with pAM552, pRibo-T and pRibo-T-v2 imaged after 48 hours at 37 °C. d. Total RNA extraction from SQ171 and SQ171fg cells growing with pAM552, pRibo-T and pRibo-T-v2. 123

Figure 3.4. Improved orthogonal pairs. a. Selection scheme to optimize orthogonal Shine-Dalgarno (SD) and anti-Shine-Dalgarno (aSD) pairs in untethered and tethered context. b. Top evolved orthogonal mRNA and 16S with predicted pairing. Selection round is noted by “round 1” or “round 2” to the right of each pair. “n” denotes number of isolated members with that sequence from the selection. 125

Figure 3.5. Improved orthogonal pair function in Ribo-T-v2. Original orthogonal Ribo-T system denoted by “v1”. a. Orthogonal expression of super folder green fluorescent protein (*sf-gfp*) in BL21(DE3) Δ upp. + pair: both o-rRNA and o-mRNA, - pair: just o-mRNA. % orthogonality shown below column labels. b. Orthogonal expression of chloramphenicol acetyltransferase (*cat*) in BL21(DE3) Δ upp. c. Orthogonal expression of *sf-gfp* in BL21 Star (DE3) strain. d. Orthogonal expression of *sf-gfp* in C321. Δ A derived strain MCJ.1217. 128

Figure 3.6. Incorporation of non-canonical amino acid p-azidophenylalanine (pAzF) by orthogonal Ribo-T. a. Combined rRNA and *sf-gfp* plasmid with *sf-gfp* gene is replaced with a 1TAG or 5TAG version to create pORT3B.gfp1TAG and pORT3B.gfp5TAG. Wild-type *rnb* operon was cloned as negative control for background orthogonal expression (pAM.B.gfp1TAG and pAM.B.gfp5TAG). b. Expression of *sf-gfp* with 1TAG or 5TAG in C321. Δ A derived strain MCJ.1217, in the presence of pAzF (+) or without pAzF (-). 131

Figure 4.1. Possible tether sites, with CP23S mutation doubling time \pm standard deviation (min) indicated for 23S circular permutations. New 16S connection points in red spheres. Structure PDB 3R8S and 4GD1. 143

Figure A.1. Testing a ribosome with stapled subunits. a. Wild-type 23S H101 and 16S h44. b. Ribo-T system⁴¹. c. Ribo-T-v2 system. d. A ribosome with stapled subunits⁹⁷. e. 1% agarose gel of total RNA extracted from SQ171fg strain⁴¹ supported by pAM552 (WT), pRibo-T plasmid, pRibo-T-v2 plasmid, and stapled ribosome plasmid. f. Orthogonal *sf-gfp* expression in BL21(DE3) Δ upp strain. g. Orthogonal *cat* expression in BL21(DE3) Δ upp strain..... 156

Figure B.1. Ribo-T strains for ribosome engineering. b. Current orthogonal system with wild-type untethered ribosomes producing the proteome for cell viability, and an orthogonal plasmid-based Ribo-T for engineering. d. In a swapped system, Ribo-T rRNA is transcribed from a plasmid-based operon, and translates the proteome, while an orthogonal untethered ribosome is used for engineering. 160

Figure B.2. S1 fast growing C549T mutation with CRISPR-Cas9. S1 gene (blue highlighted) and target gRNA sequence (green highlighted) with CGG PAM sequence (red box) shown. Homologous repair cassette introduces C549T mutation and mutated PAM sequence to AAC for colony PCR screening. 163

Figure B.3. Genome engineering with CRISPR-Cas9. a. *rrn* operon architecture and location on genome. Unique target cut sites noted by coloured squares. Modified from Maeda *et al*¹⁰⁶. b. Plasmid maps of pCas plasmid, coding for Cas9 protein and λ red machinery, and pTarget-Cm plasmid coding for targeting gRNA, and optional double-stranded DNA fixing piece. Red 'X' indicates CRISPR-Cas9 cut site and subsequent PAM mutation. c. Fixing piece for clean SQ strain. d. Fixing piece to introduce S1 fast growing C549T mutation. Orange dot indicates a mutated PAM site, but C549 unmutated S1 found by sequencing PCR product. e. Fixing piece to introduce Ribo-T cassette onto the genome to replace the wild-type *rrn*. Gels on right side of c-e show screening colony PCRs to determine genomic modification efficiencies (eff.). Unique primer binding sites for screening and watermarking are added into the clean SQ strain tRNA cassette and Ribo-T cassette (pink box). 165

List of Tables

Table 2.1. Primer pairs used for construction of circularly permuted 23S rRNA genes.	95
Table 2.2. Characterization of the growth of <i>E. coli</i> SQ171 cells expressing a pure population of ribosomes with circularly permuted 23S rRNA.	99
Table 2.3. The results of sequencing of the oligo(A) linkers T1 and T2 in pRibo-T isolated from randomly picked POP2136 clones transformed with the linker library.....	100
Table B.1. Designed target sequences for genome engineering of <i>rnn</i> operons.....	166
Table B.2. gBlocks and primers for construct assemblies. Synthesized gRNA gBlocks EDC793 and EDC794 and annotated (homology -Promoter-target sequence-gRNA scaffold-terminator- homology), with same feature mapping in EDC877-EDC888. All DNA is synthesized as single stranded DNA, unless otherwise noted as a double stranded DNA gBlock.	166
Table B.3. Primer combinations and templates. Ribo-T cassettes assembled with overall assembly PCR with pieces 1-2-3-4-5-6, and tRNA cassettes 1-7-8-9-6. Numbers 808-874 correspond to primers EDC808-EDC874.....	169
Table B.4. Strain and corresponding planned genome modifications.	169

1. Introduction

1.1 Non-standard amino acid incorporation

Life largely uses the 20 canonical α and L amino acids to produce proteins. While 20 amino acids give access to a large possible sequence space, they provide insufficient variety to create the diversity in structure and function life has evolved. Indeed, certain archaea and eubacteria genetically encode selenocysteine and pyrrolysine as 21st and 22nd amino acids¹. Furthermore, over 300 post-translational modifications (PTMs) further expand protein diversity; these including phosphorylation, amidation, prenylation, and glycosylation². The presence of these PTMs often dictates protein function and efficacy. For example, therapeutic antibody production relies on mammalian cell lines like Chinese hamster ovary (CHO) cells, because proper PTMs such as glycosylation are essential for potency, stability and immunogenicity³. Production of such proteins in mammalian cells requires expensive, fastidious, and laborious culture and production techniques that are a challenge to scale⁴. PTMs are often performed by a suite of poorly understood or difficult to control enzyme factors, limiting the production and study of these PTMs. The ability to site-specifically incorporate a PTM of interest directly via a non-canonical amino acid (ncAA), or a bio-orthogonal handle for site-specific modification after translation, could provide a promising route to controlled production of proteins with desired modifications⁵. Beyond side-chain modifications, β or D amino acid polypeptide backbone modifications could provide stable protease-resistant protein therapeutics⁶⁻¹⁰.

There are numerous strategies for incorporating ncAAs into proteins. Through chemical methods such as solid phase synthesis, ~30mer polypeptides can be synthesized with ease, incorporating virtually any number of ncAAs¹¹⁻¹³. However, significant disadvantages remain compared to translation-based polypeptide synthesis, namely limits in achievable speed, accuracy, size and scalability. Towards translation-based ncAA-containing protein synthesis, an early method is global proteome replacement of a canonical amino acid with a ncAA. This requires an auxotrophic strain in which 1 of the 20 amino acids are replaced with a close analog ncAA that can be loaded to a tRNA by the native aminoacyl tRNA synthetase (aaRS). Once sufficient biomass has accumulated, the culture is depleted of the chosen amino acid and replaced with the ncAA analog. While cell growth stops because of the incorporation of the ncAA into the proteome, the cells are viable and can incorporate the ncAA into the new proteins at all sites of the depleted canonical amino acid¹⁴. Obvious shortcomings include limits on ncAA used and lack of site-specificity due to global replacement.

The near-universal genetic code is highly redundant, providing opportunities for codon reassignment, and thus, ncAA incorporation. Most commonly used is UAG amber stop codon reassignment. In this scheme, the anti-codon of an amber suppressor tRNA is mutated to recognize the UAG stop codon. This tRNA is then charged with a non-canonical amino acid by an orthogonal aminoacyl-tRNA synthetase/tRNA_{CUA} pair, where ideally only the desired ncAA is charged onto the engineered TAG suppressor tRNA (tRNA_{CUA}). The charged suppressor tRNA then competes with release factor 1 (RF-1) to incorporate the ncAA into the growing peptide chain (Fig. 1.1).

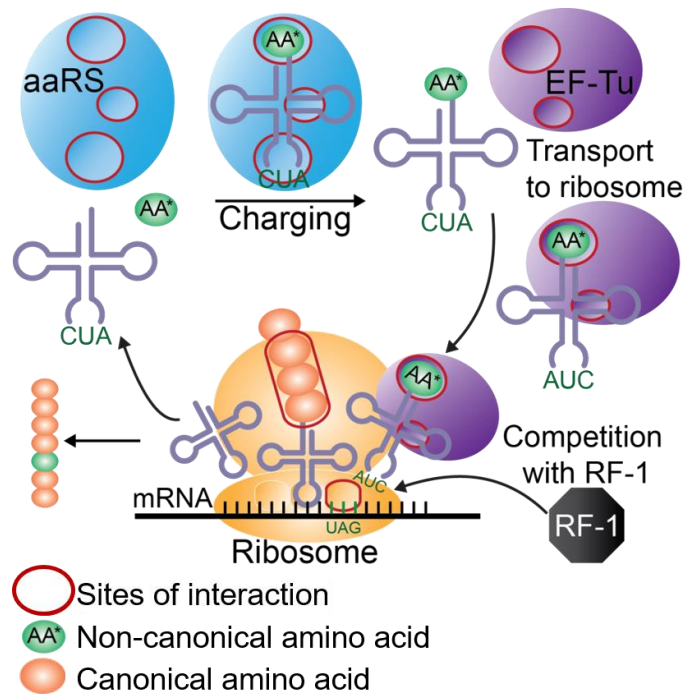


Figure 1.1 Non-canonical amino acid incorporation. Simplified cartoon of non-canonical amino acid incorporation process with UAG amber suppression. Producing proteins and peptides with non-canonical amino acids requires an expanded genetic code with multiple biological parts. These parts include (i) an open coding channel reassigned to a non-canonical monomer, (ii) monomer-transfer RNA (tRNA) substrates that can decode the open codon (that are typically produced by an orthogonal aminoacyl-tRNA synthetase (o-aaRS) specifically charging a non-canonical monomer to its orthogonal tRNA), (iii) delivery of monomer-tRNA substrates to the ribosome by elongation factor Tu (EF-Tu), and (iv) compatible ribosomes. To ensure efficient operation of a re-engineered translation apparatus, many parts must be reconfigured.

To date, over 150 non-canonical amino acids have been site-specifically incorporated into proteins in *E. coli*, yeast and mammalian cells through suppression of the TAG amber stop codon¹⁵⁻¹⁷. Such ncAA include modified backbones¹⁸, fluorophores¹⁹, PTM functional groups^{20, 21} and photo/chemically reactive side groups²², producing proteins with novel properties for diverse applications. These advancements have enabled protein function and structure studies²³, real-time biophysical probing of protein function²⁴, and development of novel therapeutic proteins²⁵. However, currently these ncAAs are still largely structurally and functionally similar to the canonical 20. Major limitations still exist with incorporating exotic side chains and modified backbones. For example, β -amino acids (amino acids with expanded backbones) can be incorporated, but in limited numbers and non-sequentially; they also require *in vitro* charging using a flexizyme ribozyme^{6, 26-28}. Limitations to these systems include (i) the lack of an aminoacyl-tRNA synthetase (aaRS) to specifically and efficiently charge the ncAA to the TAG suppressor transfer RNA (tRNA_{CUA}), (ii) non-optimal elongation factor Tu (EF-Tu) binding for the delivery of the ncAA-tRNA_{CUA} to the ribosome, and (iii) the ribosome's inherent and dynamic movement. A major breakthrough in this field would include the ability to co-evolve the system of translation (e.g., elongation factors, synthetases, and the ribosome) for the incorporation of multiple novel ncAAs. My work focuses on the ribosome as an engineering target for improving ncAA incorporation platforms.

1.2 The *Escherichia coli* ribosome

In all kingdoms of life, ribosomes are invariably composed of two subunits, small and large (30S and 50S in bacteria), each built of RNA and proteins (Fig. 1.2). The small subunit 30S particle contains the 1,542 nucleotides (nt) 16S ribosomal (r)RNA and 21 ribosomal (r)Proteins. During initiation, the Shine-Dalgarno (SD) sequence of the messenger (m)RNA is bound by the anti-SD sequence on the 3' end of the 16S rRNA. Initiation factors and fMet-tRNA associate with the 30S subunit. The large subunit 50S particle contains the 2,904 nt 23S rRNA, the 120 nt 5S rRNA, and 33 rProteins. This subunit is responsible for catalyzing the peptidyl transferase reaction and polypeptide secretion through the exit tunnel²⁹. These key functions are facilitated primarily by the 23S rRNA, making it a key target for ribosome engineering.

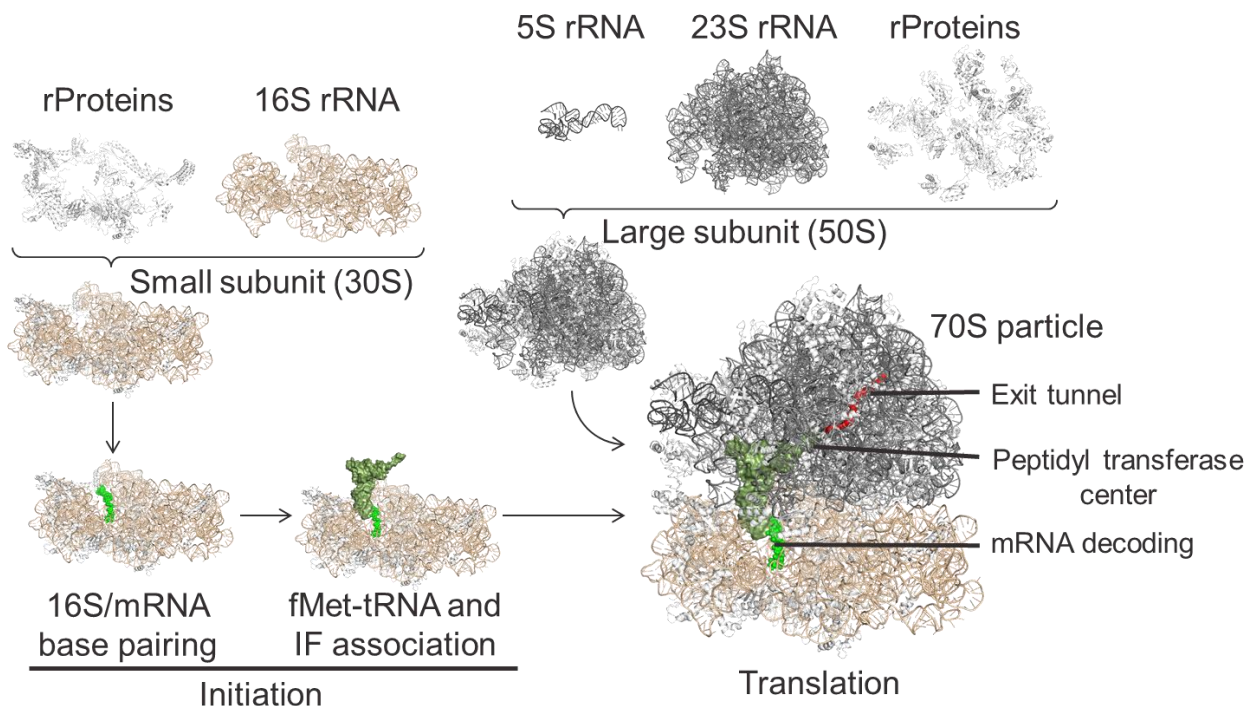


Figure 1.2 *E. coli* ribosome components, structure and function. Ribosomal proteins (rProteins) are shown in white, 16S rRNA in tan, 23S and 5S rRNA in grey. Messenger RNA is in green, tRNA in forest green, and nascent polypeptide chain in red. Crystal structures adapted from PDB 2WWL and 2WWQ.

1.3 Ribosome engineering

Cells require highly active ribosomes for life. As such, the native *E. coli* ribosome has been evolutionarily optimized for efficient incorporation of the 20 canonical amino acids, with limited mutational flexibility while maintaining cell viability. Strategies to bypass cell viability constraints for ribosome engineering are highlighted here.

1.3.1 *In vitro* ribosome engineering

The Jewett lab has pioneered the ability to build and evolve mutant ribosomes outside the cell using the integrated synthesis, assembly and translation (iSAT) platform. In this system, ribosome-free *E. coli* lysis extracts are supplied with plasmid DNA encoding the mutated rRNA operon, a reporter gene plasmid, ribosomal proteins, polymerase, an energy source, cofactors and buffers. In one test tube, rRNA is transcribed from the plasmid operon, coassembled with rProteins and sufficiently processed to produce highly active ribosomes which can translate the reporter mRNA³⁰⁻³². The system can also be coupled to evolution strategies such as ribosome display, to evolve new functionalities without the use of intact cells. This greatly expands the accessible ribosomal mutation space compared to previous *in vitro* and *in vivo* methods³³⁻³⁷.

1.3.2 *In vivo* ribosome engineering

While many advances have been achieved with cell-free systems, my work has focused on engineering *in vivo* *E. coli* based translation systems. *In vivo* ribosome engineering provides (i) easy compartmentalization and propagation of mutant plasmid-based libraries, (ii) readily available high throughput and robust selection methods, and (iii) the possibility to use these systems in virtually any lab with basic molecular biology technique capabilities.

However, the random exchange of ribosomal subunits between recurrent acts of translation presents an obstacle for engineering orthogonal cellular genetic systems. In such systems, a subpopulation of ribosomes should ideally be excluded from synthesizing endogenous proteins and instead be dedicated to the translation of a specialized orthogonal mRNA. An orthogonal and evolvable translation machine could be optimized for the functions that are cumbersome or even beyond the reach for a ‘conventional’ ribosome, such as polymerizing amino acid sequences that lead to translation arrest, utilizing alternative genetic codes or the genetically programmed incorporation of ncAAs into proteins⁵. Because the ability of a ribosome to carry out such special tasks would likely compromise its normal functions, the orthogonal translation system allows for the selection of desirable properties of the specialized ribosome without impeding the general protein synthesis carried out by native ribosomes. By placing an alternative Shine-Dalgarno (SD) sequence in a reporter mRNA and introducing the complementary changes in the anti-SD region in 16S rRNA, it is possible to redirect a subpopulation of the small ribosomal subunits to translation of a specific messenger RNA^{35, 38}(Fig. 1.3a,b). The specialized orthogonal 30S subunits have been employed for selecting mutants with new decoding properties^{37, 39}. However, because large subunits freely exchange between native and orthogonal small subunits, creating a fully orthogonal ribosome has been impossible, thereby limiting the selection or engineering of the peptidyl transferase center (PTC), the nascent peptide exit tunnel and the entire large ribosomal subunit. In this work, we offer a solution for this problem of intersubunit promiscuity by constructing a ribosome with inseparable subunits tethered with covalent linkers (named “Ribo-T”), and thus ‘married-for-life’ (Fig. 1.3c). We demonstrate that Ribo-T, which is built on the scaffold of a chimeric 4.5 kb RNA composed of 16S and 23S rRNA sequences, carries out protein synthesis without fully dissociating into individual subunits and therefore can be used for engineering a complete orthogonal translation system *in vivo* and *in vitro*.

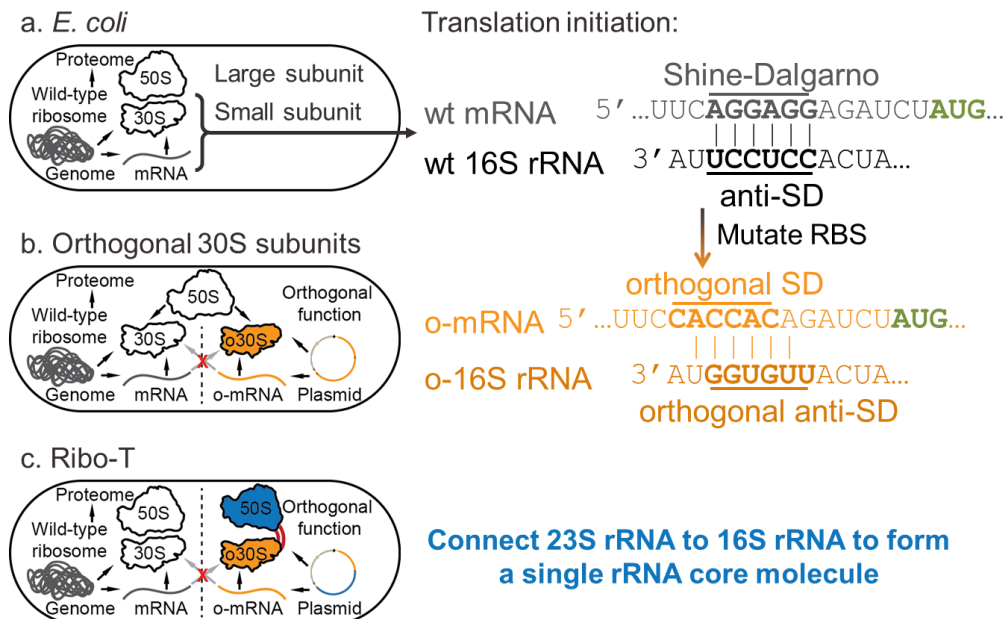


Figure 1.3 Ribosome engineering in living *E. coli*. a. Wild-type Shine-Dalgarno (SD) mediated mechanism for translation initiation. b. Mutating SD/antiSD pair creates orthogonal small subunits. The large 50S subunit works with both wild-type and orthogonal 30S subunits. c. 23S rRNA is fused with orthogonal 16S rRNA to create a ribosome with tethered subunits (Ribo-T).

1.4 Creating Ribo-T: (Design, Build, Test)ⁿ

“Persistence in science counts for a lot.”—Robert Byer⁴⁰

In October 2013, it was nearly 3 years into our pursuit towards a ribosome with tethered subunits, Ribo-T⁴¹, when I heard Dr. Robert Byer on a Nature Podcast⁴⁰. He was talking about creating a mini particle accelerator⁴², a project they had been thinking about since 1996. 17 years later, it was published. The take home message was clear; given enough time and hard work, a challenging project can succeed! Of course, I was not excited by the prospect of a 17 year PhD but in my optimism, I happily ignored this detail.

The story of Ribo-T starts in September 2010 with Michael Jewett of Northwestern University and Alexander (Shura) Mankin of University of Illinois at Chicago, hatching the idea for Ribo-T over lunch. With labs just 20 miles apart, it became a seamless ‘ping-pong’ collaboration with frequent team meetings on both campuses, easy exchange of constructs, and lots of face-to-face interactions. For me, it all started in February 2010 when I first met Mike on a recruiting weekend of Northwestern University. After discussing photography, travel, impressionist art and visionary science over beer before the department dinner, I knew he was the advisor for me. When I joined the lab in January 2011, he pitched me the Ribo-T project. I was instantly hooked.

The project was based on a deceptively simple idea: tie a large ribosomal subunit to a functionally isolated (orthogonal) small subunit. If we succeeded, the large subunit would become also functionally isolated and therefore engineerable in ways previously impossible. A simple idea, sure, but it went completely against what evolution ‘decided’ was a good design; in all kingdoms of life, across billions of years of evolution, the ribosome has remained a molecular machine composed of two completely separate subunits (Fig. 1.4A). Yet we were able to break that paradigm. Project

trajectory from conception to publication took nearly 5 years (Fig. 1.4), requiring a great deal of groundwork and learning, then rather suddenly, success. While thankfully this is far short of 17 years, why the long time for a simple idea?

1.4.1 First tries to tie: An infinite loop

While we have beautiful crystal structures of the ribosome and know a great deal about its function, it is an exceptionally intricate and complicated macromolecular RNA-based machine. Each subunit is composed of a ribosomal RNA core with ribosomal proteins, fine-tuned over billions of years of evolution. A full-on rational *de novo* design of this scope is currently insurmountable; the ribosome is too complex. Thus, as synthetic biologists we utilize the “design, build, test” engineering doctrine, but with seemingly endless “repeats” added.

Our overarching design consideration was how to form a stable linker ensuring cis-associating subunits at a site with minimal interference on ribosome functionality. Since small subunit orthogonality is imparted by the 16S core ribosomal RNA (rRNA) and the large subunit key functionality is imparted by the 23S core rRNA²⁹, we wanted to create a ribosome with a single core rRNA comprised of the 16S and 23S rRNA fused into a single RNA molecule.

Briefly, our first set of designs connected the ‘tail’ of the 23S rRNA to the ‘head’ of the 16S rRNA by a single stranded RNA tether (Fig. 1.4B). Since the native ends of the 23S and 16S rRNA are far apart (~180 Å straight distance), we moved the large subunit tether site closer to the small subunit by way of a “circular permutation” wherein the native ends of the 23S rRNA, which are located next to each other as they form a helix, are linked and new ends are created elsewhere on the subunit. We could try to use circular permutations to move the location of the 23S rRNA ends, and thus tether site, anywhere on the large subunit if—a big if—the mutation does not detrimentally

interfere with ribosome biogenesis and/or function. From a previous study⁴³ we knew that a circular permutation at 23S helix 63 could fully support cell growth, and created new ends relatively close to the small subunit (~ 110 Å from the 16S rRNA 5' end), and was away from the “busy” part of the ribosome where tRNAs enter and exit. Helix 34 is even closer (~ 75 Å) and though we did not know yet about the viability of this circular permutation (spoiler, it was not), we thought this site could work as well.

Our designs then tried to bypass native processing by moving the promoter's transcriptional start right up to the construct's 5' end and placing a self-cleaving ribozyme at the 3' end (the hammerhead ribozyme⁴⁴ and the hepatitis delta virus ribozyme⁴⁵ were tested). We then designed and built a library of tethers ranging from ~ 20 bp to ~ 1000 bp, containing repeating hairpin structures for potentially added stability from ribonucleases (Fig. 1.4B). To test these constructs, we looked for orthogonal³⁵ function *in vivo* and accumulation of a larger piece of rRNA in the cell. In short, the reality was that we had the orthogonal function (chloramphenicol acetyltransferase assay: orthogonal Ribo-T translates an orthogonal *cat* message, giving resistance to the antibiotic chloramphenicol) but no detectable full sized Ribo-T rRNA. The tether was just being cleaved. There we were, 2 full years into the project, no Ribo-T.

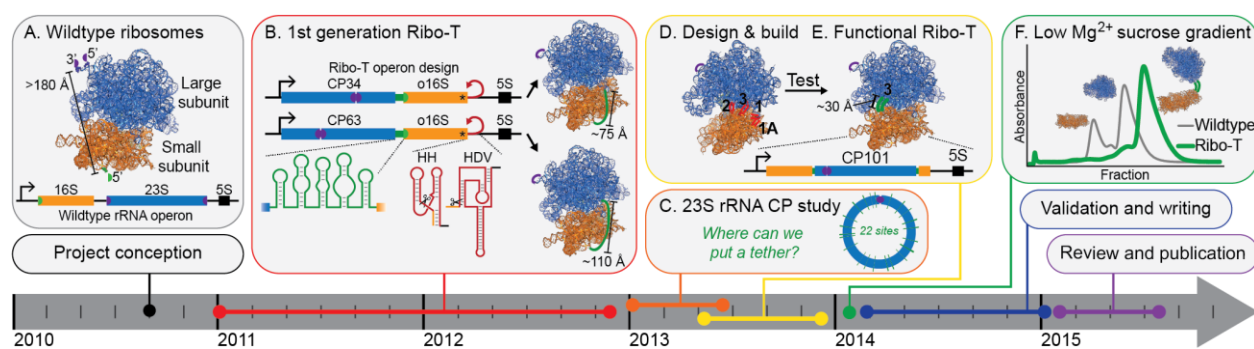


Figure 1.4 Timeline in creating Ribo-T. A) Wildtype ribosome and rRNA operon. B) First generation Ribo-T design. Circularly permuted 23S at helix 34 or 63, connected to a 16S with an orthogonal (o) mRNA recognition site (*). HH-hammerhead ribozyme, HDV-hepatitis delta virus ribozyme. C) 23S rRNA circular permutation study. D) Design, build and test of new Ribo-T structure. E) Successful Ribo-T with tether connection at large subunit 23S helix 101 and small subunit 16S helix 44. F) Sucrose gradient with fractionation experiment demonstrating stable Ribo-T tether in intact ribosomes. Crystal structures: PDB 3R8T & 4GD2.

A better-informed design

Knowing tether cleavage and possibly the processing was the issue, we wanted to explore new tether sites in order to minimize tether distance. Tether location is readily changed with a large subunit rRNA circular permutation, but this mutation is not trivial as it can greatly affect ribosome biogenesis and function. Our prior design was severely limited by the small data set that existed in the literature; only a handful of sites have been tested *in vitro*⁴⁶ and only 3 mutations of this exact type were known to be viable *in vivo*⁴³, and we were just guessing about the circular permutation at 23S Helix 34. It became clear that we needed more design flexibility than the previously known sites would allow.

Time for brute force. Towards a better-informed design, we tested 91 locations for new 23S rRNA ends, spread through the entire surface of the large subunit for their ‘circular permutability’...and just in case our ultimate goal failed we would at least have some interesting data to show for all this work. Through this study, we found 19 new viable permutants (giving us 22 total) to work with (Fig. 1.4C). Perhaps not surprising given the ever-humbling process of engineering biology, turns out our design using 23S helix 34 was doomed from the start as this circular permutation is not viable (CP719, Fig. 2.6). So much for rational design.

With this dataset in hand, we saw that several of the new locations were very close to the subunit interface. We had a fresh break-through idea: what if we not just connect one rRNA end to the end of the other, but graft the large subunit into the midst of the 16S rRNA with 2 short linkers at the interface? This way, we would have two short tethers right at the interface, not just one longer tether. This design had two other advantages: the processing enzymes which recognize the native rRNA ends will not cleave the linkers because they will be connected at non-native end locations, and the processing of 16S rRNA can be driven by the natural mechanisms because the 16S rRNA ends would remain intact.

A ribosome with tethered subunits, Ribo-T

We built a few variants (Fig. 1.4D), and tested orthogonal activity in *E. coli* with an orthogonal green fluorescent protein message: one of the constructs was slightly above background (23S helix 101/16S helix 44 connection, Fig. 1.4E). We then extracted total RNA from the cells and ran an agarose gel to separate the RNA out based on size. After *years* of cleaved tethers, we finally saw a faint full Ribo-T sized band in addition to the cell's normal untethered ribosomes rRNA bands! With this glimmer of hope, it was time for a "Hail Mary" experiment.

We wanted to see if the Ribo-T design could fully support cell growth in the absence of normal ribosomes. In a strain of *E. coli* with all the genomic rRNA operons inactivated⁴⁷, all the rRNA originates from a plasmid-based operon. Switching the small subunit mRNA recognition site from the orthogonal sequence back to wild-type, we built a simple library of 7-12 adenines on each tether, transformed these Ribo-T plasmids into the genomic rRNA deletion strain, and kicked out the old plasmid. To our amazement, colonies grew. What was going on here? Back to the total RNA gels. The first remarkable result came on October 25th 2013; instead of the typical large subunit and small subunit rRNA bands, we saw just a single major band corresponding to a Ribo-T size rRNA. It was wild to see. After all, we created the first known cells to be fully supported by a ribosome with tethered subunits! Take that evolution.

But our characterization until now was just by looking at total extracted RNA, not full intact ribosomes. The next key experiment was to check for a stable tether in the ribosome sample. Sucrose gradient fractionation separates the small subunit, large subunit, and fully complexed ribosome particles. We ran the ribosome samples in both high Mg^{2+} conditions (subunits form whole ribosome) and low Mg^{2+} conditions (subunits completely dissociate). If Ribo-T had a stable tether, we would not see the small and large subunit dissociation peaks in the low Mg^{2+} condition, but rather a single dominant peak of the subunits physically tied together.

On January 30th, 2014, Cédric Orelle, Teresa Szal and I ran the sucrose gradient fractionations at the University of Illinois at Chicago. We saved the Ribo-T low Mg^{2+} condition for last. We intently watched the absorbance peaks slowly trace out on the computer screen...no small subunit peak...no large subunit peak...just a beautiful single major peak corresponding to our Ribo-T (Fig. 1.4F). We knew we had it! Shura Mankin brought in whiskey in Falcon tubes to toast. And the rest is the paper⁴¹, after of course months of detailed validation to convince ourselves and reviewers that Ribo-T was indeed real.

1.4.2 Breaking the infinite loop

From a student's perspective, a PhD with a nice steady buildup of publishable results is ideal. You will for sure have something to graduate on if you work hard enough, even if the end goal is never fully realized. I happened to have a high-risk project as the bulk of my PhD work, and a very realistic possibility all along was that the pursuit of Ribo-T would fail, at least in my timeline as a PhD student. I am very mindful of an element of "luck" in this story; so many things had to come together just right, and there were many very reasonable points to call it quits on the project—in the early years of Ribo-T, our mantra was "if we fail, fail fast".

How did we accomplish such a seemingly impossible objective? First, we were wonderfully naïve when we started, allowing us to uninhibitedly explore the space for a few years, getting a sense for the beast. Second, we had visionary funders in the Packard Foundation, NSF, and DARPA, willing to fund a high-risk high-reward project. Third, we didn't know when to quit, so we became obsessed with getting Ribo-T. After every frustrating result and failed construct, instead of scrapping it we always picked ourselves back up and found one more thing to try.

I save the most important for last: we had the perfect team of engineers and biologists: Mike Jewett, a young, energetic, big-vision engineering professor, and Shura Mankin, an established biology professor with deep knowledge of the ribosome and lots of experience. Then there was me, a PhD student, and Cédric, a post-doc, who just didn't know any better to not take on such a high-risk project. Our team was rounded out with wonderful people who loved the science and the pursuit of something challenging. Furthermore, having the team all in the Chicago area enabled frequent face-to-face team meetings and social events. It was genuinely fun, and we became very close accordingly. While it may be sappy, it's nevertheless true: Ribo-T gave me colleagues I now hold as dear friends.

Retrospection of course comes at the end of a big project: would I join this type of project again given the long term unpredictable (Design, Build, Test)ⁿ process? Absolutely I would. This type of work has everything I love about science and engineering: getting obsessed with a fascinating problem, doing things never done before, working on a diverse team towards a single goal, and having fun doing it because you are working with friends. And as with any human endeavor, there is a wonderful chaos of unpredictability about the process, both humbling and exhilarating. But when that gamble pays off after years of hard work, you feel so alive. I'll be chasing that feeling again for sure, even if it takes the full 17 years next time.

1.4.3 Acknowledgements

First and foremost, thank you to team Ribo-T: Cédric Orelle, Teresa Szal, Tanja Florin, Alexander S. Mankin, and my mentor Michael C. Jewett. Thanks to Paul D. Carlson, Adam J. Hockenberry and Jennifer A. Schoborg for comments and discussion on this piece.

1.4.4 Publication

Section 1.4 was a solicited ACS Synthetic Biology viewpoint piece about our Ribo-T paper.

E.D.C. wrote the piece.

Carlson, E.D. (2015) Creating Ribo-T: (Design, Build, Test)ⁿ. ACS synthetic biology, 4, 1173-1175.

2. Protein synthesis by ribosomes with tethered subunits

2.1 Abstract

The bipartite structure of the ribosome likely reflects its evolutionary origin from two independent primordial ribozymes, one putatively associated with non-templated peptide synthesis and another involved in RNA replication^{48, 49}. Through billions of years of evolution from the last universal common ancestor to the modern extant species, the ribosomal subunits have never been united into a single entity suggesting that the ability of the subunits to separate from each other is highly advantageous for protein synthesis. During translation the small and large subunits accomplish distinct but complementary functions: while the small subunit decodes the genetic information encoded in mRNA, the large subunit catalyzes polymerization of amino acids into protein and is also responsible for protein excretion. The independent but coordinated functions of the subunits, including their ability to associate at the initiation phase, move relative to each other during elongation, and dissociate after release of the completed protein, are an established paradigm of the genetically-programmed protein synthesis. Furthermore, the autonomy of the subunits is presumed to be critical not only for their functions in protein synthesis but also during their biogenesis where dedicated assembly factors keep immature ribosomal subunits apart and prevent them from engagement in translation⁵⁰.

The ability of the subunits to reversibly associate and dissociate at initiation and termination steps of translation, respectively, and move relative to each other during elongation is considered a fundamental property of the ribosome. Free exchange of the subunits limits the development of specialized genetic systems that could be evolved for novel functions without interfering with native translation. Here we show that ribosomes with tethered and thus inseparable subunits (Ribo-T) are

capable of successfully carrying out protein synthesis. By engineering a hybrid rRNA composed of small and large subunit rRNA sequences, we produced a functional ribosome in which the subunits are covalently linked into a single entity by short RNA linkers. Strikingly, Ribo-T was not only functional *in vitro*, but was able to support cell growth even in the absence of wild type ribosomes. We used Ribo-T to create the first fully orthogonal ribosome-mRNA system and demonstrated its evolvability by selecting otherwise dominantly lethal rRNA mutations in the peptidyl transferase center that facilitate translation of problematic protein sequences. Ribo-T can be used for exploring poorly understood functions of the ribosome, enabling orthogonal genetic systems, and engineering ribosomes with new functions.

2.2 First tries to tie

Since specificity of mRNA selection is dictated by the small subunit rRNA, the orthogonality of the full ribosome could be achieved by linking the small and large subunit rRNA into a continuous molecule. A successful chimeric 16S-23S construct has to satisfy a number of criteria: 1) it must properly interact with the ribosomal proteins and biogenesis factors in order to support functional folding and assembly of the subunits; 2) the 16S-23S rRNA hybrid should avoid cleavage by ribonucleases of rRNA processing and be resistant to the action of other cellular nucleases; 3) the linker(s) connecting 16S and 23S rRNAs should be sufficiently short to ensure cis-association of the conjoined subunits yet long enough to provide sufficient freedom for the subunit movement required for efficient translation initiation, processive elongation and successful peptide release. In the native ribosome, the ends of 16S and 23S rRNA are exposed on the solvent-accessible surface of the subunits and are far ($>170 \text{ \AA}$) apart. Connecting them directly in a head-to-tail fashion seemed impractical: the long RNA linker would be fully accessible to cellular nucleases and thus, highly unstable.

The simplest design would be to directly link one end of the 23S rRNA to the 16S rRNA with a single-stranded RNA linker. However, we thought this distance was too far to form a stable tether (~ 180 Å direct distance, PDB 3R8T and 4GD2). This first set of designs looked for a shorter tether site away from the “busy” area of the ribosome where the incoming mRNA interacts with tRNAs. Also, since the anti-Shine-Dalgarno site endowing small subunit orthogonality sits at the 3’ end of the 16S rRNA, we wanted to first try linking the 23S rRNA to the 5’ end of the 16S to avoid tether interference with the anti-SD function. Conveniently, the 23S rRNA 5’ and 3’ ends form a helix; these ends can be connected and new 5’ and 3’ ends created elsewhere on the 23S rRNA molecule, termed a “circular permutation”. Previous to our work, Kitahara *et al.*⁴³ showed that a circular permutation at 23S rRNA Helix 63 could fully support cell growth. In this construct, the native 23S 5’ and 3’ ends are linked with a tetra loop, and new 5’ and 3’ ends are opened at Helix 63 (Fig. 2.1). The new 5’ and 3’ ends in this cp63 mutant are relatively close to the 16S 5’ end (~ 110 Å, PDB 3R8T and 4GD2). Helix 34 is also close (~ 75 Å, PDB 3R8T and 4GD2), so this site could work as well (though our study, described in the next section, showed this site was non-viable). We had two variants designed, CP63-o16S and CP34-o16S, both with an orthogonal anti-Shine-Dalgarno for orthogonal expression³⁵.

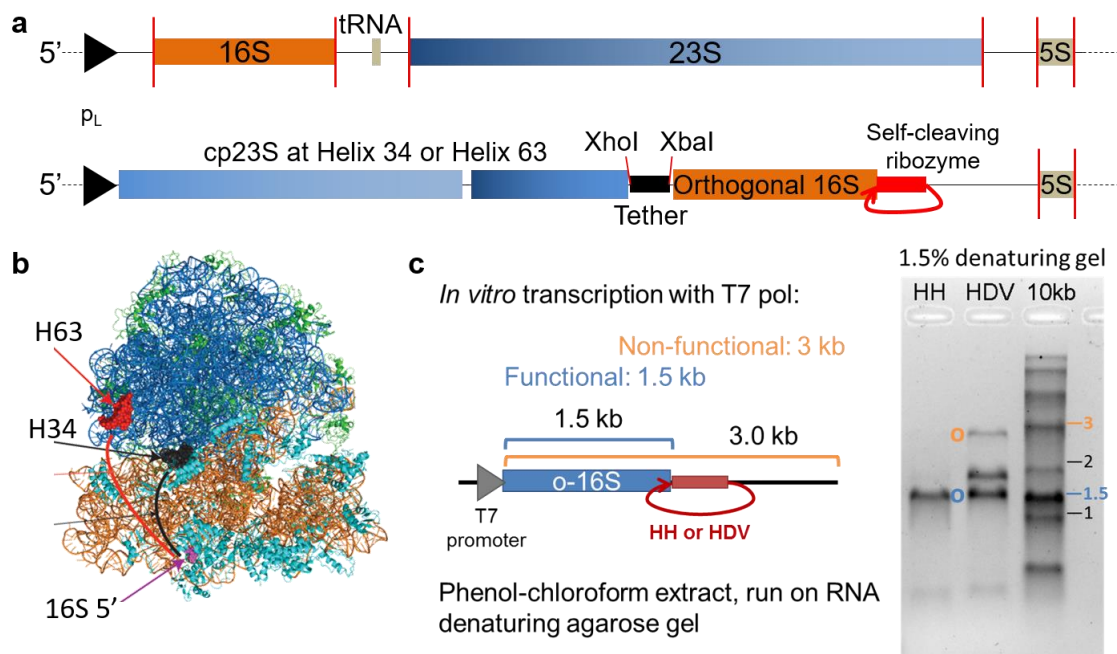


Figure 2.1. a. DNA operons of wild-type *mmB* operon (top) and rearranged Ribo-T initial tries ribosomes with a tether connecting a circularly permuted 23S gene and orthogonal 16S rRNA. XhoI and XbaI sites allow for tether incorporation. b. Ribosome crystal structure with initial tether sites chosen at 23S helix 34 (H34) and 23S helix 63 (H63). An RNA tether will connect either H34 or H63 to the 16S 5' end. c. Testing hammerhead (HH) and hepatitis delta virus (HDV) efficiencies using *in vitro* transcription reactions and denaturing RNA electrophoresis gel.

Ribosomal RNA is transcribed as a long piece of RNA, which is then cut down to the mature 16S, 23S and 5S by RNAses that recognize the processing stems, unique to each rRNA piece²⁹. With the 5' end is the 23S and the 3' the 16S, this processing would likely be disrupted and the Ribo-T construct left unprocessed. We decided to try bypassing processing stems completely by moving the promoter's transcriptional start up to the 5' end of the construct and placing a self-cleaving ribozyme at the 3' end. We incorporated the hammerhead ribozyme⁴⁴ or the hepatitis delta virus ribozyme⁴⁵ into the constructs (Fig. 2.1a). An *in vitro* transcription reaction followed by incubation at 37 °C for 1 hour, and a denaturing RNA gel revealed partial cleavage of the hepatitis delta virus ribozyme construct, and near complete cleavage of the hammerhead ribozyme construct (Fig. 2.1c).

Finally, given this design had a single strand of RNA as the connection, we were very concerned with degradation in the cell since unstructured RNA is highly susceptible to degradation *in vivo*⁵¹. We designed a library of varying tether lengths from about 100 bp to 1000 bp, containing repeating stable hairpin structures⁵¹ for potentially added stability (Fig. 2.2b). Tether libraries were assembled from primers coding for hairpin loops, and inserted into the Ribo-T CP63-o16S and CP34-o16S via incorporated *XhoI* and *XbaI* restriction sites (Fig. 2.2). Final testing of these constructs looked for orthogonal function *in vivo* and accumulation of a larger piece of rRNA in the cell. We observed expression of a cognate orthogonal chloramphenicol acetyltransferase gene, but no detectable Ribo-T sized rRNA, leading us to conclude that the tether was being readily cleaved in the cell.

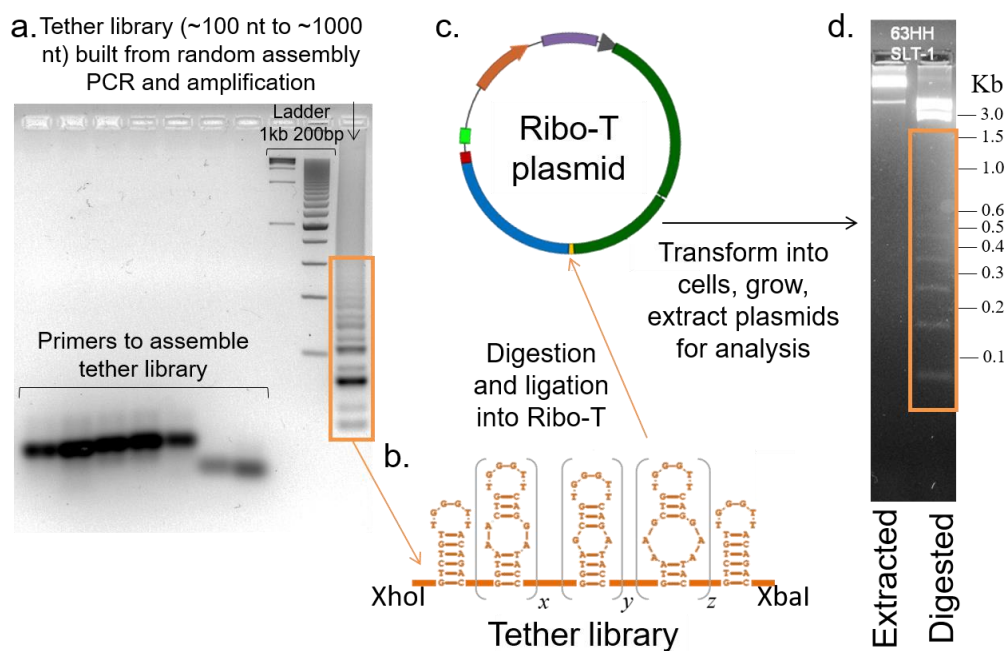


Figure 2.2. Tether library generation. a. Agarose gel showing individual primers (7 left lanes) and PCR assembled into a library of tethers (rightmost lane). b. Library and Ribo-T plasmid are digested with *XhoI* and *XbaI* restriction enzymes. c. Digested tether library and plasmid backbone are ligated to form a plasmid with Ribo-T. d. Plasmids are extracted from cells. Undigested (left) and *XhoI/XbaI* digested plasmids (right) run on an agarose gel to confirm library integration.

2.3 Circular permutations of 23S rRNA

2.3.1 Introduction

With tether degradation being an issue, we considered an alternative design of a 16S-23S chimera in which the 23S rRNA would be ‘grafted’ into the 16S rRNA with the bridges connecting 16S and 23S rRNA sequences located close to each other at the rim of the subunits interface. This design would minimize tether length, providing potentially greater protection from RNase degradation in the cell. To identify potential linking sites, we took advantage of the proximity of the 5’ and 3’ ends of 23S rRNA in the structure of the mature ribosome to connect the native 23S rRNA ends and generate new ends at a different location (Fig. 2.3). This circular permutation (cp) approach has been pioneered by Polacek and coworkers, who showed that cp23S rRNA associates with ribosomal proteins into a catalytically-active 50S subunit *in vitro*⁴⁶, while a subsequent pilot study showed that three 23S rRNA cp variants could assemble into a functional subunit *in vivo*⁴³. However, there are many more possible large subunit helices. There are many factors determining cp23S viability in the cell including disruption of ribosome biogenesis pathways, deleterious effects on ribosome function during initiation, elongation and/or termination, and negative effects on translation factor interactions. These complex and likely confounding aspects require a screen for viable 23S rRNA circular permutations. However, the construction and testing methods of previous studies⁴³ are tedious and not scalable, so we first set out to develop more high-throughput construction and screening methods to screen all the helices of the large subunit.

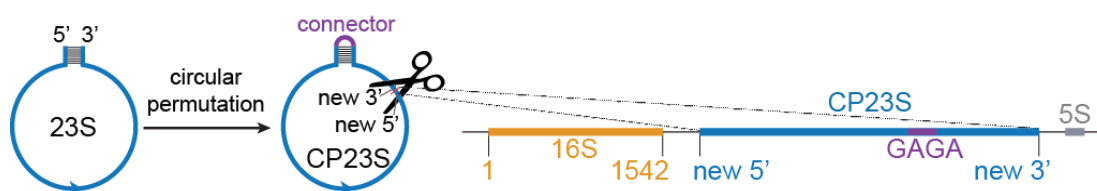


Figure 2.3. The general scheme of constructing rRNA operon in which the mature 23S rRNA gene sequence is replaced with the circularly permuted gene.

2.3.2 Methods

We prepared a comprehensive collection of 91 cp23S rRNA mutants with new 5' and 3' ends placed in the apex loops and some internal loops of nearly every 23S rRNA hairpin (Fig. 2.4a-c). The cp23S rRNA sequences were introduced in place of the wt 23S rRNA gene in the *rmb* operon of pAM552 plasmid (Fig. 2.4a-c, Fig. 2.5a) and the resulting constructs were transformed in the *E. coli* SQ171 cells lacking chromosomal rRNA alleles⁴⁷. An erythromycin resistance mutation A2058G was introduced in the cp23S constructs to facilitate selection of the functional cp23S rRNA variants.

Preparation of circularly permuted variants of the 23S rRNA

The A2058G mutation was introduced into the pAM552 plasmid (Fig. 2.5a) by inverse PCR using primers CCGTCTTGCCGCGGGTAC and GTGTACCCGCGGCAAGACGGGAAGACCCCGTGAACC (the underlined sequence is complementary to the second primer and the mutation is shown by italicized bold character) followed by re-circularization by Gibson assembly reaction⁵². A 23S-A2058G gene with native 5' and 3' ends linked by a GAGA tetra-loop was generated by inverse PCR using primers GGTAAAGCCTCACGGTTC and CCGTGAGGCTTAACCGAGAGGTTAAGCGACTAAGCGTAC (GAGA tetra loop in bold) and pAM552-A2058G as template. Purified PCR product (50 ng) was circularized by Gibson assembly reaction for 1 hour at 50 °C. The resulting circular 23S rRNA gene was then cloned at its native unique *EagI* restriction site (position 1905 in wt 23S rRNA gene) into T7-FLAGTM-4 plasmid (Sigma Aldrich) as follows. The circularized 23S rRNA gene was amplified by inverse PCR using primers GAGACACAACGTGGCTTTCCGGCCGTAACCTATAACG and CACTCGTCGAGATCGATCTTCGGCCGCCGTTTACC (added homology to the T7-FLAGTM-4 vector underlined) and Gibson-assembled with the T7-FLAGTM-4 vector amplified with the primers AAGATCGATCTCGACGAGTG and GAAAGCCACGTTGTGTCTC. The cloned circularly permuted 23S rRNA gene in the resulting plasmid pCP23S-*EagI* containing a pBR322 origin of replication and KanR selective marker (Fig. 2-6a) was fully sequenced.

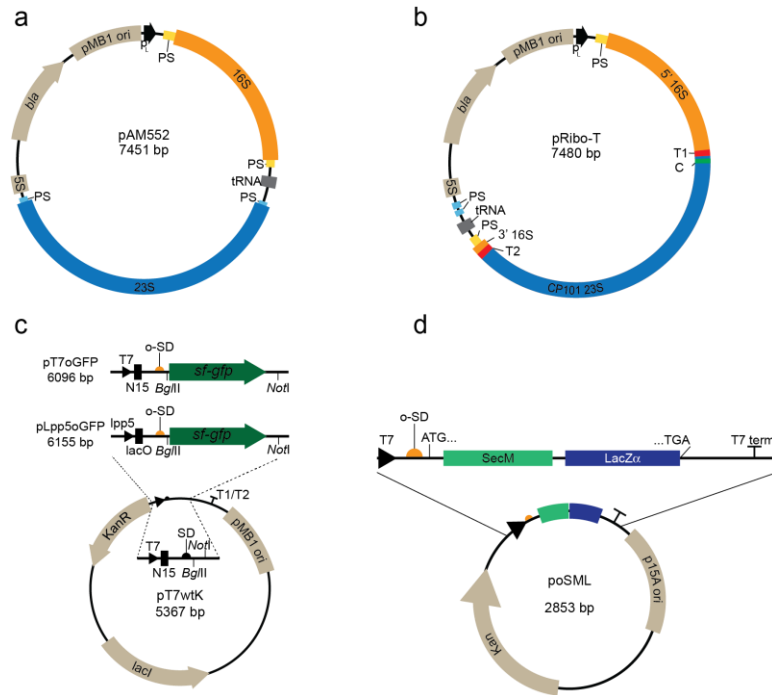


Figure 2.5. Key plasmids. a, pAM552 plasmid is a derivative of pLK35⁵³ from which the unessential segments of the pBR322 cloning vector have been removed. pAM552 contains the entire *rrnB* operon of *E. coli* under the control of the phage lambda P_L promoter which is constitutively active in the conventional *E. coli* strains but is silent at 30° in the strain POP2136 (30°C) carrying the *cI857* gene of the temperature-sensitive lambda repressor⁵⁴. The 16S rRNA gene is shown in orange with the 16S rRNA processing stem sequences indicated in yellow. The 23S rRNA gene is blue and the corresponding processing stem sequences are light blue. The intergenic tRNA^{Glu} gene is shown in dark grey. b, The map of the pRibo-T8/9 plasmid derived from pAM552. The native 5' and 3' ends of the 23S rRNA were linked via a tetranucleotide sequence GAGA (connector C shown in green), and circularly permuted 23 rRNA gene, 'opened' in the apex loop of H101, was inserted in the apex loop of 16S rRNA helix h44 via an A₈ linker T1 and an A₉ linker T2 (red bars). c, The map of the backbone plasmid pT7wtK and the reporter plasmids pT7oGFP and pLpp5oGFP, expressing *sf-gfp* controlled by an orthogonal SD sequence (orange semi-circle) under T7 or *lpp5* promoters (black triangles). d, The map of the pACYC177-derived plasmid containing *secM/lacZα* reporter gene controlled by the T7 promoter (black triangle) and alternative SD sequence (orange semi-circle). The sequence of the *secM-lacZα* reporter matches that in the originally described plasmid pNH122⁵⁵.

The pCP23S-EagI plasmid was then digested with EagI (New England Biolabs) for 1 hour at 37 °C, and the CP 23S rRNA gene was isolated from a SYBRSafe-stained 0.7% agarose gel using a E.Z.N.A. Gel Extraction kit (Omega). The 23S rRNA was circularized by T4 DNA ligase (New England Biolabs) in a 50 µl reaction with 2.5 ng/µl DNA for 14 hrs at 16 °C, followed by heat inactivation at 65 °C for 10 minutes. The reaction was diluted 1:100 for use as a template in the PCR reactions for generating the circular permutants (Fig. 2.4a, c).

Ninety-one CP23S mutants were designed by introducing new 23S rRNA 5' and 3' ends at most of the apex loops and some internal loops of rRNA helices to assure spatial proximity of the new rRNA termini in the fully assembled 50S ribosomal subunit. Each CP23S rRNA gene was PCR-amplified in a 40 µl reaction using Phusion High Fidelity DNA polymerase (New England Biolabs) with primer pairs shown in Table 2.1 and 4 µl of the 1:100 diluted 23S circular ligation reaction as template. Each primer pair adds to the 5' and 3' ends of the amplified CP23S gene 20 bp of homology to the 23S rRNA processing stem retained in the target vector pAM552-Δ23S-AflII (described below). PCR reactions catalyzed by the Phusion High Fidelity DNA polymerase (NEB) were run under the following conditions: 98 °C, 10 min followed by 25 cycles (98 °C, 30 sec; 60 °C, 30 sec; 72 °C, 180 sec), followed by the final incubation for 15 min at 72 °C. The reaction product was purified using E.Z.N.A. Cycle Pure kit (Omega) and the size of the amplified DNA was confirmed by electrophoresis in a 1% agarose gel. For CPs with off target bands (12 CPs total), the PCR product of the correct size was extracted from the agarose gel.

To minimize PCR errors in generating the vector backbone, which carried 16S and 5S rRNA sequences, and prevent carry-through of the wt *rrnB* operon, universal backbone vector pAM552-Δ23S-AflII lacking the 23S rRNA gene and containing added AflII restriction site for cloning of CP23S was prepared. The plasmid pAM552-AflII was constructed from pAM552 by adding AflII

restriction sites within the terminal stem of the wt 23S rRNA gene by introducing the G2C and C2901G mutations. First the G2C mutation was introduced by inverse PCR using 5'-phosphorylated primers CTTAAGCGACTAAGCGTACAC and CTCACAACCCGAAGATGTTTC, followed by blunt-end ligation, transformation into *E. coli* POP2136⁵⁴ electrocompetent cells, plating on LB-agar plates supplemented with 50 µg/ml carbenicillin, growth overnight at 30 °C, single colony isolation and sequencing. The C2901G mutation was added by the same method using 5'-phosphorylated primers GCTTACAACGCCGAAGCTG and TTAAGCCTCACGGTTCATTAG. The introduced mutations preserved the integrity of the 23S rRNA terminal stem and did not affect growth of SQ171 cells expressing only ribosomes with the pAM552-AflIII-encoded rRNA (growth rates 53.9 ± 1.0 min for SQ171 cells transformed with pAM552 and 53.3 ± 2.4 min for SQ171 transformed with pAM552-AflIII, as determined from 4 separate colonies each on Biotek Synergy H1 plate readers in 96 well flat bottom plates (Costar) in 100 µl LB supplemented with 50 µg/ml carbenicillin, 37°C, linear shaking with 2 mm amplitude, at 731 cycles per min). To remove the 23S rRNA gene, pAM552-AflIII was digested with AflIII (NEB) for 1 hr at 37 °C, the backbone portion of the vector was gel-purified and ligated with T4 DNA ligase (New England Biolabs) overnight at 16 °C. It was then transformed into POP2136 cells, plated on LB/agar plates supplemented with 50 µg/ml carbenicillin, and grown at 30 °C. Plasmids from several colonies were isolated and fully sequenced. The resulting pAM552-Δ23S-AflIII plasmid contains the 16S rRNA, 23S processing stems with an added AflIII restriction site, 5S rRNA, and β-lactamase resistance gene and ColE1 ori (Fig. 2.4b). Vector backbone was prepared by digesting pAM552-Δ23S-AflIII with AflIII restriction enzyme at 37 °C for 2 hrs and purification using an E.Z.N.A. Cycle Pure kit.

All the CP23S constructs were assembled in parallel by Gibson assembly⁵² reaction (Fig. 2.4c) in a 96-well PCR plate. For each CP23S target, 50 ng of AflIII-digested purified backbone was added to 3-fold molar excess of the PCR-amplified and purified CP23S insert. Gibson assembly mix¹ (15 μ l) was added, the final volumes brought to 48 μ l with nuclease-free water, and incubated at 50 °C for 1 hr in the PCR machine. No CP23S insert was added to the negative control reaction. To check the efficiency of DNA assembly, 2 μ l of selected assembly reactions were transformed into electrocompetent POP2136 cells. Following 1 hour recovery at 37 °C in SOC media, a quarter of each transformation was plated on LB-agar plates supplemented with 50 μ g/ml carbenicillin and grown for 20 hours at 30 °C. A typical CP23S assembly reaction generated 30-120 POP2136 colonies with the control reaction generating only few colonies.

Testing cp23S rRNA constructs

Transformation of SQ171/pCSacB rubidium chloride-competent cells was carried out in a 96-well plate. Two μ l of the Gibson Assembly reactions were added to 20 μ l competent cells in the pre-chilled plate. After 45 min incubation in ice/water bath, 45 sec at 42°C and 2 min on ice, 130 μ l of SOC medium were added to the wells and the plate was incubated 2 hr at 37°C with shaking at 600 rpm on a microplate shaker. Forty μ l of medium were then transferred from each well to the wells of another 96-well plate containing 120 μ l SOC supplemented with 100 μ g/ml ampicillin and 0.25% sucrose. The plate was incubated overnight at 37°C with shaking at 600 rpm. A 96-pin replicator was used to spot aliquots of the cultures onto a rectangular LB agar plate containing 100 μ g/ml ampicillin, 5% sucrose and 1 mg/ml erythromycin. The plate was incubated overnight at 37°C and the appearance of Amp^r/Ery^r transformants was recorded. The completeness of the replacement of the wild type pCSacB plasmid with the plasmids carrying circularly permuted 23S rRNA gene was verified by PCR using a mixture of three primers: primer 1 (GCAGATTAGCACGTCCTTCA) complementary to the 23S rRNA

segment 50-69, primer 2 (CGTTGAGCTAACCGGTTACTA) containing the sequence of the 23S rRNA segment 2863-2882, and primer 3 (GGGTGATGTTTGAGATATTTGCT) corresponding to the sequence of the 16S/23S intergenic spacer 139 – 116 bp upstream from the 23S rRNA gene in *rrnB* (Fig. 2.4d). The combination of the primers 1 and 3 produces a 207 bp PCR band if wild type *rrn* operon is present; the combination of the primers 1 and 2 produces a 112 bp PCR band on the templates with circularly permuted 23S rRNA gene (Fig. 2.4e).

To reduce the number of false-negative cp23S rRNA variants, the experiment was repeated one more time using de novo assembled Gibson reactions with the cp23S rRNA constructs that failed to replace pCSacB in the first experiment. Two additional functional cp23S rRNA constructs were recovered from the second attempt. Altogether, 22 cp23S rRNA variants were able to replace pCSacB in the SQ171 cells. CP23S identity was confirmed by plasmid sequencing. Growth rates were analyzed on Biotek Synergy H1 plate readers in 96 well flat bottom plates (Costar) in 100 μ L LB with 50 μ g/ml carbenicillin. Doubling times and final OD₆₀₀ after 18 hours are shown in Table 2.2.

2.3.3 Results and discussion

Escherichia coli ribosome synthesis and assembly (biogenesis) is a tightly regulated and ordered process with complex folding and assembly steps²⁹. Understanding the complexities of this process is key for ribosome engineering efforts. One aspect of understanding is the order in which the rRNA is transcribed. To study this, 91 circular permutations were built and evaluated on the ability to support cell growth in *E. coli* without genomic copies of wild-type rRNA. Twenty-two engineered constructs were able to replace the SQ171 resident plasmid pCSacB which carries wt *rnm* operon (Fig. 2.6), producing erythromycin-resistant cells with the large ribosomal subunit containing exclusively cp23S rRNA. Most of these mutants had new 23S rRNA ends at the subunit solvent side, including several locations close to the interface rim (Fig. 2.7). This work provides a more thorough understanding of ribosome biogenesis *in vivo*, and informs ongoing ribosomal engineering efforts.

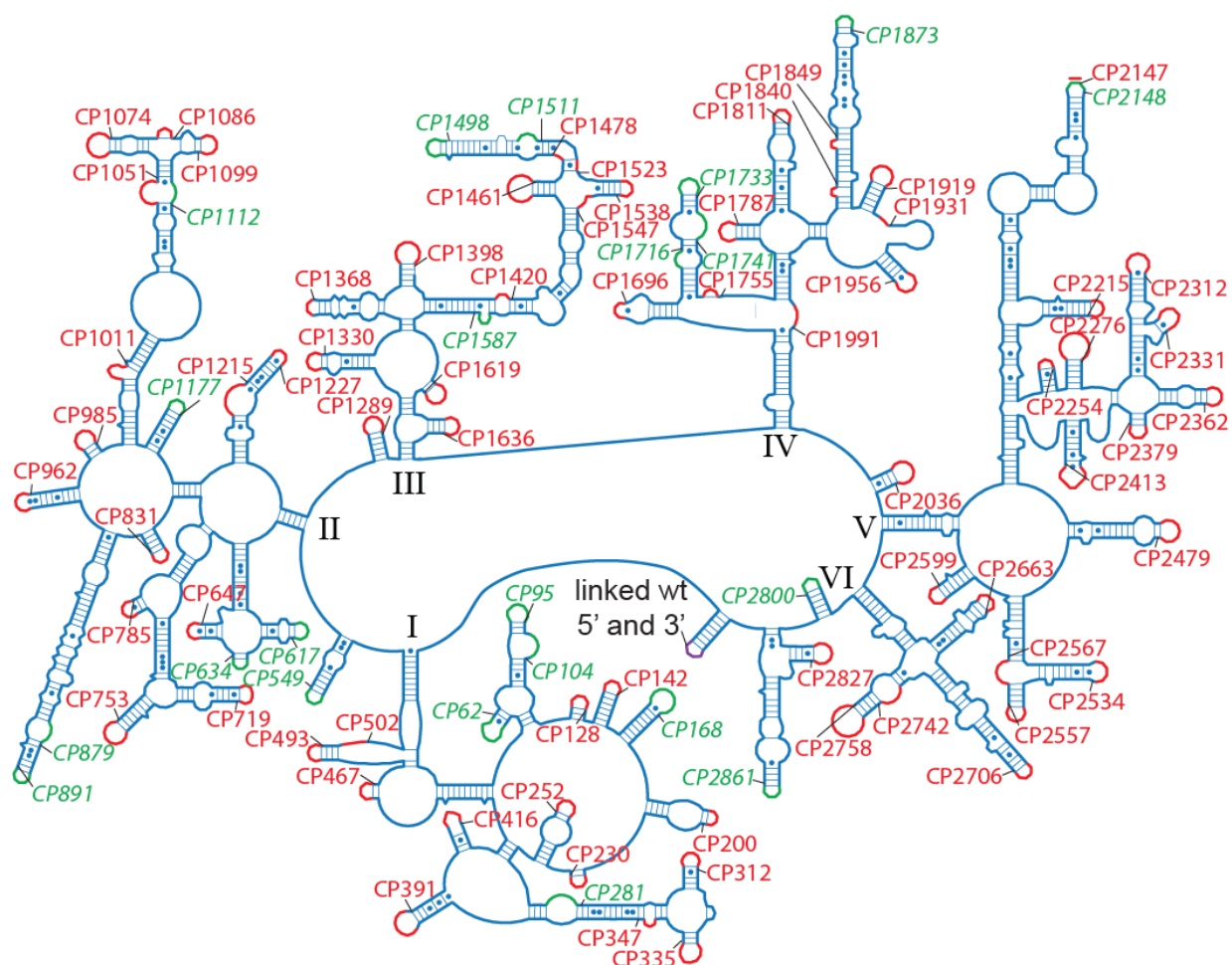


Figure 2.6. Global screening of circularly permuted 23S rRNAs identifies variants capable of replacing the natural 23S rRNA in a functional ribosome. Secondary structure diagram of 23S rRNA⁵⁶ showing the spectrum of the CP constructs tested for their ability to support cell growth in the absence of wild type ribosomes. The new ends of the CP variants of 23S rRNA were introduced in the apex or internal loops of the rRNA hairpins. The corresponding constructs are named per the position of the new 5' end in the structure of the wt mature 23S rRNA (*e.g.*, CP104). The names of the constructs (and the corresponding rRNA hairpin loops) that can support cell growth are shown in green and those that failed to produce sufficiently active ribosomes are shown in red. To assess viability, two independent biological replicates for each CP were carried out. For all viable CP constructs the lack of wt rRNA genes was verified by PCR as shown in the Extended Data Fig. 2 and the identity of CP constructs in the resulting clones was verified by plasmid sequencing.

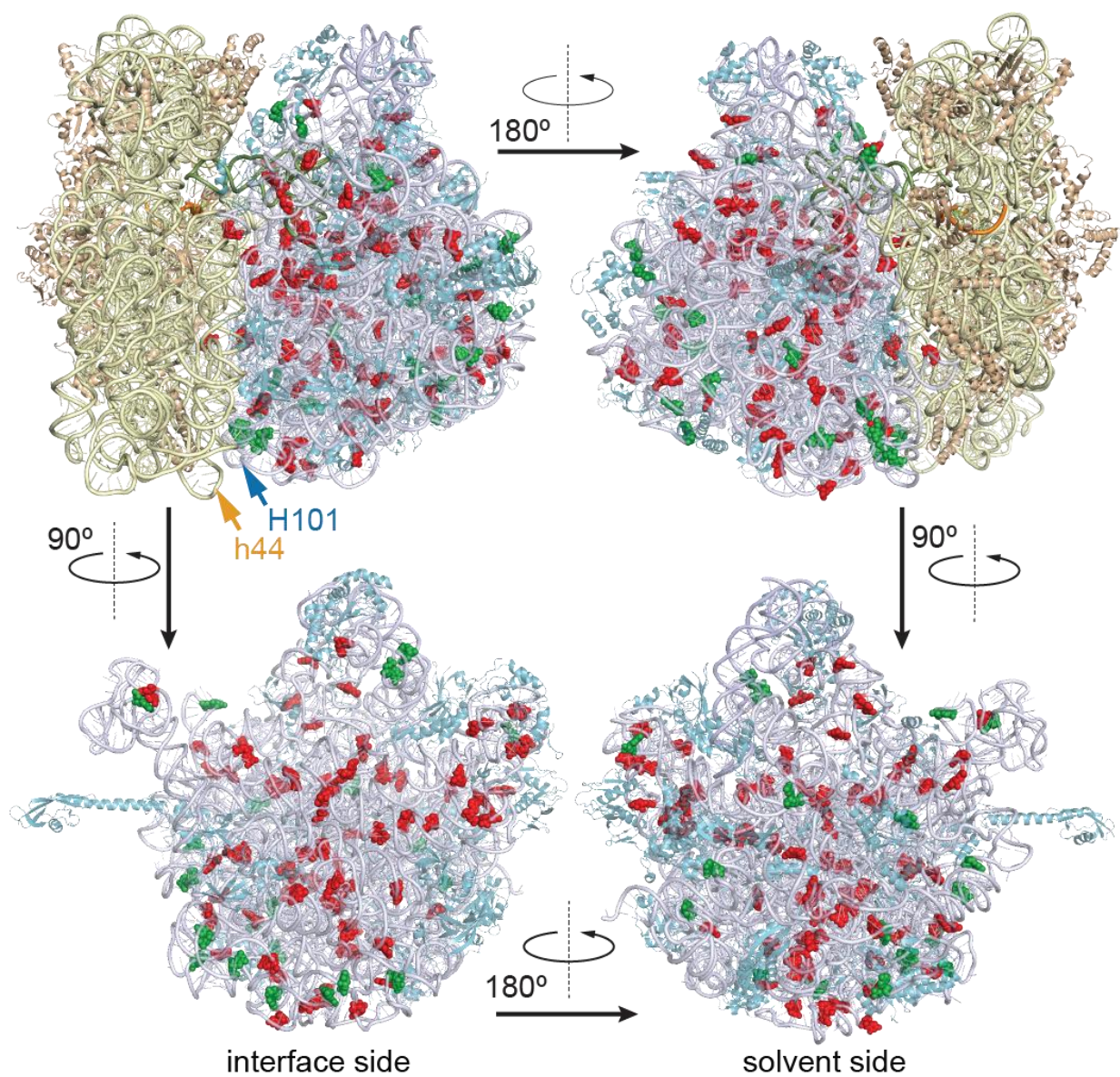


Figure 2.7. Circularly permuted 23S rRNA mutation mapped to ribosome crystal structure. (Top) The location of the new ends of CP variants of the 23S rRNA in the crystallographic structure of the *E. coli* 70S ribosome⁵⁷ (PDB 3R8T and 4GD2). Spheres represent the atoms of the nucleotides corresponding to the new 5' and 3' ends. The ends of the viable CP variants are green and those of the non-viable versions are red. The loops of helices h44 and H101 in the small and large subunit rRNA, respectively, used for subsequent experiments, are indicated by arrows. (Bottom) Same as above, but after removal of the small subunit. Two views represent the interface and solvent sides of the large ribosomal subunit.

2.4 A ribosome with tethered subunits, Ribo-T

We engineered an *E. coli* ribosome with a 50S large subunit physically tethered to a 30S small subunit via the core ribosomal RNA of the two subunits; the two separate 30S and 50S ribosomal RNA core molecules are linked to create a single RNA molecule for the ribosomal cores. This major advancement now links key 50S ribosome function to 30S orthogonality, allowing for unprecedented engineering of the ribosome in living cells. After screening 91 possible tether sites on the large subunit, and now select a tether site connecting the two subunits. We show extensive testing confirming that Ribo-T assembles *in vivo*, and that the tether is very stable and remains intact. Furthermore, Ribo-T is functional, able to synthesize proteins with about 50% the speed of wild-type ribosomes (*in vitro* testing of purified Ribo-T). This may seem like a significant hit in functionality, but recall that Ribo-T has non-trivial rearrangements in structure. As such, remarkably, we have a strain of *E. coli* that operates solely with Ribo-T ribosomes.

2.4.1 Introduction

One of the viable mutants (CP2861, Fig. 2.6 and Fig. 2.7) had the 5' and 3' ends of the cp23S rRNA within the loop of helix 101 (H101), right across from the apex loop of the 16S rRNA helix 44 (h44) (Fig. 2.7 and Fig. 2.8b,c). The length of h44 varies among different species⁵⁸ and the sequence of its terminal loop can tolerate significant sequence alterations⁵⁹. The proximity of h44 and H101 loops seemed to open an attractive opportunity for bridging the subunits by engineering a hybrid 16S/23S rRNA molecule in which the complete cp23S rRNA sequence would be grafted in the loop of 16S rRNA h44 (Fig. 2.8a). In such a construct, the processing sequences flanking the ends of the mature 16S rRNA would remain intact providing for the proper maturation of the 16S rRNA termini, whereas endonuclease processing signals of the large subunit rRNA would be eliminated thereby preventing cleavage of the mature 23S rRNA out from the hybrid molecule.

Approximately 30Å separate the tips of the h44 and H101 loops in the classic (non-rotated) state of the ribosome while in the rotated ribosome in the hybrid state the distance increases to ca. 40 Å^{57, 60-62} (Fig. 2.9). Thus the RNA linkers needed to be sufficiently long to span this distance and to allow for subunit ratcheting during protein synthesis^{63, 64}. Being unable to accurately predict the optimal length of the linkers, we prepared a library of constructs, pRibo-T, in which the length of two tethers, T1 connecting G1453 of the 16S rRNA with C2858 in 23S rRNA and T2 linking 16S G1454 with 23S C2857, varied from 7 to 12 adenine residues, providing tethers sufficiently long to connect the two subunits (Fig. 2.8c).

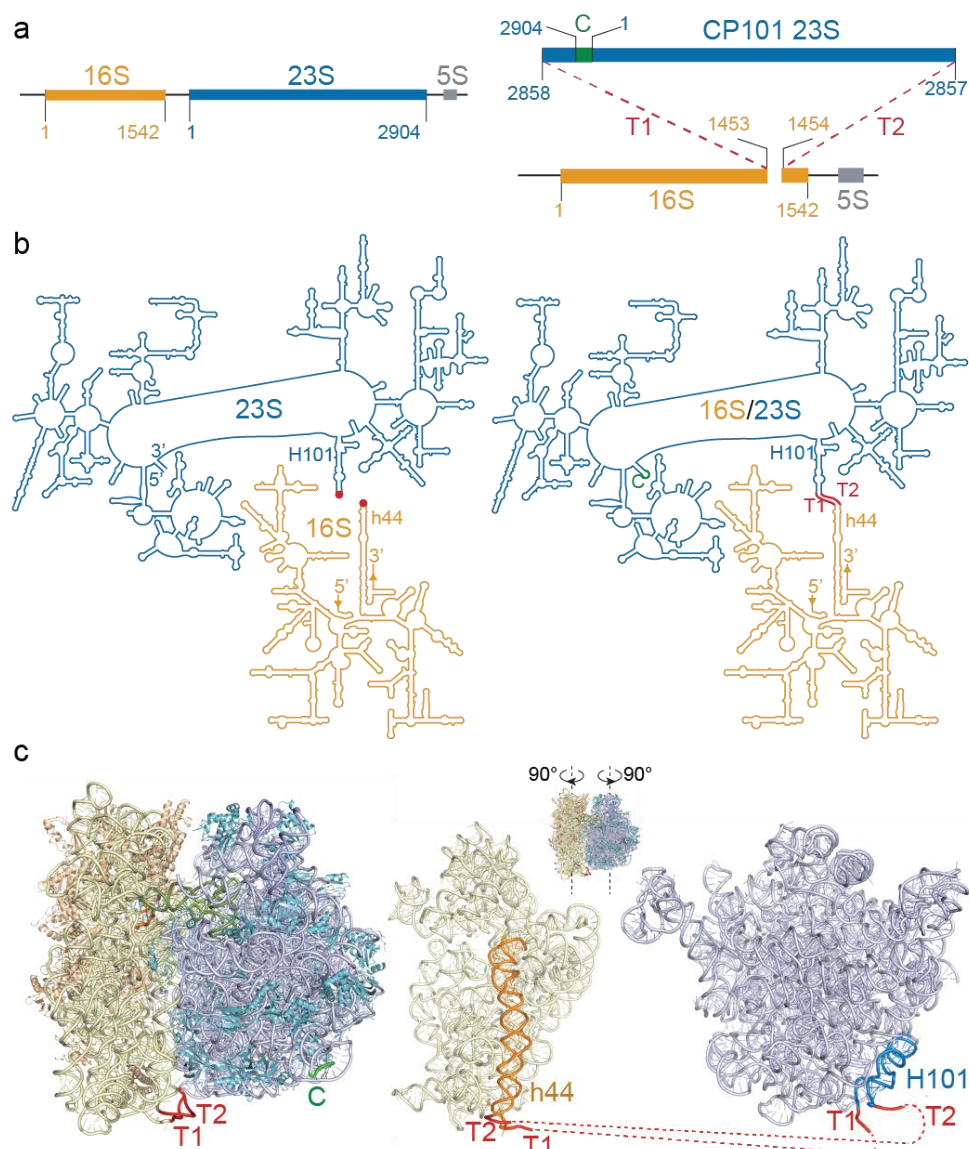


Figure 2.8. Ribo-T design. **a**, Wild type (left) and Ribo-T (right) rRNA genes. In the bacterial wild type rRNA operon (e.g., *E. coli rrnB* operon shown in the figure), small and large subunit rRNAs are excised from the primary transcript and processed to form mature individual 16S, 23S and 5S rRNA. In Ribo-T, the circularly permuted 23S rRNA gene, ‘closed’ at its native ends with a 4 nt long connector **C** and ‘opened’ in the loop of H101, is inserted via short tethers **T1** and **T2** into the apex loop of h44 in the 16S rRNA gene. The resulting hybrid rRNA gene is transcribed as a single chimeric 16S/23S rRNA with its 5’ and 3’ ends likely processed by the enzymes of 16S rRNA maturation. **b**, Secondary structure of the mature wild type (left) and Ribo-T (right) rRNAs. The red dots in wild type 16S and 23S rRNA indicate the apex loops of h44 and H101, which in Ribo-T are connected by tethers **T1** and **T2**. The arrows at the 16S rRNA ends and the tethers in the Ribo-T map indicate the direction of transcription of the chimeric 16S/23S rRNA. **c**, The locations of the **T1** and **T2** tethers in the three-dimensional model of Ribo-T (based on the structure of *E. coli* ribosome in the unrotated state⁵⁷ (PDB 3R8T and 4GD2)). In the small subunit, 16S rRNA and small subunit proteins are colored yellow and orange, respectively; in the large subunit 23S rRNA and 5S rRNA are colored blue and cyan; the P site-bound tRNA is olive; the connector **C** linking native 5’ and 3’ ends of the 23S rRNA is green and the tethers **T1** and **T2** linking 16S and 23S rRNA are red. On the right, the ribosome has been opened as a book exposing the subunit interface sides. Helices h44 (16S) and H101 (23S) are highlighted in orange and blue, respectively. Ribosomal proteins are removed for clarity.

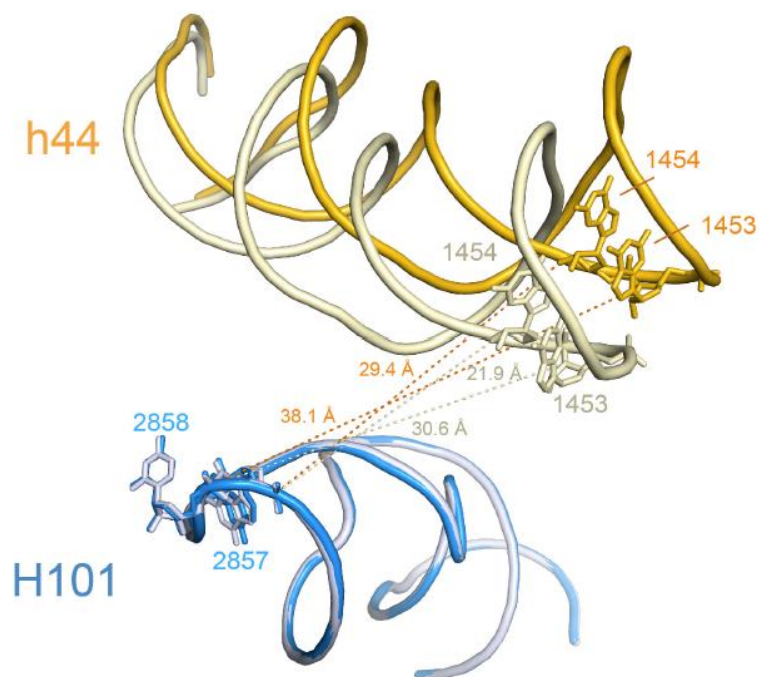


Figure 2.9. The Ribo-T tethers allow for the ribosome ratcheting. Distance changes (Å) between the 16S rRNA and 23S rRNA residues h44 and H101 connected by the oligo(A) linkers in Ribo-T when the ribosome undergoes the transition from the classic to the rotated state. The distances between the 5' phosphorus atoms of the corresponding nucleotides are shown. 16S and 23S rRNAs in the non-rotated state are tan and pale blue, and in the rotated state are gold and blue, respectively. The structures of the *E. coli* ribosomes used for measuring the distances and generating the figure have PDB accession numbers 3R8T and 4GD2 (non-rotated state) and 3R8S and 4GD1 (rotated state).

2.4.2 Methods

Construction of pRibo-T

To avoid generation of mutations in the 23S rRNA gene during PCR amplification for Gibson assembly, the 23S rRNA gene variant circularly permuted at H101 (corresponding to CP2861 from Fig. 2.6) was first cloned in the pUC18 vector. For that, the 23S rRNA gene circularly permuted at H101 was PCR-amplified from circularized 23S rRNA gene prepared in the circular permutation study (Fig. 2.4) using the high-fidelity AccuPrime Taq polymerase (Life Technologies) and primers containing *Bam*HI restriction sites (shown in bold) TATT**GGATCC**GATGCGTTGAGCTAACCGGTA and TTAT**GGATCC**TGCGCTTACACACCCGGCCTAT. The amplified fragment was cut with *Bam*HI and cloned in dephosphorylated *Bam*HI-cut pUC18 plasmid. A plasmid containing CP101 23S rRNA (pUC23S) was fully sequenced to verify the lack of mutations in the 23S rRNA gene.

For preparation of pRibo-T (Fig. 2.5), pAM552-Δ23S-AflII plasmid (Fig. 2.4) served as a recipient for the CP101 23S rRNA gene. The CP101 23S rRNA gene was excised from the pUC23S plasmid by *Bam*HI digestion and gel purified. To graft the CP101 23S rRNA gene into the 16S rRNA gene, the plasmid backbone was prepared by PCR-amplifying the plasmid pAM552-Δ23S-AflII (5 ng in 50 μl reaction) using primers introducing poly-A linkers and sequences corresponding to H101 of 23S rRNA (underlined) and h44 in 16S rRNA (italicized) TTAGTACCGGTTAGCTCAACGCATCG (T)₇₋₁₂ *CGAAGGTTAAGCTACCTACTTCTTTTGC* (reverse primer with tether T1) and TTGATAGCCGGGTGTGTAAGCGCAG (A)₇₋₁₂ *GGAGGGCGCTTACCACTTTGT* (forward primer with tether T2). The PCR reaction, which was catalyzed by Phusion High Fidelity DNA polymerase, was carried out under the following conditions: 98°C for 2 min followed by 30 cycles of (98°C, 30 sec; 62°C, 30 sec; 72°C, 2 min) followed by 72°C for 5 min. The resulting 4.6 kb PCR fragment was treated with *Dpn*I for 4 hr at 37°C and purified using Wizard SV Gel and PCR Clean-Up kit (Promega). The PCR-amplified

plasmid backbone and the gel-purified CP101 23S rRNA gene fragment were combined in a Gibson Assembly reaction. Five μl of the reaction mixture was transformed into 50 μl electrocompetent POP2136 *E. coli* cells. Cells were plated onto LB/agar plate supplemented with 100 $\mu\text{g}/\text{ml}$ ampicillin. After 24 hr incubation at 30°C, the colonies appeared. Seventeen colonies were picked, grown in LB/ampicillin at 30°C, plasmids were isolated and linkers were sequenced using the primers GAACCTTACCTGGTCTTGACATC (corresponding to the 16S rRNA sequence 976-998) and ATATCGACGGCGGTGTTTG (corresponding to the 23S rRNA sequence 2476-2495) to verify the complexity of the linker library (Table 2.3). All the colonies were then washed off the plate and total plasmid was extracted and used to transform SQ171 competent cells.

Functional replacement of the wild-type ribosome by Ribo-T

SQ171 cells carrying pCSacB plasmid, which contains wt *rmb* operon, were transformed with the total pRibo-T preparation isolated from the POP2136 cells. Briefly, 250 ng of plasmid preparation were added to 250 μl of rubidium chloride-competent cells. Cells were incubated 45 min on ice, 45 sec at 42°C and 2 more min on ice followed by addition of 1 ml SOC medium and incubation at 37°C for 2 hours with shaking. A 150 μl aliquot of the culture was transferred to 1.85 ml SOC supplemented with 100 $\mu\text{g}/\text{ml}$ ampicillin and 0.25% sucrose (final concentrations) and grown overnight at 37°C with shaking. Cells were spun down and plated on an LB agar plate containing 100 $\mu\text{g}/\text{ml}$ ampicillin, 5% sucrose and 1 mg/ml erythromycin. Eighty of the colonies that appeared after 48 hrs incubation of the plate at 37°C were inoculated in 2 ml LB supplemented with 100 $\mu\text{g}/\text{ml}$ ampicillin and grown for 48 hrs. The growth rate of ~30 clones that managed to grow during that period was then assessed in LB/ampicillin medium in the 96-well plate. Plasmids were isolated from 6 faster growing clones and linkers were sequenced. The linker T1 in five sequenced clones was composed of 9 adenines and linker

T2 was composed of 8 adenines, while one clone had the reverse combination. Total RNA was extracted from these clones using RNeasy Mini Kit (Qiagen) and analyzed by agarose electrophoresis. The successful replacement of the wild type pCSacB plasmid with the pRibo-T plasmids carrying Ribo-T was verified by PCR using primers GACAGTTCGGTCCCTATCTG (corresponding to the 23S rRNA sequence 2599-2618) and TTAAGCCTCACGGTTCATTAG (complementary to the 23S rRNA sequence 2880-2900) and additionally verified by primer extension on the total cellular rRNA as indicated in Fig. 2.11c. The growth of the cells was monitored at 37 °C in 150 µl of LB supplemented with 100 µg/ml of ampicillin in the wells of a 96-well plate in the TECAN microplate reader (15 min orbital shaking with a 3 mm amplitude followed by 5 min rest prior to reading). The doubling time (τ) values estimated from the logarithmic parts of the growth curves are indicated in Fig. 2.11a.

Polysome analysis

The cultures of cells (250 ml) of the SQ171fg strain transformed with either pAM552 (WT) or pRibo-T8/9 were grown at 37°C with vigorous shaking. When the optical density reached A_{600} 0.4-0.7, chloramphenicol solution was added to obtain final concentration of 125 µg/ml and, after 5 min, cells were pelleted by centrifugation at 4°C. Polysomes were prepared following the published protocol²⁹ by freezing-thawing in the lysis buffer (20 mM Tris-HCl, pH 7.5, 15 mM MgCl₂) supplemented with 1 mg/ml lysozyme 0.25 % sodium deoxycholate and 2 U of RQ1 DNase (Promega). The lysates were centrifuged at 20,000g for 30 min at 4°C and polysomes-containing supernatants ($20 A_{260}$) were loaded onto the 12 ml 10%-50% sucrose gradient (buffer: 20 mM Tris-HCl, pH 7.5, 10 mM MgCl₂, 100 mM NH₄Cl₂, 2 mM β -mercaptoethanol). Polysomes were resolved by centrifugation in a SW-41 rotor (39,000 rpm, 3 hr, 4°C). Gradients were fractionated using BioComp Instrument gradient fractionator and fractions were collected in the wells of a 96-well plate. Appropriate fractions were pooled, ribosomes were ethanol-precipitated and resuspended in 200 µl

of buffer containing 300 mM sodium acetate, pH 5.5, 5 mM EDTA, 0.5% SDS. rRNA was isolated by successive extractions with phenol (pH 6.6), phenol/chloroform and chloroform. After ethanol precipitation, RNA was analyzed by non-denaturing agarose gel electrophoresis.

Analysis of protein synthesis rate and proteins synthesized in Ribo-T cells

Protein synthesis rate in SQ171fg cells expressing either wt ribosomes (plasmid pAM552) or Ribo-T (pRibo-T plasmid) was measured by following incorporation of [³⁵S]-methionine into proteins as described⁶⁵. Specifically, 0.25 μCi of [³⁵S]-methionine (specific activity 1,175 Ci/mmol) (ARC) was added to 1 ml of exponentially growing cells at 37°C and after 45 sec incubation proteins were precipitated by addition of 1 ml of ice-cold 25% trichloroacetic acid (TCA) containing 2% casamino acids. After incubating for 30 min on ice and then 30 min at 100°C, samples were passed through G4 glass fiber filters. The filters were washed three times with 3 ml of ice cold 5% TCA, and once with 3 ml of acetone and air dried, and the amount of retained radioactivity was determined by scintillation counting. Preliminary measurements of the time course of [³⁵S]-methionine incorporation in the faster-growing SQ171fg/pAM552 cells showed that radioactivity curve plateaus after 120 sec of incubation of cells with [³⁵S]-methionine.

Exponential cultures (250 ml) of the SQ171fg strain transformed with either pAM552 (A2058G) or pRibo-T8/9 growing in LB medium supplemented with 100 μg/ml of ampicillin and 50 μg/ml of spectinomycin were harvested by centrifugation and cells were flash-frozen in liquid nitrogen. Protein isolation and two-dimensional gel electrophoresis was performed by Kendrick Labs, Inc. (Madison, WI).

Preparation of Ribo-T and wild type ribosomes and analysis of their RNA and protein content

Ribosomes were prepared from the exponentially growing cells of the SQ171fg strain transformed with either pAM552 (WT) or pRibo-T8/9 as described³⁴. RNA was phenol extracted, precipitated as previously described and resolved by electrophoresis in a denaturing 6% (acrylamide : bis-acrylamide ratio 1 : 19 w/w) polyacrylamide gel (for the 5S rRNA analysis) or 4% (acrylamide : bis-acrylamide ratio 1 : 29 w/w) polyacrylamide gel (for the analysis of large rRNAs).

Ribo-T associated ribosomal proteins were analyzed by mass spectrometry at the Proteomics Center of Excellence, Northwestern University. Ribosomes were precipitated by incubation in 20% trichloroacetic acid at 4 °C overnight and centrifugation at 14,000 g for 10 min. Precipitated ribosomes were washed once with cold 10% trichloroacetic acid and twice with acetone. The pellet was air dried for 10-20 min prior to resuspension in 20 µl 8 M urea. Proteins were reduced with 10 mM dithiothreitol and cysteine residues alkylated with 50 mM iodoacetamide in the final volume of 160 µl. Sequencing grade trypsin (Promega) was added at a 1:50 enzyme:protein ratio and after overnight digestion at room temperature, the reaction was stopped by addition of formic acid to 1%. Following digestion, peptides were desalted using C18 Spin columns (Pierce, cat # 89870) and lyophilized. Amino reactive TMT reagents (126/127, Thermo Scientific, cat# 90065) was used for peptide labeling. The reagents were dissolved in 41 µl acetonitrile and added to the lyophilized peptides dissolved in 100 µl of 100 mM triethylammonium bicarbonate. After 1 hr at room temperature, the reaction was quenched by adding 8 µl of 5% hydroxylamine. Following labeling, the two samples under analysis were mixed in 1:1 ratio. Peptides were desalted using C18 ZipTip Pipette Tips (EMD Millipore) and resuspended in 30 µL of solvent A (95% water, 5% acetonitrile, 0.2% formic acid).

Peptides were analyzed using nanoelectrospray ionization on an Orbitrap Elite mass spectrometer (Thermo Scientific). Proteome Discoverer (Thermo Scientific) and the Sequest algorithm was used for data analysis. Data was searched against a custom database containing UniProt entries using *Escherichia coli* taxonomy, allowing 3 missed cleavages, 10 ppm precursor tolerance, and carbamidomethylation of cysteine as a static modification. Variable modifications included oxidation of methionine, TMT of lysine and N-terminal TMT. For quantification via the reporter ions the intensity of the signal closest to the theoretical m/z , within a ± 10 ppm window, was recorded. Reporter ion intensities were adjusted based on the overlap of isotopic envelopes of all reporter ions as recommended by the manufacturer. Only peptides with high confidence were used for quantification. Ratios of 126/127 were normalized based on median.

Sucrose gradient analysis of ribosomes and ribosomal subunits

Wild type 70S ribosomes or Ribo-T isolated from SQ171fg cells as described above were diluted ca. 70 fold in high Mg^{2+} buffer (20 mM Tris-HCl, pH 7.5, 100 mM NH_4Cl , 2 mM 2-mercaptoethanol, 15 mM $MgCl_2$) or low Mg^{2+} buffer (20 mM Tris-HCl, pH 7.5, 100 mM NH_4Cl , 2 mM 2-mercaptoethanol, 1.5 mM $MgCl_2$). After incubation for 30 min at 4°C, ribosomes and subunits were resolved in 10-40% 12 ml sucrose gradients prepared with the same buffers. Gradients were centrifuged in the SW41 rotor at 38,000 rpm for 3 hr at 4°C. Ribosome profiles were then analyzed using gradient fractionator (BioComp Instrument).

Probing the structure of the Ribo-T tethers

The structure of the tethers was probed by dimethylsulfate (DMS) modification following a published protocol⁶⁶. Briefly, 10 pmol of Ribo-T or WT ribosomes were activated by incubation for 5 min at 42°C in 50 µl of buffer 80 mM HEPES-KOH, pH 7.6, 15 mM MgCl₂, 100 mM NH₄Cl containing 20 U of RiboLock RI RNase inhibitor (Thermo Fisher Scientific). Two µl of DMS (SIGMA) diluted 1:10 in ethanol were added (2 µl of ethanol were added to the unmodified controls) and samples were incubated for 10 min at 37°C. The modification reaction was stopped and rRNA extracted as described⁶⁶. Primer extensions were carried out using the primers GACTGCCAGGGCATCCACCG and AAGGTTAAGCCTCACGG (for tether T1) or CCCTACGGTTACCTTGTTACG for tether T2.

Additionally, the integrity of the tethers in the Ribo-T preparation was tested by extension of the primers annealing immediately 3' to the tether. Primer GTACCGTTAGCTCAACGCATC was extended by reverse transcriptase across tether T1 in the presence of dATP, dTTP, dGTP and ddCTP and primer CACAAAGTGGTAAGCGCCCTCCT was extended across tether T2 in the presence of dATP, dTTP, dCTP and ddGTP.

Testing Ribo-T activity in cell-free translation system

DNA template containing the T7 promoter and the gene of the superfolder green fluorescence protein⁶⁷ was PCR amplified from a pY71-sfGFP plasmid⁶⁸ using primers TAATACGACTCACTATAGGG and CTCCTTTTCGGGCTTTGTT. GFP mRNA was prepared by *in vitro* transcription and purified by size-exclusion chromatography on a Sephadex G50 mini-column, phenol extraction and ethanol precipitation. The transcript was translated in the Δ(ribosome, amino acid, tRNA) PURExpress system kit (New England Biolabs). A typical translation reaction was assembled in a total volume of 10 µl and contained 2 µl of the kit solution A, 1.2 µl of factor mixture, 1 µl amino acid mixture (3 mM each),

1 μ l tRNA (20 μ g/ml), 0.4 μ l Ribolock RNase inhibitor (40U/ μ l), 5 μ g (\sim 20 pmol) GFP transcript and 22 pmol of wild type ribosomes or Ribo-T. Samples were placed in wells of a 384-well black wall/clear flat bottom tissue-culture plate (BD Biosciences) and covered with the lid. Reactions were incubated at 37°C in a microplate reader (Tecan), and fluorescence values were recorded every 20 min at $\lambda_{\text{Exc}}=488$ nm and $\lambda_{\text{Em}}=520$ nm over 7 hrs. Protein synthesis rates were calculated by linear regression over the time points 0, 40 and 60 min with a $R^2>0.9$ using the trendline function of Excel (Microsoft). Time point 20 min was not taken into consideration because the plate was switched from ice to 37 °C at time 0.

Transcription/translation of the DHFR template supplied with the Δ (ribosome, amino acid, tRNA) PURExpress kit (New England Biolabs) was carried in the presence of [35 S] L-methionine (1175 Ci/mmol) using manufacturers protocol. A typical 5 μ l reaction, assembled as described above but using 50 ng of the DNA template, was supplemented with 5 μ Ci [35 S] L-methionine and 10 pmol of wild type or Ribo-T ribosomes. When needed, the reactions were supplemented with 50 μ M erythromycin. Reactions were incubated 2 hours at 37°C and protein products were analyzed by SDS gel electrophoresis in 16.5% Bis-Tris gels (Biorad) using NuPAGE MES/SDS running buffer (Invitrogen). Gels were stained, dried and exposed to a phosphorimager screen overnight. Radioactive bands were visualized by Typhoon phosphorimager (GE Healthcare).

Toe-printing analysis

Toe-printing was performed as previously described^{69, 70}. When needed, the threonyl-tRNA synthetase inhibitor borrelidin or the initiation inhibitor thiostrepton were added to the reactions to the final concentrations of 50 μ M.

2.4.3 Results and discussion

The ribosomes with tethered subunits can support protein synthesis and cell growth

Transformation of SQ171 cells with the prepared Ribo-T tether library of 7-12A at each tether, and plating the transformants onto LB agar plates containing ampicillin, erythromycin (for selection for the engineered plasmid) and sucrose (for counter selection of the wt *rnn* pCSacB plasmid) resulted in appearance of several slowly growing colonies. The pattern of RNA extracted from several clones that were able to grow in liquid culture was strikingly different from the familiar total RNA picture: the conventional prominent bands corresponding to 16S and 23S rRNA were replaced with a single major RNA species with the electrophoretic mobility corresponding to the 16S/23S chimera (Fig. 2.10a). This result indicated that translation in the engineer cells was likely carried out exclusively by Ribo-T and revealed for the first time that the bipartite nature of the ribosome is dispensable for successful protein synthesis.

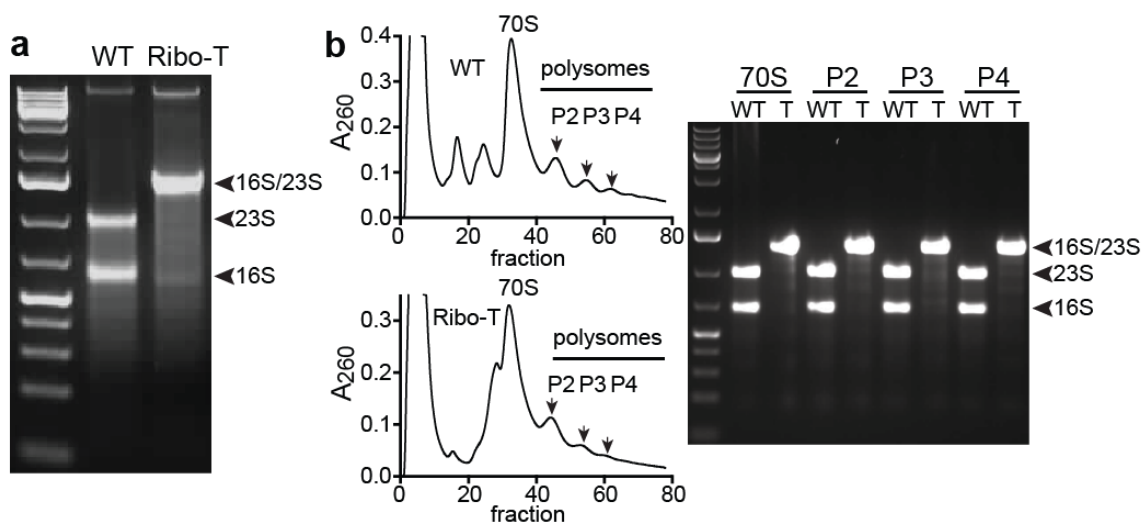


Figure 2.10. Ribo-T supporting cell growth and actively translating **a**, Agarose gel electrophoresis of total RNA prepared from SQ171 cells expressing wt ribosomes ("WT") or Ribo-T. The gel is representative of 5 independent biological replicates. A faint band in the Ribo-T sample migrating slightly faster than 16S rRNA likely represents a small fraction of Ribo-T with a cleaved linker seen in some preparations. **b**, (left) Sucrose gradient fractionation of polysomes prepared from cells expressing wt ribosomes (upper panel) or Ribo-T (lower panel). The position of the peaks corresponding to monosomes (70S), disomes (P2), trisomes (P3) and tetrasomes (P4) are indicated by arrows. (right) The agarose electrophoresis analysis of RNA extracted from the corresponding sucrose gradient peaks is shown.

Only two combinations of linkers, 8A/9A or 9A/8A for T1 and T2, respectively, were found in the 6 best-growing clones. The clone with the pRibo-T plasmid containing the 8A/9A linkers (pRibo-T8/9), which in some subsequent experiments showed slightly better behavior than the pRibo-T9/8 clones, was chosen for further investigation. The original 8A/9A clone, although viable, grew rather slowly (doubling time 107 ± 3 min compared to 35 ± 1 min for SQ171 cells expressing wt ribosomes), exhibited poor recovery from the stationary phase and low cell density at saturation (Fig. 2.11a). To select a 'healthier' variant of the SQ171 cells carrying Ribo-T8/9, we repeatedly passaged the cells in the liquid culture (resulting in approximately 100 generations) after which faster growing colonies appeared on the plates. One of these clones, SQ171fg (for fast growing), showed shorter doubling time (70 ± 2 min) (Fig. 2.11a), more rapid recovery from the stationary phase and a higher density at saturation compared to the original Ribo-T cells (reaching OD_{600} of ca. 5 when grown in a flask, an increase of 1.7-fold compared to the original SQ171 strain). PCR and primer extension analysis confirmed the lack of the wt rDNA and rRNA respectively, reinforcing the notion that every ribosome in this strain was assembled with the engineered hybrid 16S-23S rRNA (Fig. 2.11b,c).

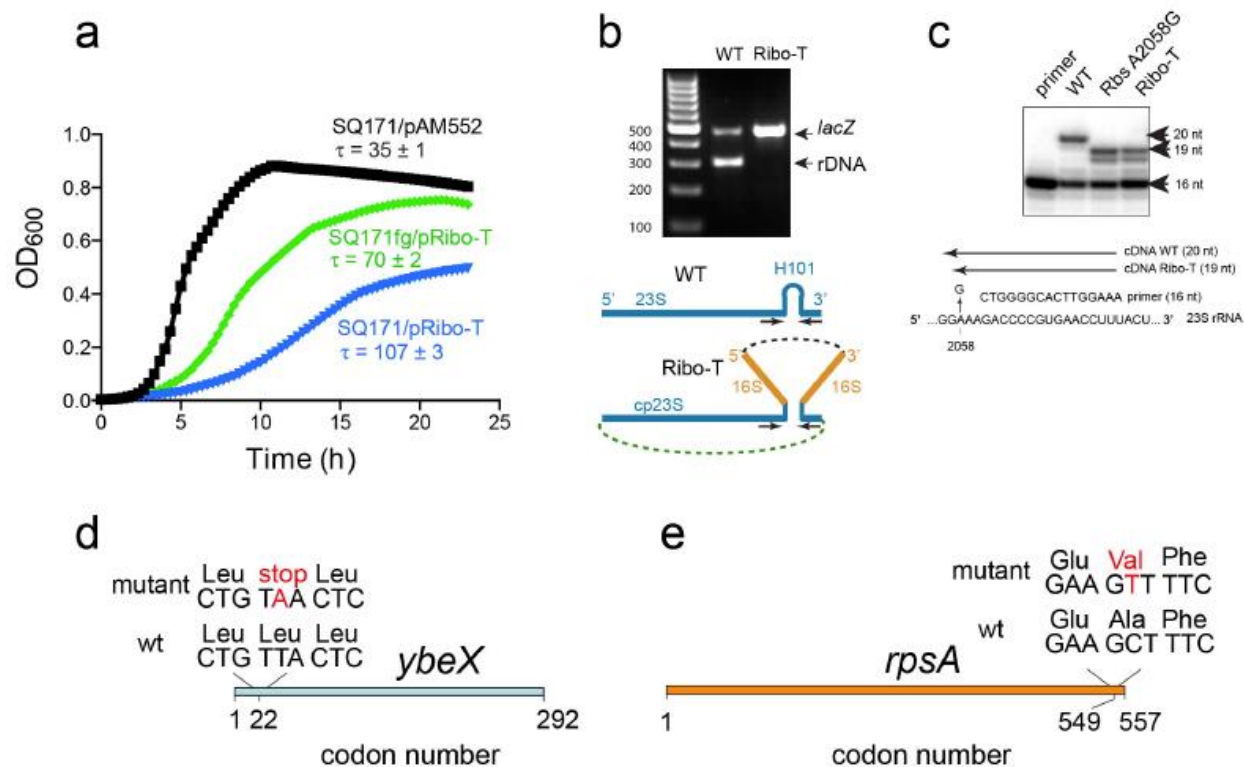


Figure 2.11. Chromosomal mutations enhance growth of SQ171 cells in which Ribo-T completely replace wt ribosomes. a, Growth curves of the parental SQ171 cells transformed with the pAM552(G2058) plasmid (black curve) or pRibo-T8/9 plasmid (blue curve) or selected fast growing mutant (SQ171fg) transformed with pRibo-T8/9 (green curve). The cells express homogeneous populations of ribosomes (wt for pAM552 transformants or Ribo-T for the pRibo-T8/9 transformants, see panels b and c). b, PCR analysis of rDNA in the SQ171fg strain transformed with pRibo-T8/9 (the SQ110 strain that carries a single chromosomal copy of *rnm* allele served as a wt control). The PCR primers amplify the 302 bp 23S rRNA gene segment 'across' the H101 hairpin in wild type rDNA. In pRibo-T, the primer annealing sites are more than 4.8 kb apart (black dashed line), which prevents formation of the PCR product. Two additional primers designed to amplify a 467 bp fragment from the *lacZ* gene were included in the same PCR reaction as an internal control. The gel is representative of 2 independent biological experiments. c, Primer extension analysis of rRNA expressed in the SQ171fg cells transformed with pAM552 (WT), pAM552 with the A2058G mutation, or pRibo-T8/9 which carries the A2058G mutation. Primer extension was carried out in the presence of dTTP and ddCTP. Because Ribo-T contains the A2058G mutation in the 23S rRNA sequence, the generated cDNA is one nucleotide shorter than the one generated on the wild type 23S rRNA template. The lack of the 20 nt cDNA band in the Ribo-T sample demonstrates the absence of wt 23S rRNA in the SQ171fg cells transformed with pRibo-T8/9. The gel is representative of 3 independent biological experiments. d, e, Chromosomal mutations in SQ171fg: d, a nonsense mutation in the Leu codon 22 of the *ybeX* gene encoding protein similar to Mg²⁺/Co²⁺ efflux transporter; e, a missense mutation in the codon 549 of the *rpsA* gene encoding ribosomal protein S1.

Because the pRibo-T8/9 plasmid from the SQ171fg clone was unaltered, we sequenced the entire genome and found mutations in two loci: a nonsense mutation in codon 22 of the *ybeX* gene encoding a protein similar to Mg^{2+}/Co^{2+} efflux transporters (Fig. 2.11d) and a missense (Ala-to-Val) mutation in codon 550 of the *rpsA* gene encoding ribosomal protein S1 (Fig. 2.11e). Since the engineered *ybeX* knock-out mutant of the SQ171 cells did not show improved growth when transformed with the pRibo-T8/9 plasmid (doubling time 137 ± 4 min), we believe that either the mutant S1 protein or its combined effect with the truncated Mg^{2+} transporter account for the fast-growth phenotype of the Ribo-T expressing SQ171fg mutant cells.

To verify that translation of proteins in SQ171fg/pRibo-T cells (hence force referred to as Ribo-T cells) was indeed carried out by the ribosome with the tethered subunits, we further examined the integrity of Ribo-T rRNA. Analysis of Ribo-T preparations in a denaturing polyacrylamide gel showed only very faint bands corresponding to truncated 16S rRNA and 23S rRNA species (marked by asterisks in Fig. 2.12a) resulting likely from the cleavage of Ribo-T at T1 and T2 linkers either in the cell or during Ribo-T isolation. In most of the multiple Ribo-T preparations, these cleavage products accounted for less than 4% of the total Ribo-T rRNA, with none of the preparations exceeding 7% cleavage. Importantly, in some of the preparations, these bands were completely absent (*e.g.*, lane 2 in Fig. 2.12a) showing that more than 99% of Ribo-T remained intact. Furthermore, primer extension across the linkers T1 and T2 did not show any major stops attesting to the general stability of the oligo(A) linkers (Fig. 2.12d).

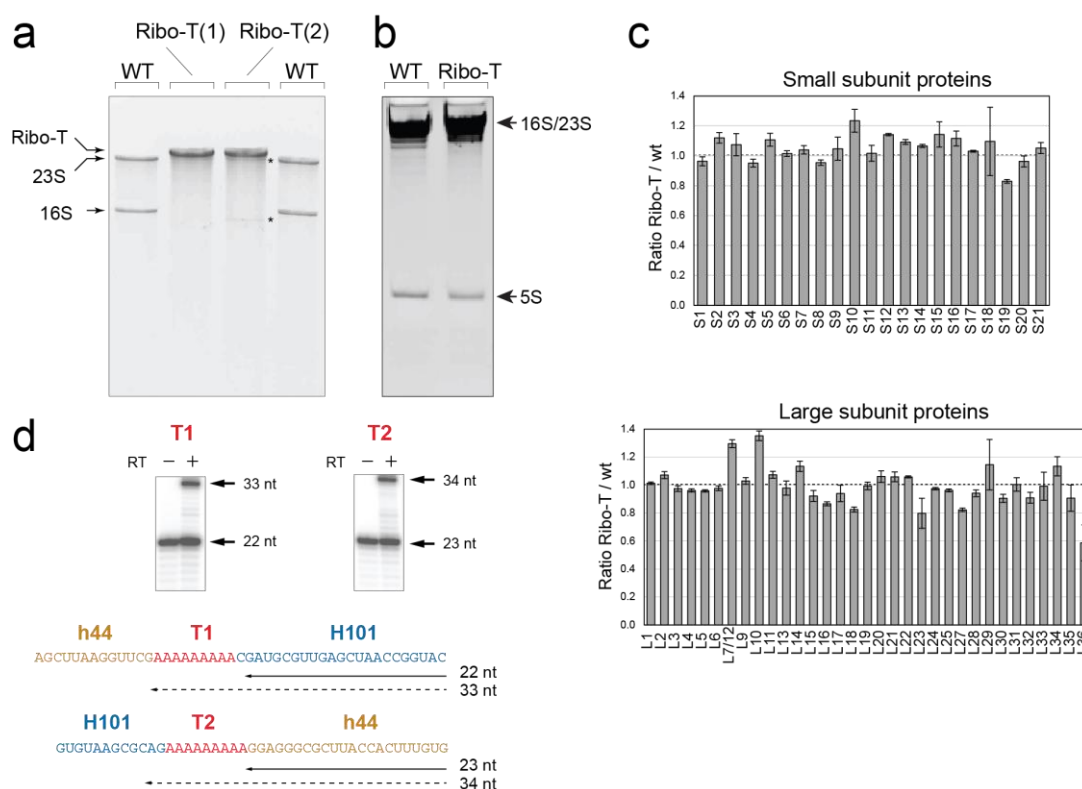


Figure 2.12. Ribo-T composition and integrity of the linkers. a, b, Analysis of rRNA extracted from the isolated wild-type ribosomes or Ribo-T in a denaturing 4% (a) or 8% (b) polyacrylamide gel. a, Ribo-T(1) and Ribo-T(2) represent two individual preparations with Ribo-T(2) isolated following the standard procedure (see Methods), and Ribo-T(1) isolated by immediate pelleting through the sucrose cushion after the cell lysis. The faint bands in the Ribo-T2 preparation indicated by the asterisks could be occasionally seen in some preparations; they probably represent rRNA fragments generated by cleavage of the linkers in a small fraction of Ribo-T either in the cell or during Ribo-T preparation. b, 5S rRNA is present in Ribo-T. c, The relative abundance of small and large subunit proteins in Ribo-T in comparison with wild-type ribosome as determined by mass spectrometry (protein L26 could not be reliably quantified in Ribo-T and wild-type ribosomes). The data represent the average of three technical replicates, and error bars indicate the s.d. d, Analysis of the integrity of the T1 and T2 linkers in a Ribo-T preparation by primer extension. The 22-nucleotide-long primer was extended across the T1 linker in the presence of ddCTP terminator and the 23S-nucleotide-long primer was extended across the T2 linker in the presence of ddGTP terminator. Control samples (2) represent the unextended primers. The gels are representative of two independent experiments.

Protein synthesis rate in the Ribo-T cells reached 50.5 ± 3.5 % of that in cells with the wild type ribosome (Fig. 2.13a) and thus cannot be accounted for by a small fraction of Ribo-T with the cleaved linkers. However, to establish beyond any doubt that translation of proteins in the engineered cells is indeed carried out by intact Ribo-T (as opposed to Ribo-T with cleaved tethers) we tested whether Ribo-T or cleaved Ribo-T species were preferentially present in polysomes. Gel electrophoretic analysis of rRNA found in polysomes prepared from Ribo-T cells unambiguously showed the predominant presence of the ca. 4,500 nucleotide-long 16S-23S hybrid rRNA and the relative lack of any cleaved rRNA (Fig. 2.10b), providing a clear evidence that intact Ribo-T composed of covalently-linked subunits is capable of carrying protein synthesis *in vivo*. 2D-gel analysis showed that the absolute majority of the proteins present in SQ171 cells that express only wt ribosomes are also efficiently synthesized in the Ribo-T cells (Fig. 2.13b,c) revealing that physical separation of the ribosomal subunits is not required for efficient translation of the majority of cellular polypeptides.

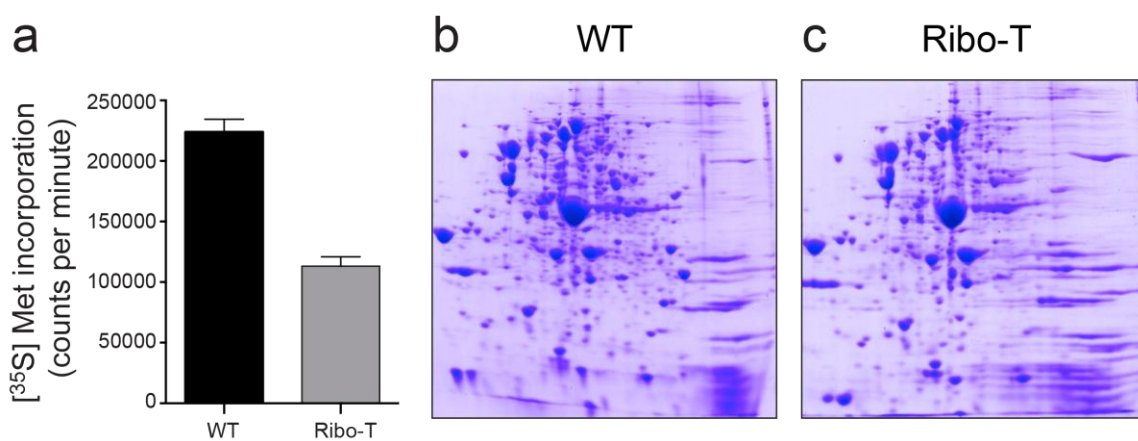


Figure 2.13. Ribo-T can successfully translate most cellular polypeptides. a, Protein synthesis rate in SQ171fg cells expressing wild-type ribosomes or Ribo-T. Protein synthesis was measured by quantifying the incorporation of [³⁵S] L-methionine into TCA-insoluble protein fraction during a 45-s incubation at 37 °C in minimal medium. The bar graphs represent the average values of experiments performed in two biological replicates each done in two technical duplicates. Error bars denote s.d. b, c, 2D gel electrophoresis analysis of the proteins expressed in exponentially growing SQ171 transformed with pAM552 (A2058G) (b) or pRibo-T (c).

Composition and properties of Ribo-T

We isolated ribosomes with tethered subunits from Ribo-T cells and characterized their composition and properties. Although Ribo-T assembly pathway must be principally different from that of the normal ribosome, the tethered ribosome contains an apparently equimolar amount of 5S rRNA and the full complement of ribosomal proteins present in quantities closely matching the composition of the wt ribosome (Fig. 2.12b,c). Chemical probing of the structure of h44 and H101 in wt ribosome and in Ribo-T showed that the 16S and 23S rRNA hairpins remain largely unperturbed, while the T1 and T2 linkers are highly accessible for modification by dimethylsulfate indicating that they are exposed to the solvent (Fig. 2.14).

Sucrose gradient analysis of Ribo-T showed that at 15 mM Mg^{2+} the majority of the ribosomal material sedimented as a 70S peak with a minor faster-sedimenting peak likely representing Ribo-T dimers, possibly arising due to cross-ribosome subunit association in a small fraction of Ribo-T (Fig. 2.15a). At a lower Mg^{2+} concentration (1.5 mM), when the native ribosome completely dissociates into 30S and 50S subunits, Ribo-T continues to sediment as a single peak with an apparent sedimentation velocity corresponding to 65S (Fig. 2.15a). The distinctive (and expected) resistance of Ribo-T to subunit dissociation suggests a possible venue for isolating pure Ribo-T even from the cells containing mixed population of wild type and Ribo-T ribosomes.

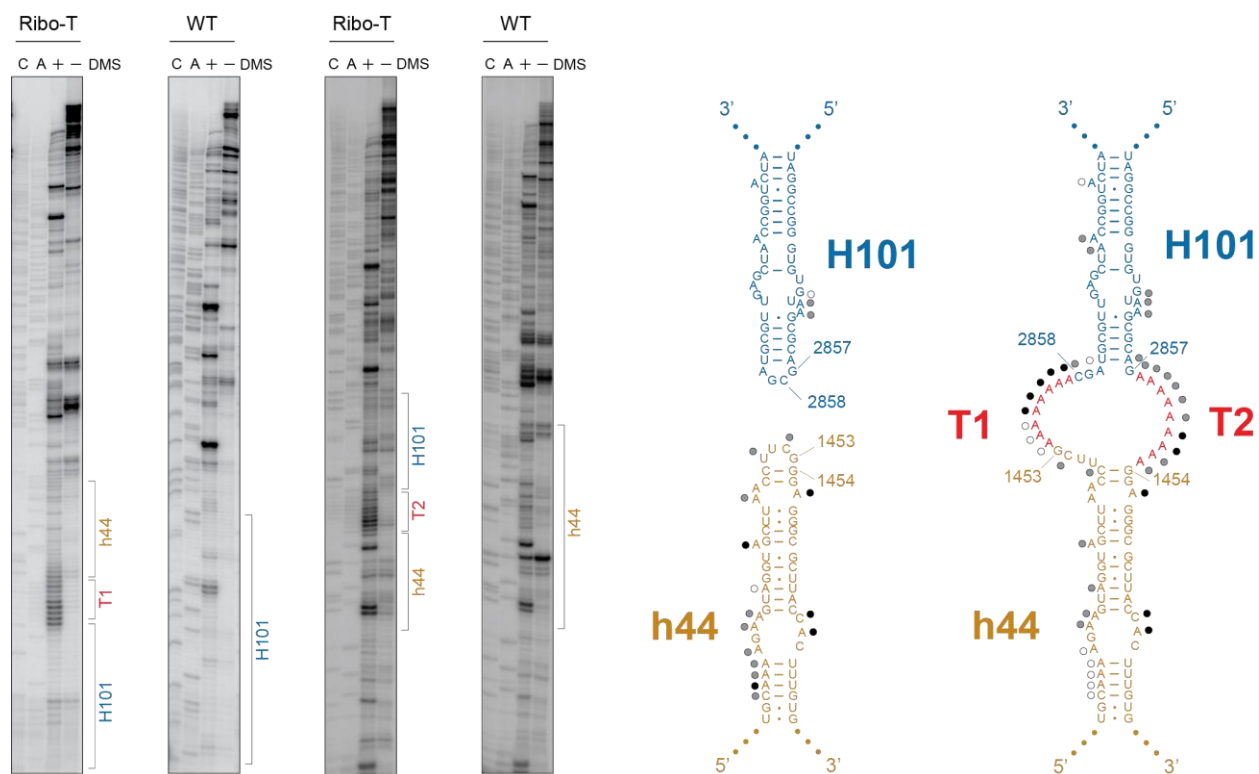


Figure 2.14. Chemical probing of the structure of the Ribo-T linkers. Ribo-T or wt ribosomes were modified by dimethylsulfate and extracted rRNA was subjected to primer extension analysis. In each gel, the left two lanes ('C' and 'A') represent sequencing reactions followed by dimethylsulfate-modified sample and control (unmodified) RNA. The diagrams on the right represent the secondary structures of helices H101 and h44 in wild type ribosomes (left) and Ribo-T (right) with the nucleotide residues modified strongly, moderately and weakly indicated by black, gray and white circles, respectively. The shown gels are representative of two independent experiments.

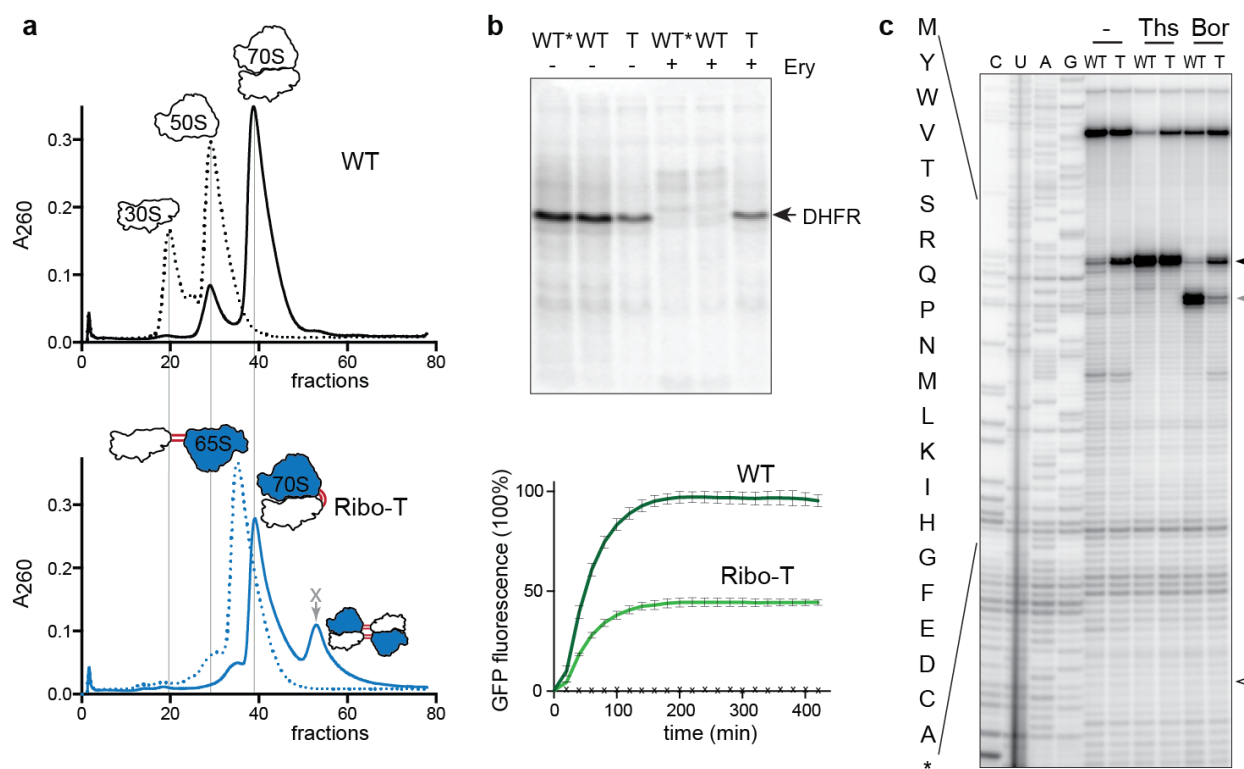


Figure 2.15. Functional characterization of Ribo-T. a, Sucrose gradient analysis of wild-type ribosomes (top) and Ribo-T (bottom) under 15mM MgCl₂ (solid line) or 1.5mM MgCl₂ subunit dissociating conditions (dotted line). The peak marked with grey arrow and 'X' may represent Ribo-T dimers. The result was qualitatively verified in an independent experiment performed at Mg²⁺ concentrations 1.5mM and 10mM. b, In vitro translation of proteins by isolated Ribo-T. Top, SDS-PAGE analysis of the dihydrofolate reductase (DHFR) protein synthesized in the Dribosome PURExpress system supplemented with purified wild-type ribosomes or Ribo-T (T); wild-type ribosomes provided with the kit (WT*) were used as a control. The transcription-translation reaction was carried out in the presence of [³⁵S]L-methionine in the absence or presence of 50 mM erythromycin (ERY). The A2058G mutation in Ribo-T renders the Ribo-T-driven translation resistant to the antibiotic. The 'no erythromycin' samples are a representative result of two independent biological experiments. Bottom, time course of sfGFP protein expression in the Δ ribosome PURExpress system supplemented with purified wild-type (black) or Ribo-T (grey) ribosomes. The kobs rates (385 ± 13 relative fluorescent units (RFU) min⁻¹ (mean \pm s.d.) for wild-type, 177 ± 6 RFU min⁻¹ for RiboT) were determined from the initial slopes. The activity of both ribosomes was fully inhibited by 50 mg ml⁻¹ chloramphenicol (time points indicated by x). Each curve is an average of two independent biological replicates, with error bars indicating the s.d. c, Toeprinting analysis of translation of a 20-codon synthetic gene RST1⁷⁰ by wild-type ribosomes or Ribo-T. The antibiotic thiostrepton (THS), present at 50 mM, arrests the initiating ribosome at the start codon⁷¹ (black arrowhead). The threonyl-tRNA synthetase inhibitor borrelidin (BOR) arrests translation at the fourth codon of RST1 mRNA (grey arrowhead)⁷⁰. The position of a toeprint band that would correspond to the ribosome that has reached the RST1 stop codon is shown by an open arrowhead. A more pronounced toeprint band at the start codon in the samples lacking thiostrepton indicates that Ribo-T departs from the initiation codon slower than wild-type ribosomes. A weaker borrelidin-specific band observed in the Ribo-T sample suggests that under our experimental conditions, fewer Ribo-T compared to wild-type ribosomes were able to reach the fifth codon, apparently owing to slower initiation.

Ribo-T functions in cell-free protein synthesis

We further tested activity of isolated Ribo-T in PURExpress cell-free translation system³³ lacking native ribosomes. Ribo-T efficiently synthesized the 18 kDa dihydrofolate reductase (DHFR) (Fig. 2.15b). By following the kinetics of accumulation of functional 27 kDa super folder green fluorescent protein (sf-GFP)⁶⁷, we calculated that the rate of Ribo-T-catalyzed protein synthesis reaches ca. 45% of that of the wt ribosomes (Fig. 2.15b). To assess which translation step is the most problematic for Ribo-T, progression of Ribo-T through a short synthetic gene was analyzed by toe-printing⁷⁰ (Fig. 2.15c). Here a more pronounced band of the ribosomes at the ORF start codon indicated that Ribo-T may be somewhat impaired in translation initiation at a step subsequent to the start codon recognition. Similarly slow initiation was observed during *in vitro* translation of several other genes (data not shown). Because increasing the concentration of initiation factors could not rescue the translation initiation defect (data not shown), it is unlikely to stem from a lower affinity of the factors for Ribo-T, but the true nature of this effect will require further investigation.

2.5 An expanded mutation space *in vivo*

2.5.1 Introduction

To test the utility of Ribo-T as a fully orthogonal translation machine, we next engineered a specialized version of Ribo-T (oRibo-T) committed to translation of a particular orthogonal cellular mRNA. By modifying the Shine-Dalgarno sequence of an mRNA and the corresponding complementary sequence in 16S ribosomal (r)RNA, specialized small subunits have been created in bacteria capable of translating only a specific type of engineered mRNAs but excluded from translating “normal” cellular mRNAs³⁵⁻³⁹. Until our work, this technique was limited to the small subunit because large subunits freely exchange between pools of native and orthogonal 30S subunits. Accordingly, key ribosomal functions residing on the large subunit (*e.g.*, peptide bond formation and protein excretion) are not orthogonal. With the Ribo-T system working to support cell growth, our next objective was to create the orthogonal Ribo-T system to enable *in vivo* ribosome engineering efforts.

2.5.2 Methods

Construction of the plasmids for testing oRibo-T activity in vivo

The backbone plasmid pT7wtK (Fig. 2.5c) was first prepared from the commercial plasmid T7-FLAGTM-4 (Sigma Aldrich) by introducing the following changes. First, the *bla* gene was deleted using inverse PCR with phosphorylated primers TAACTGTCAGACCAAGTTTACTC and ACTCTTCCTTTTTCAATATTATTGAAG and Phusion High Fidelity DNA polymerase. Following purification with E.Z.N.A. Cycle Pure kit, DNA was blunt-end ligated for 14 hours at 16 °C using T4 DNA ligase, and transformed into electrocompetent DH5 α *E. coli* cells and plated on LB-agar supplemented with 30 μ g/ml kanamycin. Next, a *Bgl*II-*Not*I cloning site was introduced using phosphorylated primers

AGATCTGTTGCTACGCAGCGTT**GCGGCCGC**TGAAGATCGATCTCGACC

and

GCCTCCTATGAAAAATAACAGATATAGTCTCCCTATAGTGAGTCGTATTAGG, with *Bgl*II and *Not*I sites in bold. A sequence 3' of the T7 promoter, termed N15 (underlined), optimized for T7 expression of an orthogonal gene³⁶ was introduced on one of the primers. Purified PCR product was blunt-end ligated with T4 DNA ligase for 14 hours at 16 °C, transformed into DH5 α electrocompetent cells and plated on LB-agar supplemented with 30 μ g/ml kanamycin. The resulting plasmid pT7wtK contains a T7 promoter, wild-type SD sequence, a *Bgl*II-*Not*I cloning site, T1/T2 terminator, pMB1 origin of replication, a *lac*I gene and a kanamycin resistance gene.

To create plasmid pT7wtGFP, primers GGTGGT**AGATCT**ATGAGCAAAGGTGAAGAAC and GGTGGT**CGGCCCGC**GGGCTTTGTTAGCAG were used to PCR amplify the *sf-gfp* gene from pY71-sfGFP⁶⁸, adding *Bgl*II and *Not*I restriction sites (bold) at the ends of the *sf-gfp* PCR product. Purified PCR product and plasmid pT7wtK were digested with *Bgl*II and *Not*I (New England Biolabs) for 1 hour at 37 °C. The pT7wtK digested vector was treated with alkaline phosphatase CIP (New England Biolabs) for 1 hour at 37 °C. Both reactions were purified with E.Z.N.A. Cycle Pure kit. The *sf-gfp* insert was added in 3-fold molar excess to 50 ng pT7wtK backbone, and ligated with T4 DNA ligase (NEB) for 14 hrs at 16 °C, transformed into DH5 α electrocompetent cells and plated on LB-agar supplemented with 30 μ g/ml kanamycin.

To create pT7oGFP (Fig. 2.5c) containing *sf-gfp* whose translation is controlled by an orthogonal SD sequence, the wild-type SD sequence of pT7wtGFP (AGGAGG) was mutated to an orthogonal sequence CACCAC³⁵ by inverse PCR using phosphorylated primers ATGAGCAAAGGTGAAGAAC and AGATCTGTGGTGTGAAAAATAACAGATATAGTCTC. PCR product purified with E.Z.N.A. Cycle Pure kit was blunt-end ligated with T4 DNA ligase for 14 hours at 16 °C, transformed into electrocompetent DH5 α cells and plated on LB-agar supplemented with 30 μ g/ml kanamycin.

Finally, the T7 promoter was replaced with the *lpp5* promoter⁷². To achieve that, inverse PCR was performed using pT7oGFP as template and phosphorylated primers TATACTTGT**GGAATTGTGAGCGGATAACAATT**CTATATCTGTTATTTTTTCA and ACACAAAGTTTTTTATGTTGTCAATTTTTTTTGATAGTGAGTCGTATTAGGATC, (the *lpp* promoter is underlined). The *lacO* site (bold) was included in order to provide for inducible expression in POP2136 strain controlled with isopropyl β -D-1-thiogalactopyranoside (IPTG). DNA was purified, blunt-end ligated, transformed into DH5 α cells and plated on LB-agar supplemented with 30 μ g/ml kanamycin. The resulting plasmid pLpp5oGFP (Fig. 2.5c) contains a *lpp5* promoter, *lacO* site, orthogonal SD sequence, *sf-gfp* gene, T1/T2 terminator, pMB1 origin of replication, a *lacI* gene and a kanamycin resistance gene.

The anti-Shine-Dalgarno sequence of pRibo-T 16S rRNA was mutated from wild-type (5'-TCACCTCCTTA-3') to an orthogonal sequence (5'-TCAT**TTGTGG**TA-3')³⁵ by inverse PCR using phosphorylated primers CCTTAAAGAAGCGTACTTTGTAG and TACCACAATGATCCAACCGCAGG, pRibo-T as template and Phusion High Fidelity DNA polymerase. PCR was run at the following conditions: 98 °C, 3 min followed by 25 cycles (98 °C, 30 sec; 55 °C, 30 sec; 72 °C, 120 sec), followed by final extension 72 °C, 10 min. Correct size band was purified by agarose gel electrophoresis and extracted using the E.Z.N.A. Gel Extraction kit. It was circularized by blunt-end ligation and transformed into POP2136 electrocompetent cells. Cells were plated on LB/agar plates supplemented with 50 μ g/ml carbenicillin and grown at 30 °C overnight. Colonies were isolated and poRibo-T was fully sequenced.

Testing activity of oRibo-T in vivo

Electrocompetent POP2136 cells were transformed with the following plasmid combinations: i) pAM552 and pT7wtK (no *gfp* control), ii) pAM552 and pLpp5oGFP, iii) pAM552o and pLpp5oGFP and iv) poRibo-T1 and pLpp5oGFP. Transformants were plated on LB plates supplemented with 50 µg/ml carbenicillin and 30 µg/ml kanamycin and incubated for 24 hours at 30 °C. Wells of a 96-well plate with low evaporation lid (Costar) was filled with 100 µl of LB media supplemented with 50 µg/ml carbenicillin and 30 µg/ml kanamycin. The wells were inoculated with colonies from each plasmid combination above (six colonies each), and incubated at 30 °C for 14 hours with shaking. Clear bottom chimney wells of another 96-well plate (Costar) were filled with 100 µL of LB media supplemented with 50 µg/ml carbenicillin, 30 µg/ml kanamycin, and 1 mM IPTG. The plate was inoculated with 2 µl of saturated initial inoculation plate, and incubated with linear shaking (731 cycles per min) for 16 hrs at 42 °C on a Biotek Synergy H1 plate reader, with continuous monitoring of cell density (A_{600}) and *sf-gfp* fluorescence (excitation 485 and emission 528 with sensitivity setting at 80).

Testing oRibo-T activity in cell-free translation system

Ribosomes (wt) or oRibo-T (mixed with wt ribosomes) were prepared from SQ171fg cells transformed with pAM552 or poRibo-T1, respectively. An orthogonal *sf-gfp* gene was PCR amplified from the plasmid pT7oGFP using primers TAATACGACTCACTATAGGG and ACTCGTCGAGATCGATCT. The transcription-translation reaction was carried out in Δ (ribosome, amino acid, tRNA) PURExpress system as described above. The 7.5 µl reactions were supplemented with 18.75 ng DNA template and 7.5 pmol ribosomes and when needed, clindamycin or pactamycin were added to the reactions to the final concentrations of 50 µM or 100 µM respectively.

For *in vitro* translation of an orthogonal *secM-lacZ α* template it was PCR amplified from the poSML plasmid using a direct primer TAATACGACTCACTATAGGG corresponding to the T7 promoter and a reverse primer TTCCAGTCACGACGTT, which allowed preserving 18 codons after the SecM arrest site. mRNA was prepared by *in vitro* transcription and purified. It was then translated in the Δ (ribosome, amino acid, tRNA) PURExpress system assembled in a total volume of 5 μ l and containing 1 μ l of the kit solution A, 0.6 μ l of factor mixture, 0.5 μ l amino acid mixture (3 mM each) lacking methionine, 0.2 μ l of [³⁵S] L-methionine 8.5 μ M (1175 Ci/mmol), 0.5 μ l tRNA (20 μ g/ml), 0.2 μ l Ribolock RNase inhibitor (40U/ μ l), 100 μ M pactamycin, 10 pmol transcript and 10 pmol of total ribosomes. Translation was carried out for 5 min at 37°C, followed by addition of 1 μ g of RNase A and incubation for 5 min at 37°C. Translation products were analyzed in 16.5% Tricine SDS polyacrylamide gel⁷³. The gel was stained, dried, and exposed to a phosphorimager screen overnight.

Construction of C41(DE3)/ Δ lacZ58(M15)

The Δ lacZ58(M15) allele required for alpha complementation was transduced from the *E. coli* strain K1342 (*E. coli* Genetic Stock Center, Yale) into *E. coli* C41(DE3) strain by P1 phage transduction protocol⁷⁴. Transductants were selected on LB agar supplemented with 10 μ g/ml tetracycline. Then colonies were re-streaked on LB-agar plates containing 10 μ g/ml tetracycline, 200 μ M IPTG and 80 μ g/ml X-Gal. The replacement of wt *lacZ* with the Δ lacZ58(M15) allele was verified by PCR using primers ACCATGATTACGGATTCCTGG and CCGTTGCACCACAGATGAA (the sizes of the expected PCR products are 467 bp for wt and 374 bp for the mutant).

Construction of the orthogonal secM-lacZ α reporter poSML

The backbone of the pACYC177 vector was PCR-amplified using primers ATCTCATGACCAAAATCCCTTAACGTGAGT and GCGGTTAGCTTTTACCCCTGCATCTTTGAG. A 568 bp DNA fragment whose ends overlapped with the amplified pACYC177 backbone and which contained T7 promoter, the orthogonal SD sequence CACCAC³⁵, the *secM*(121-166)-*lacZ α* fusion from the plasmid pNH122⁵⁵, was synthesized by Integrated DNA Technologies. The pACYC177 backbone and the *secM/lacZ α* construct were combined using Gibson Assembly and introduced in the C41(DE3)/ Δ lacZ58(M15) cells.

Construction of the 2451/2452 mutant poRibo-T library and selecting mutants capable of alleviating SecM-mediated translation arrest

A library of A2451N/C2452N mutants was generated by inverse PCR using plasmid poRibo-T2 as a template, Phusion High Fidelity DNA polymerase, and primers AGGCTGATACCGCCAAG and CTCTTGGGCGGTATCAGCCT~~NN~~TATCCCCGGAGTACCTTTTATC, with added sequence (underlined) used for re-circularization with Gibson assembly. PCR reaction was carried out under the following conditions: 98 °C, 3 min followed by 25 cycles (98 °C, 30 sec; 55 °C, 30 sec; 72 °C, 120 sec), followed by final extension 72 °C, 10 min. The PCR-amplified DNA band was purified by extraction from the agarose gel with an E.Z.N.A. Gel Extraction kit, and re-circularized by Gibson assembly for 1 hour at 50 °C. Two μ l of the reaction were transformed into electrocompetent POP2136 cells plated on LB plates supplemented with 50 μ g/ml carbenicillin and grown for 24 hrs at 30 °C. Individual colonies were picked and sequenced to identify all possible 16 variants of the library.

The C41(DE3)/ Δ lacZ58(M15) cells were transformed with the poSML reporter plasmid Fig. 2.5d) and plated on LB-agar containing 50 μ g/ml kanamycin. One of the colonies, which appeared after overnight incubation at 37°C, was inoculated into liquid culture, grown in the presence of 50 μ g/ml kanamycin and cells were rendered chemically competent. Cells were transformed with the pooled library of sixteen 2451/2452 mutants. Transformed cells were plated on LB agar containing 50 μ g/ml kanamycin, 100 μ g/ml ampicillin, IPTG 0.5 mM, X-Gal 40 μ g/ml and 2 mM lacZ inhibitor phenylethyl- β -d-thiogalactopyranoside (PETG). Plates were incubated at 37°C for 24 hours and photographed. 16 white colonies or 15 blue colonies were inoculated in 5 ml of LB medium supplemented with 100 μ g/ml ampicillin and grown overnight. The plasmids were isolated and the identities of nucleotide residues at the position 2451 and 2452 of the 23S rRNA were analyzed by sequencing. Alternatively, the poSML-transformed C41(DE3)/ Δ lacZ58(M15) cells were transformed with individual plasmids representing all possible 16 variants of the nucleotide combinations at positions 2451 and 2452. The poRibo-T2 plasmid carrying A2058G mutation was used as a control. In addition, the poRibo-T2 plasmid carrying the U2585G mutation was included in the transformation experiment. The transformed cells were plated on LB/agar containing 50 μ g/ml kanamycin and 100 μ g/ml ampicillin and incubated overnight at 37°C. Three colonies from each transformation were then streaked on LB/agar plates containing 50 μ g/ml kanamycin and 100 μ g/ml ampicillin and supplemented with 0.5 mM IPTG, 40 μ g/ml X-Gal and 2 mM PETG. Plates were incubated at 37°C for 22 hours and photographed.

2.5.3 Results and discussion

To create the orthogonal Ribo-T system, the wt anti-SD 3' end of the 16S-23S hybrid RNA was altered from ACCUCCUUA to AUUGUGGUA³⁵ producing a poRibo-T1 construct. When poRibo-T1 was introduced in the *E. coli* (POP2136 strain) carrying the *sf-gfp* gene with the SD sequence CACCAC cognate to the oRibo-T³⁵ (Fig. 2.5c, pLpp5oGFP), notable GFP expression was observed (Fig. 2.16a), demonstrating the activity of oRibo-T in the cell. The preparation of ribosomes from the poRibo-T1 transformed cells (which contains a mixture of wt and oRibo-T ribosomes) was able to translate the orthogonal *sf-gfp* gene in a cell-free system (green dotted line in Fig. 2.16b). However, *in vitro* translation of this reporter was not fully orthogonal because some GFP expression was observed even with the preparation containing exclusively wt ribosomes (pink dotted line in Fig. 2.16b). To assess the contribution of oRibo-T for *in vitro* expression of the orthogonal *sf-gfp*, we took advantage of the A2058G mutation in poRibo-T1, which rendered ribosomes resistant to macrolide (*e.g.*, erythromycin) and lincosamide (*e.g.*, clindamycin) antibiotics. Addition of clindamycin to the reaction with wt ribosomes completely inhibited expression of the reporter (pink solid line in Fig. 2.16b), whereas significant expression of GFP was observed in the reaction carrying the oRibo-T preparation (green solid line in Fig. 2.16b), fully attributable to the *in vitro* activity of the engineered orthogonal ribosome.

Selective inhibition of wt ribosomes in the oRibo-T preparation could be a useful tool for *in vitro* applications. Importantly, the unique nature of Ribo-T allows for utilizing antibiotic resistance mutations in any of the ribosomal subunits. We demonstrated this by introducing a G693A mutation in the 16S rRNA segment of oRibo-T, which rendered it resistant to the small subunit-targeting antibiotic pactamycin^{70,75}. Pactamycin (100 μ M) completely inhibited the activity of the wt ribosomes in the PURE translation system, whereas oRibo-T (G693A) remained fully active (Fig. 2.16c).

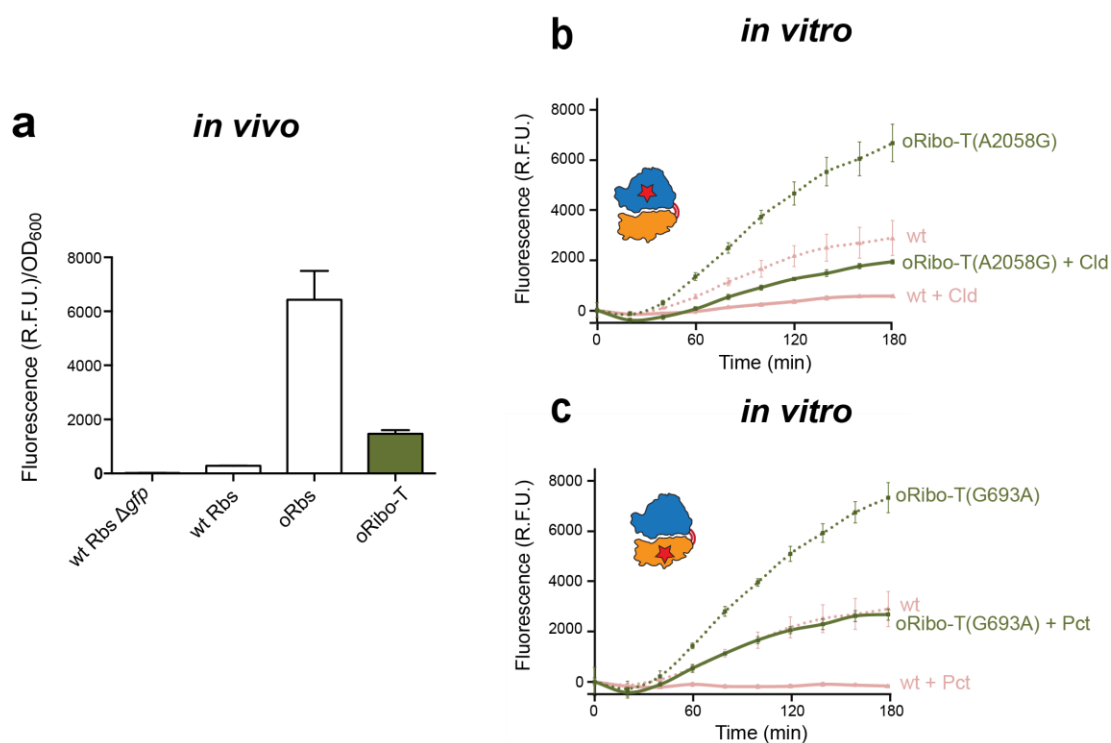


Figure 2.16. Translation of the orthogonal *sf-gfp* gene by oRibo-T *in vivo* and *in vitro*. a, Expression of an orthogonal *sf-gfp* reporter in the *E. coli* POP2136 cells transformed with pAM552 plasmid encoding wt rRNA (wt Rbs), pAM552 with an orthogonal SD sequence in 16S rRNA of a non-tethered ribosome (oRbs) or poRibo-T1 expressing an orthogonal Ribo-T (green bar). Cells lacking *gfp* reporter (wt Rbs Δgfp) were used as a background fluorescence control. The data represent the average value of six biological replicates in technical triplicates with the error bars indicating the standard deviation. b, *In vitro* translation of the orthogonal *sf-gfp* reporter by non-tethered non-orthogonal wt ribosomes (pink lines), or oRibo-T(A2058G) (which also contained cellular wt ribosomes) (green lines). The dotted lines correspond to the translation reactions without antibiotic and solid lines represent reactions supplemented with 50 μM clindamycin (Cld). c, same as b, but oRibo-T contained a G693A mutation instead of A2058G and clindamycin was replaced with 100 μM pactamycin (Pct). The red star in the cartoons indicate the ribosomal subunit carrying the antibiotic resistance mutation. Graphs in b and c are each representative of two biological replicates each done in technical triplicates with the error bars indicating the standard deviation in the shown experiment.

The evolvability of oRibo-T is revealed by selection of gain-of-function mutations in the peptidyl transferase center

We next used the oRibo-T system to search for gain of function mutations in the PTC, which could facilitate translation of a problematic protein sequence by the ribosome. Such experiments would require highly efficient transformation of the recipient cells with poRibo-T constructs. We noted, however, that in contrast to the selected SQ171fg cells, transformation of several *E. coli* strains (e.g. JM109, BL21 or C41) with poRibo-T1 was rather poor and resulted in slowly growing colonies, which varied significantly in size (Fig. 2.17). Fortuitously, in the course of these experiments we isolated a spontaneous mutant plasmid, poRibo-T2, which showed notably improved transformation efficiency and produced evenly-sized colonies which appeared on the plate after an overnight incubation (as opposed to a 36 hr incubation for the poRibo-T1 transformants) (Fig. 2.17). Sequencing showed that poRibo-T2 acquired a single mutation in the P_L promoter that controls Ribo-T expression, which altered its '-10' box from GATACT to TATACT bringing it closer to the TATAAT consensus. Although we do not fully understand why the promoter mutation improves performance of poRibo-T (as well as of non-orthogonal pRibo-T) in the 'unselected' *E. coli* cells, all the subsequent *in vivo* experiments were carried out using the poRibo-T2-derived constructs.

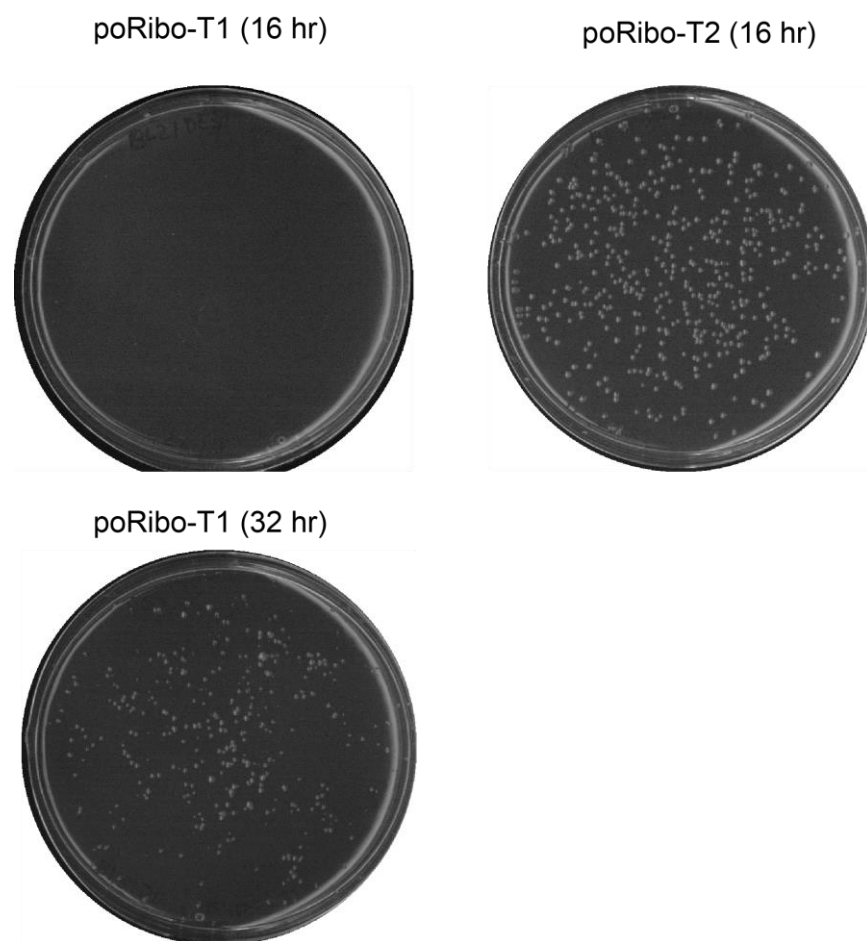


Figure 2.17. Promoter mutation in oRibo-T improves transformation of the *E. coli* cells. Transformation of BL21 cells with the original poRibo-T1 construct and with poRibo-T2 construct carrying a point mutation in the '-10' box of the P_L promoter controlling oRibo-T transcription. The plates show representative results of three independent biological experiments.

Translation of the *secM* gene, which regulates the expression of the essential SecA ATPase involved in protein secretion, is controlled by nascent peptide-dependent translation arrest. The ribosome stalls when it reaches the Pro₁₆₆ codon of *secM* because specific interactions of the SecM nascent chain with the ribosomal exit tunnel impair the PTC function preventing the transfer of the 165-amino acid long peptide to the incoming prolyltransfer-RNA (Pro-tRNA). Thus, the SecM polypeptide represents a classic example of an amino acid sequence whose translation is problematic for the ribosome⁵⁵. Several mutations in the ribosomal exit tunnel (*e.g.*, A2058G) have been previously identified as relieving translation arrest possibly by disrupting the nascent chain-ribosome interactions^{55, 71, 76}. However, exploring the role of the PTC in the mechanism of the translation arrest and identifying the catalytic center mutations alleviating ribosome stalling during SecM translation has been impossible so far because of the lethal nature of the mutations in the PTC active site^{77, 78}. To search for the translation arrest bypass mutations in the PTC, we removed the A2058G mutation from poRibo-T2 and engineered an orthogonal SecM-based reporter, poSML (Fig. 2.18a, Fig. 2.5b,d). In the pACYC177-based poSML, the reporter gene, equipped with an orthogonal SD sequence, includes 46 codons of *secM*, encoding the problematic amino acid sequence, fused in frame in front of the *lacZα* gene⁵⁵ (Fig. 2.18a). When the reporter plasmid was introduced in the poRibo-T2 transformed C41(DE3) cells capable of α -complementation, colonies formed on the indicator plates were white (data not shown), likely because SecM-induced translation arrest prevents oRibo-T from reaching the *lacZα* segment of the reporter mRNA.

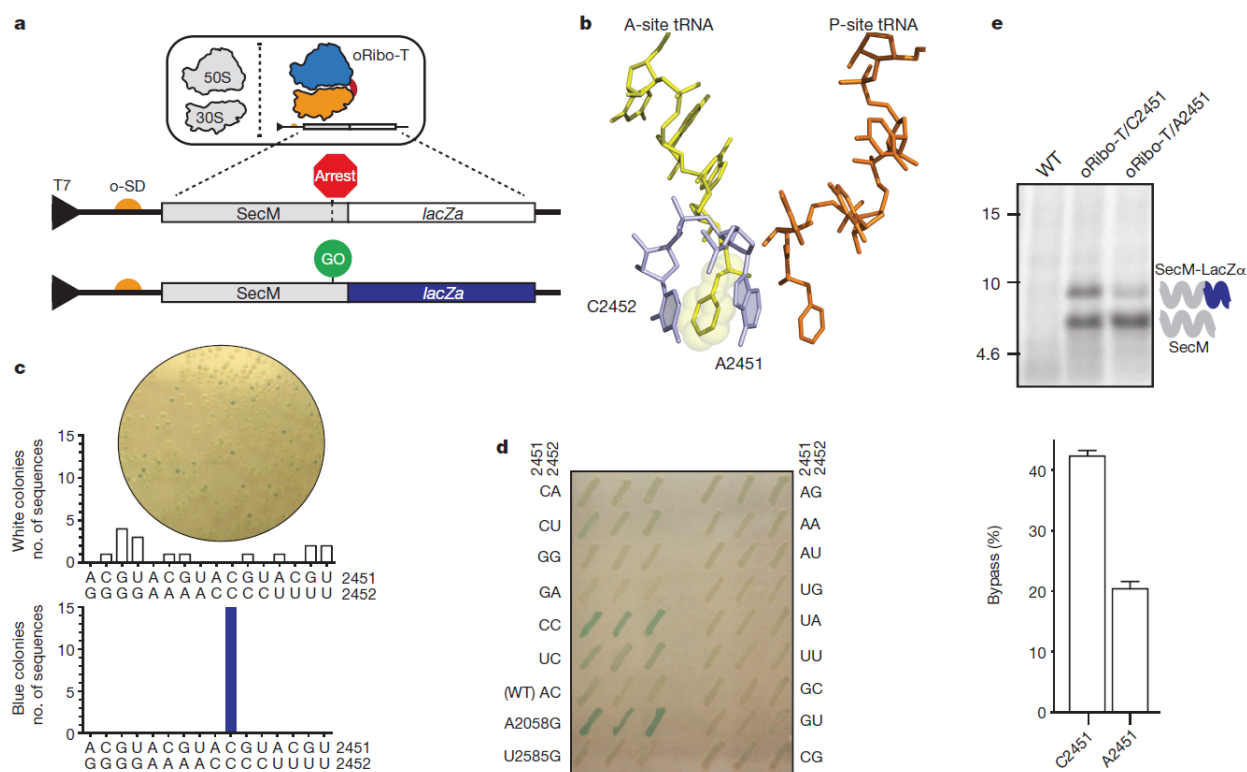


Figure 2.18. Evolving Ribo-T to identify gain-of-function PTC mutations that facilitate synthesis of problematic amino acid sequences. a, The SecM-LacZa reporter with an orthogonal Shine-Dalgarno (o-SD) sequence is translated in the cell by oRibo-T. SecM-dependent ribosome stalling prevents expression of the lacZa gene unless a ribosomal mutation allows for bypass of the SecM arrest site. b, The placement of Phe-tRNAs bound in the P-site (orange) and A-site (yellow) of the PTC⁶¹. The conserved 23S rRNA residues A2451 and C2452 (blue) form the amino acid side-chain binding pocket in the A-site. c, Top, colonies formed on X-gal/isopropyl β -D-1-thiogalactopyranoside (IPTG) plates by the *E. coli* C41 cells transformed with the *secM-lacZa* reporter plasmid and a library of poRibo-T2 plasmids with the PTC mutations at positions 2451 and 2452. Bottom, identity of 2451 and 2452 residues in poRibo-T2 plasmids isolated from randomly picked 16 white colonies and 15 blue colonies. d, The *E. coli* C41 cells transformed with the *secM-lacZa* reporter and individual poRibo-T2 plasmids with different nucleotide combinations at positions 2451 and 2452. The transformed cells were initially plated on LB agar antibiotic plate without X-gal or IPTG (all colonies pale), and three randomly picked transformants were then streaked on the shown indicator plate containing X-gal and IPTG. The poRibo-T2 mutant with the A2058G mutation, which is known to enhance the bypass of the SecM arrest sequence⁵⁵, was used as a positive control. A mutation of another essential PTC nucleotide (U2585G), which has been proposed to be implicated in some translation arrest scenarios⁷⁹, showed no effect on SecM arrest. The photographs of the agar plates in c and d have been contrast-enhanced for better colour separation. e, The A2451C mutation enhances bypass of the SecM stalling sequence by oRibo-T in vitro. The orthogonal construct containing *secM* stalling sequence fused in frame to the truncated *lacZa* gene was translated in the Δ ribosome PURExpress cell-free translation system supplemented with wild-type non-tethered ribosomes or preparations of oRibo-T (A2451 or C2451). The Ribo-T constructs carried the pactamycin-resistance mutation G693A in 16S rRNA, and the reactions were carried out in the presence of pactamycin, which, in addition to the presence of an orthogonal Shine-Dalgarno sequence, ensured that the reporter is translated exclusively by oRibo-T (see the control wild-type lane with no translation products). Numbers on the left indicate the size (kDa) of molecular mass markers. The bar graph at the bottom shows the efficiency of bypass (ratio between the full-size and SecM-arrested translation products). A representative gel of two independent experiments is shown, with error bars indicating the s.d.

We then engineered a library of oRibo-T mutants with alterations in rRNA residues in the PTC A site since it has been proposed to play a key role in the mechanism of ribosome stalling^{55, 71, 76}. In addition, the ability to manipulate the ribosomal A-site could be crucial for future efforts to engineer ribosomes capable of programmed polymerization of unnatural amino acids and backbone-modified analogs. Two splayed-out residues, A2451 and C2452, whose mutations are dominantly lethal in *E. coli*^{77, 78}, form the pocket that accommodates the amino acid side chain of the A site-bound aminoacyl-tRNA^{61, 80} (Fig. 2.18b). Thus, the poRibo-T2 library we prepared contained each of the 16 possible dinucleotide combinations at positions 2451-2452 in the 23S rRNA segment of oRibo-T.

Strikingly, when the C41(DE3) cells with the poSML plasmid were transformed with the poRibo-T2 2451/2452 library and plated on indicator plates, some of the colonies appeared notably blue-colored (Fig. 2.18c). This meant that some of the oRibo-T mutants were able to bypass the SecM-induced arrest and continue active translation through the *lacZα* segment of the reporter. Sequencing 15 blue colonies showed that they all carried a C2451-C2452 sequence (the A2451C mutation) in the PTC. In contrast, none of the 16 analyzed 'white' colonies had this sequence and instead exhibited a variety of dinucleotide combinations at positions 2451-2452 (Fig. 2.18c). Because of the relatively small size of the 2451/2452 mutant library, we verified these results by introducing 16 individual poRibo-T2 plasmids with all possible 2451-2452 mutations into poSML-transformed C41(DE3) cells. Importantly, all the individual oRibo-T 2451/2452 mutants were viable confirming that oRibo-T is suitable for expression of dominantly lethal 23S rRNA mutations and indicating a low degree of cross-association of Ribo-T with free wt 30S subunits. Three transformants of each type were then tested on the indicator plate.

Consistent with the previous result (Fig. 2.18c), the A2451C mutation confers the most pronounced blue color of the transformants, comparable to that seen in cells expressing oRibo-T with the tunnel mutation A2058G (Fig. 2.18d). The A2451U mutation also increased the blue hue of the cells although to a lesser extent. Our results suggested that the A2451C (and A2451U) mutants were not only functional in cellular protein synthesis but in addition gained the ability to bypass translation arrest caused by the problematic SecM sequence. Interestingly, a mutation of another essential nucleotide in the PTC (U2585G), which has been proposed to be implicated in some translation arrest scenarios⁷⁹, showed no effect on SecM arrest. We verified the discovered role of A2451 in the mechanism of SecM translation arrest by testing the expression of the orthogonal *secM-lacZ* reporter *in vitro* by isolated wt or A2451C mutant oRibo-T.

In order to assure that the *in vitro* effects are attributed exclusively to oRibo-T, a pactamycin resistance mutation G693A^{70, 75} was introduced in the 16S segment of oRibo-T constructs and cell-free translation in the PURE system was carried out in the presence of pactamycin. Under our experimental conditions, only a small fraction of original oRibo-T were able to bypass the SecM arrest signal and synthesize the full-size hybrid protein (Fig. 2.18e, lane oRibo-T(A2451)). In contrast the A2451C mutant was able to bypass the SecM arrest site twice as efficiently as the unmodified oRibo-T [Fig. 2.18e, lane oRibo-T(C2451)], confirming that the selected (and otherwise lethal) mutation has altered the functional properties of the PTC and improved the ability of oRibo-T to polymerize a polypeptide sequence problematic for wt ribosome. These results provide the first direct experimental evidence of a direct involvement of the PTC A site in the mechanism of nascent peptide-dependent ribosome stalling and suggest that interactions between the proline moiety of Pro-tRNA and the A-site rRNA residues are critical for the SecM-induced translation arrest.

2.6 Conclusions and future directions

By engineering Ribo-T, a ribosome with inseparable tethered subunits, and demonstrating its functionality *in vivo* and *in vitro*, we have revised one of the key paradigms of molecular biology: that successful expression of the cellular genome requires reversible association and dissociation of the ribosome into individual subunits. Although the ability of translation initiation by 70S ribosome at leaderless mRNAs has been previously demonstrated⁸¹, it was surprising that non-dissociating ribosomes would be active enough to account for expression of the entire bacterial genome at a sufficient level for active cell growth and proliferation. This finding in turn opened the unprecedented possibility to engineer a fully orthogonal, and most importantly evolvable, gene expression system in the cell where an entire specialized ribosome, not only the mRNA-interacting small subunit, is dedicated to translation of a defined genetic template. As a proof of principle we showed that oRibo-T can be used for engineering and studying in cells the mutations of functionally-critical rRNA residues, a task that would be difficult or impossible to achieve in any other system. This shows that Ribo-T may find important implications in exploring poorly understood functions of the ribosome in protein synthesis. Furthermore, the opportunity provided by the oRibo-T system to dramatically modify the catalytic properties of the protein synthesis machine, opens up exciting prospects for engineering or evolving the ability of the ribosome to synthesize genetically-encoded polymers with principally new properties both *in vivo* and *in vitro*.

In the near term, we will evolve Ribo-T to incorporate exotic substrates (nonstandard amino acids) with much greater efficiency compared to current NSAA incorporation systems⁵. This work changes one of the key paradigms of molecular biology and sets the stage for engineering an orthogonal translation system where a sub-fraction of cellular ribosomes could be dedicated to a specific task, such as translation of a particular protein, incorporation of specific unnatural amino acids or using an alternative genetic code. For example, Ribo-T could enable new drugs and protein therapeutics, boot-up orthogonal translation networks in cells for synthetic biology applications, and provide a route towards materials that are impossible to make today that rely on an expanded chemistry of life.

2.7 Additional information

2.7.1 Acknowledgements

We thank I. Ntai and the Proteomics Center of Excellence at Northwestern University for mass spectrometry analysis, K. N. Swonger, C. Burghard, E.M. Fulk, V. Raghavan and N. Aleksashin for help with some experiments, K. Ito for providing the sequence of the pNH122 *secM-lacZ* reporter, Y. Polikanov for help in preparing ribosome images, J. Lee for assistance in genome sequence analysis, S. Sothiselvam and J. Marks for stimulating discussions and suggestions and N. Vazquez-Laslop for insightful advices on the project and critical reading of the manuscript. This work was supported by the Defense Advanced Research Projects Agency [N66001-12-C-4211], the National Science Foundation grants MCB-0943393 (to MCJ) and MCB-1244455 (to ASM) and the David and Lucille Packard Foundation Fellowship [2011-37152] (to MCJ).

2.7.2 Author Contributions

MCJ and ASM designed the study, analyzed results, and wrote the paper. CO and EDC designed and performed experiments and analyzed data. TS and TF performed experiments.

2.7.3 Publishing and Patent information

Published manuscript

Orelle, C.*, Carlson, E.D.*, Szal, T., Florin, T., Jewett, M.C. and Mankin, A.S. (2015) Protein synthesis by ribosomes with tethered subunits. *Nature*, 524, 119-1244.

*Contributed equally

Patent application

Orelle, C., Carlson, E.D., Szal, T., Jewett, M.C. & Mankin, A.S. Methods of making tethered ribosomes. (2015) PCT/US2015/033221

2.8 Tables

Table 2.1. Primer pairs used for construction of circularly permuted 23S rRNA genes.

Primer name ^{a)}	Primer sequence 5'→3' ^{b)}
CP67_60-F	AACATCTTCGGGTTGTGAGcTTAAGCTGCGATAAGCGTCG
CP67_60-R	ACAGCTTCGGCGTTGTAAGcTTAAGCCACGTCCTTCATCG
CP95_87-F	AACATCTTCGGGTTGTGAGcTTAAGCACCGTTATAACCGGCGATTTTC
CP95_87-R	ACAGCTTCGGCGTTGTAAGcTTAAGCACCTTACCGACGCTTATC
CP104_97-F	AACATCTTCGGGTTGTGAGcTTAAGCACCGGCGATTTCCG
CP104_97-R	ACAGCTTCGGCGTTGTAAGcTTAAGCGGTTTCATATCACCTTACC
CP128_123-F	AACATCTTCGGGTTGTGAGcTTAAGCCCCAGTGTGTTTCGAC
CP128_123-R	ACAGCTTCGGCGTTGTAAGcTTAAGCCCCATTTCGGAAATCG
CP142_137-F	AACATCTTCGGGTTGTGAGcTTAAGCACACACTATCATTAACTGAATC
CP142_137-R	ACAGCTTCGGCGTTGTAAGcTTAAGCACACACTGGGTTTCC
CP168_158-F	AACATCTTCGGGTTGTGAGcTTAAGCGGTTAATGAGGCGAAC
CP168_158-R	ACAGCTTCGGCGTTGTAAGcTTAAGCAGTTAATGATAGTGTGTGTC
CP200_195-F	AACATCTTCGGGTTGTGAGcTTAAGCTCTAAGTACCCCGAGG
CP200_195-R	ACAGCTTCGGCGTTGTAAGcTTAAGCTCAGTTCCCCCGGTTTC
CP230_225-F	AACATCTTCGGGTTGTGAGcTTAAGCGAGATTCCCCCAGTAG
CP230_225-R	ACAGCTTCGGCGTTGTAAGcTTAAGCGATTCTTTTCTCGGGGTAC
CP252_246-F	AACATCTTCGGGTTGTGAGcTTAAGCGCGAACGGGGAGCAG
CP252_246-R	ACAGCTTCGGCGTTGTAAGcTTAAGCGCTACTGGGGGAATCTC
CP281_274-F	AACATCTTCGGGTTGTGAGcTTAAGCCAGTGTGTGTGTAGTG
CP281_274-R	ACAGCTTCGGCGTTGTAAGcTTAAGCGCTCTGGGCTGCTC
CP312_305-F	AACATCTTCGGGTTGTGAGcTTAAGCGGCGCGGATACAG
CP312_305-R	ACAGCTTCGGCGTTGTAAGcTTAAGCGACGCTTCCACTAACAC
CP335_327-F	AACATCTTCGGGTTGTGAGcTTAAGCCCCGTACACAAAATGCAC
CP335_327-R	ACAGCTTCGGCGTTGTAAGcTTAAGCCCCTGTATCGCGCGCCTTTC
CP347_343-F	AACATCTTCGGGTTGTGAGcTTAAGCAATGCACATGCTGTGAG
CP347_343-R	ACAGCTTCGGCGTTGTAAGcTTAAGCGTGTACGGGGCTGTC
CP391_383-F	AACATCTTCGGGTTGTGAGcTTAAGCATCCTGTCTGAATATGG
CP391_383-R	ACAGCTTCGGCGTTGTAAGcTTAAGCGTCCCGCCCTACTC
CP416_411-F	AACATCTTCGGGTTGTGAGcTTAAGCTCCTCCAAGGCTAAATAC
CP416_411-R	ACAGCTTCGGCGTTGTAAGcTTAAGCCCCCATATTTCAGACAG
CP467_462-F	AACATCTTCGGGTTGTGAGcTTAAGCGGGAAAGCGAAAAGAAC
CP467_462-R	ACAGCTTCGGCGTTGTAAGcTTAAGCGGTAAGTACTGGTTCACTATCG
CP493_487-F	AACATCTTCGGGTTGTGAGcTTAAGCGGGGAGTAAAAAGAAC
CP493_487-R	ACAGCTTCGGCGTTGTAAGcTTAAGCGGGGTTCTTTTCGCCTTTC
CP502_497-F	AACATCTTCGGGTTGTGAGcTTAAGCAAAGAACCTGAAACCGTG
CP502_497-R	ACAGCTTCGGCGTTGTAAGcTTAAGCTCCCCTCGCCGGGGTTC
CP549_544-F	AACATCTTCGGGTTGTGAGcTTAAGCGCGTGTGACTGCGTACC
CP549_544-R	ACAGCTTCGGCGTTGTAAGcTTAAGCGCGTGTGCTCCCACTG
CP617_611-F	AACATCTTCGGGTTGTGAGcTTAAGCGGGGAGCCGAAGG
CP617_611-R	ACAGCTTCGGCGTTGTAAGcTTAAGCGGTTAACCTTGCTACAG
CP634_629-F	AACATCTTCGGGTTGTGAGcTTAAGCCCGAGTCTTAACTGG
CP634_629-R	ACAGCTTCGGCGTTGTAAGcTTAAGCCCTTCGGCTCCCCTATTTC
CP647_641-F	AACATCTTCGGGTTGTGAGcTTAAGCGGGCGTTAAGTTGCAGG
CP647_641-R	ACAGCTTCGGCGTTGTAAGcTTAAGCAGACTCGGTTTCCCTTC
CP719_712-F	AACATCTTCGGGTTGTGAGcTTAAGCCTAACTGGAGGACC
CP719_712-R	ACAGCTTCGGCGTTGTAAGcTTAAGCCCAACCTTCAACCTG
CP753_744-F	AACATCTTCGGGTTGTGAGcTTAAGCATTAGCGGATGACTTGTG

Primer name ^{a)}	Primer sequence 5'→3' ^{b)}
CP753_744-R	ACAGCTTCGGCGTTGTAAAGcTTAAGCATTAGTCGGTTCGGTCC
CP785_779-F	AACATCTTCGGGTTGTGAGcTTAAGCGCCAATCAAACCGGGAG
CP785_779-R	ACAGCTTCGGCGTTGTAAAGcTTAAGCACCCCCAGCCACAAG
CP831_826-F	AACATCTTCGGGTTGTGAGcTTAAGCGTAGCGCCTCGTGAATTC
CP831_826-R	ACAGCTTCGGCGTTGTAAAGcTTAAGCATAGCTTTCGGGGAGAACC
CP879_875-F	AACATCTTCGGGTTGTGAGcTTAAGCGGGGGTCATCCCGAC
CP879_875-R	ACAGCTTCGGCGTTGTAAAGcTTAAGCCCGAAACAGTGTCTACC
CP891_885-F	AACATCTTCGGGTTGTGAGcTTAAGCGACTTACCAACCCGATG
CP891_885-R	ACAGCTTCGGCGTTGTAAAGcTTAAGCGACCCCTTGCCGAAAC
CP962_955-F	AACATCTTCGGGTTGTGAGcTTAAGCGTCCGTCGTGAAGAGG
CP962_955-R	ACAGCTTCGGCGTTGTAAAGcTTAAGCACCCGCGTGTGTC
CP985_978-F	AACATCTTCGGGTTGTGAGcTTAAGCCCAGACCGCCAGC
CP985_978-R	ACAGCTTCGGCGTTGTAAAGcTTAAGCCCTCTTCACGACGGAC
CP1011_1004-F	AACATCTTCGGGTTGTGAGcTTAAGCGTCATGGTTAAGTGGGAAAC
CP1011_1004-R	ACAGCTTCGGCGTTGTAAAGcTTAAGCACCTTAGCTGGCGGTC
CP1051_1043-F	AACATCTTCGGGTTGTGAGcTTAAGCGCCAGGATGTTGGCTTAG
CP1051_1043-R	ACAGCTTCGGCGTTGTAAAGcTTAAGCGCCTTCCCACATCGTTTC
CP1074_1064-F	AACATCTTCGGGTTGTGAGcTTAAGCGCCATCATTTAAAGAAAGC
CP1074_1064-R	ACAGCTTCGGCGTTGTAAAGcTTAAGCGCCAACATCCTGGCTG
CP1086_1082-F	AACATCTTCGGGTTGTGAGcTTAAGCAGAAAGCGTAATAGCTCAC
CP1086_1082-R	ACAGCTTCGGCGTTGTAAAGcTTAAGCAATGATGGCTGCTTCTAAG
CP1099_1092-F	AACATCTTCGGGTTGTGAGcTTAAGCGCTCACTGGTTCGAG
CP1099_1092-R	ACAGCTTCGGCGTTGTAAAGcTTAAGCGCTTCTTTAAATGATGGCTG
CP1112_1108-F	AACATCTTCGGGTTGTGAGcTTAAGCGTCGGCCTGCGCGGAAG
CP1112_1108-R	ACAGCTTCGGCGTTGTAAAGcTTAAGCACCAAGTGTGAGCTATTACGCTTTC
CP1177_1172-F	AACATCTTCGGGTTGTGAGcTTAAGCGCGTTGTTGGGTAGG
CP1177_1172-R	ACAGCTTCGGCGTTGTAAAGcTTAAGCGCGTCGCTGCC
CP1215_1208-F	AACATCTTCGGGTTGTGAGcTTAAGCGGTGTGCTGTGAGG
CP1215_1208-R	ACAGCTTCGGCGTTGTAAAGcTTAAGCGGCTTACAGAACGCTC
CP1227_1222-F	AACATCTTCGGGTTGTGAGcTTAAGCGGCATGCTGGAGG
CP1227_1222-R	ACAGCTTCGGCGTTGTAAAGcTTAAGCAGCACACCTTCGCAG
CP1289_1281-F	AACATCTTCGGGTTGTGAGcTTAAGCCCCGCTCGCCGGAAG
CP1289_1281-R	ACAGCTTCGGCGTTGTAAAGcTTAAGCCCCGCTTTATCGTTACTTATG
CP1330_1324-F	AACATCTTCGGGTTGTGAGcTTAAGCCGGGGCAGGGTG
CP1330_1324-R	ACAGCTTCGGCGTTGTAAAGcTTAAGCCGTTGGACAGGAACC
CP1368_1363-F	AACATCTTCGGGTTGTGAGcTTAAGCGGCGTAGTCGATGG
CP1368_1363-R	ACAGCTTCGGCGTTGTAAAGcTTAAGCGCCTCGCCTTAGG
CP1398_1389-F	AACATCTTCGGGTTGTGAGcTTAAGCCCTGTACTTGGTGTAC
CP1398_1389-R	ACAGCTTCGGCGTTGTAAAGcTTAAGCCCTGTTTCCCATCGAC
CP1420_1417-F	AACATCTTCGGGTTGTGAGcTTAAGCAGGGGGGACGGAG
CP1420_1417-R	ACAGCTTCGGCGTTGTAAAGcTTAAGCGCAGTAACACCAAGTACAG
CP1461_1450-F	AACATCTTCGGGTTGTGAGcTTAAGCCCCGGTTAAGCGTG
CP1461_1450-R	ACAGCTTCGGCGTTGTAAAGcTTAAGCCCCGGCCAACATAG
CP1478_1474-F	AACATCTTCGGGTTGTGAGcTTAAGCGGCTGGTTTTCCAGG
CP1478_1474-R	ACAGCTTCGGCGTTGTAAAGcTTAAGCACGCTTAAACCGGGAC
CP1498_1492-F	AACATCTTCGGGTTGTGAGcTTAAGCCCGGAAAATCAAGGCTG
CP1498_1492-R	ACAGCTTCGGCGTTGTAAAGcTTAAGCCCTGGAAAACCAGCCTAC
CP1511_1508-F	AACATCTTCGGGTTGTGAGcTTAAGCGCTGAGGCCTGATG
CP1511_1508-R	ACAGCTTCGGCGTTGTAAAGcTTAAGCTGATTTTTCCGGATTTGC
CP1523_1520-F	AACATCTTCGGGTTGTGAGcTTAAGCTGACGAGGCACTACG
CP1523_1520-R	ACAGCTTCGGCGTTGTAAAGcTTAAGCACGCCTCAGCCTTG
CP1538_1533-F	AACATCTTCGGGTTGTGAGcTTAAGCGTGCTGAAGCAACAAATG

Primer name ^{a)}	Primer sequence 5'→3' ^{b)}
CP1538_1533-R	ACAGCTTCGGCGTTGTGAAGcTTAAGCGTGCCTCGTCATCACC
CP1547_1543-F	AACATCTTCGGGTTGTGAGcTTAAGCCAACAAATGCCCTGC
CP1547_1543-R	ACAGCTTCGGCGTTGTGAAGcTTAAGCCAGCACCGTAGTGC
CP1587_1582-F	AACATCTTCGGGTTGTGAGcTTAAGCGGTAACATCAAATCGTAC
CP1587_1582-R	ACAGCTTCGGCGTTGTGAAGcTTAAGCGCTTAGAGGCTTTTCC
CP1619_1612-F	AACATCTTCGGGTTGTGAGcTTAAGCGGTGGTCAGGTAGAG
CP1619_1612-R	ACAGCTTCGGCGTTGTGAAGcTTAAGCGGTTTGGGGTACGATTTG
CP1636_1630-F	AACATCTTCGGGTTGTGAGcTTAAGCTACCAAGGCGCTTG
CP1636_1630-R	ACAGCTTCGGCGTTGTGAAGcTTAAGCTACCTGACCACCTGTG
CP1696_1691-F	AACATCTTCGGGTTGTGAGcTTAAGCGGAGAAGGCACGCTG
CP1696_1691-R	ACAGCTTCGGCGTTGTGAAGcTTAAGCGTTACGGCACCATTTTG
CP1716_1712-F	AACATCTTCGGGTTGTGAGcTTAAGCTAGGTGAGGTCCCTC
CP1716_1712-R	ACAGCTTCGGCGTTGTGAAGcTTAAGCATCAGCGTGCCTTC
CP1733_1727-F	AACATCTTCGGGTTGTGAGcTTAAGCGGATGGAGCTGAAATC
CP1733_1727-R	ACAGCTTCGGCGTTGTGAAGcTTAAGCGGACCTCACCTACATATC
CP1741_1736-F	AACATCTTCGGGTTGTGAGcTTAAGCCTGAAATCAGTCGAAGATAC
CP1741_1736-R	ACAGCTTCGGCGTTGTGAAGcTTAAGCATCCGCGAGGGACCTC
CP1756_1752-F	AACATCTTCGGGTTGTGAGcTTAAGCGATAACCAGCTGGCTG
CP1756_1752-R	ACAGCTTCGGCGTTGTGAAGcTTAAGCGACTGATTTTCAGCTCC
CP1787_1777-F	AACATCTTCGGGTTGTGAGcTTAAGCACACAGCACTGTGC
CP1787_1777-R	ACAGCTTCGGCGTTGTGAAGcTTAAGCACAGTTGCAGCCAG
CP1811_1806-F	AACATCTTCGGGTTGTGAGcTTAAGCGTGACGTATACGGTG
CP1811_1806-R	ACAGCTTCGGCGTTGTGAAGcTTAAGCGTGTTCACAGTGC
CP1840_1837-F	AACATCTTCGGGTTGTGAGcTTAAGCGTGCCGGAAGGTTAATTG
CP1840_1837-R	ACAGCTTCGGCGTTGTGAAGcTTAAGCGGCAGGCGTCACAC
CP1849_1846-F	AACATCTTCGGGTTGTGAGcTTAAGCGGTTAATTTGATGGGGTTAG
CP1849_1846-R	ACAGCTTCGGCGTTGTGAAGcTTAAGCCCGCACCGGGCAG
CP1873_1868-F	AACATCTTCGGGTTGTGAGcTTAAGCGGAAGCTCTTGATC
CP1873_1868-R	ACAGCTTCGGCGTTGTGAAGcTTAAGCGCTAACCCCATCAATTAAC
CP1919_1911-F	AACATCTTCGGGTTGTGAGcTTAAGCACGGTCTTAAGGTAGC
CP1919_1911-R	ACAGCTTCGGCGTTGTGAAGcTTAAGCACGGCCGCGCTTAC
CP1931_1926-F	AACATCTTCGGGTTGTGAGcTTAAGCTAGCGAAATTCCTTGTCG
CP1931_1926-R	ACAGCTTCGGCGTTGTGAAGcTTAAGCAGGACCGTTATAGTTACG
CP1956_1950-F	AACATCTTCGGGTTGTGAGcTTAAGCTCCGACCTGCACG
CP1956_1950-R	ACAGCTTCGGCGTTGTGAAGcTTAAGCCCCGACAAGGAATTTTC
CP1991_1988-F	AACATCTTCGGGTTGTGAGcTTAAGCTGTCTCCACCCGAG
CP1991_1988-R	ACAGCTTCGGCGTTGTGAAGcTTAAGCCTGGCCATCATTACG
CP2036_2027-F	AACATCTTCGGGTTGTGAGcTTAAGCCAGTGTACCCGCGGCAAG
CP2036_2027-R	ACAGCTTCGGCGTTGTGAAGcTTAAGCCAGCGAGTTCAATTTCACTG
CP2147_2144-F	AACATCTTCGGGTTGTGAGcTTAAGCAGTCTGCATGGAGC
CP2147_2144-R	ACAGCTTCGGCGTTGTGAAGcTTAAGCCGTCCACACTTCAAAG
CP2148_2143-F	AACATCTTCGGGTTGTGAGcTTAAGCGTCTGCATGGAGCCGAC
CP2148_2143-R	ACAGCTTCGGCGTTGTGAAGcTTAAGCGTCCACACTTCAAAGCCTC
CP2215_2209-F	AACATCTTCGGGTTGTGAGcTTAAGCCGGGTTGCGGACAG
CP2215_2209-R	ACAGCTTCGGCGTTGTGAAGcTTAAGCCGGGTC AACGTTAGAAC
CP2254_2250-F	AACATCTTCGGGTTGTGAGcTTAAGCCGGTCTCCTCCTAAAGAG
CP2254_2250-R	ACAGCTTCGGCGTTGTGAAGcTTAAGCCAGTCAAACCTACCCACC
CP2276_2264-F	AACATCTTCGGGTTGTGAGcTTAAGCGGAGGAGCACGAAGG
CP2276_2264-R	ACAGCTTCGGCGTTGTGAAGcTTAAGCGGAGGAGACCGCCCCAG
CP2312_2304-F	AACATCTTCGGGTTGTGAGcTTAAGCTCAGGAGGTTAGTGC
CP2312_2304-R	ACAGCTTCGGCGTTGTGAAGcTTAAGCCAGGATTAGCCAACC
CP2331_2324-F	AACATCTTCGGGTTGTGAGcTTAAGCGCATAAGCCAGCTTGAC

Primer name ^{a)}	Primer sequence 5'→3' ^{b)}
CP2331_2324-R	ACAGCTTCGGCGTTGTAAAGcTTAAGCACTAACCTCCTGATGTCC
CP2362_2355-F	AACATCTTCGGGTTGTGAGcTTAAGCCGCGAGCAGGTGC
CP2362_2355-R	ACAGCTTCGGCGTTGTAAAGcTTAAGCCGCTCGCAGTCAAG
CP2379_2374-F	AACATCTTCGGGTTGTGAGcTTAAGCGCAGGTCATAGTGATCC
CP2379_2374-R	ACAGCTTCGGCGTTGTAAAGcTTAAGCGCACCTGCTCGCGCCGTC
CP2413_2404-F	AACATCTTCGGGTTGTGAGcTTAAGCGGGCCATCGCTCAAC
CP2413_2404-R	ACAGCTTCGGCGTTGTAAAGcTTAAGCAGAACCACCGGATC
CP2479_2471-F	AACATCTTCGGGTTGTGAGcTTAAGCTCGACGGCGGTGTTG
CP2479_2471-R	ACAGCTTCGGCGTTGTAAAGcTTAAGCTCTTGGGCGGTATCAG
CP2534_2529-F	AACATCTTCGGGTTGTGAGcTTAAGCAGGTCCCAAGGGTATG
CP2534_2529-R	ACAGCTTCGGCGTTGTAAAGcTTAAGCCAGCCCCAGGATGTG
CP2557_2551-F	AACATCTTCGGGTTGTGAGcTTAAGCGCCATTTAAAGTGGTACG
CP2557_2551-R	ACAGCTTCGGCGTTGTAAAGcTTAAGCGCCATACCCTTGGGAC
CP2567_2561-F	AACATCTTCGGGTTGTGAGcTTAAGCGTGGTACGCGAGCTG
CP2567_2561-R	ACAGCTTCGGCGTTGTAAAGcTTAAGCATGGCGAACAGCCATAC
CP2599_2594-F	AACATCTTCGGGTTGTGAGcTTAAGCGACAGTTCGGTCCCTATC
CP2599_2594-R	ACAGCTTCGGCGTTGTAAAGcTTAAGCGACGTTCTAAACCCAGC
CP2663_2658-F	AACATCTTCGGGTTGTGAGcTTAAGCGGACCGGAGTGGAC
CP2663_2658-R	ACAGCTTCGGCGTTGTAAAGcTTAAGCGTACTAGGAGCAGC
CP2706_2701-F	AACATCTTCGGGTTGTGAGcTTAAGCATGGCACTGCCCGGTAG
CP2706_2701-R	ACAGCTTCGGCGTTGTAAAGcTTAAGCATGACAACCCGAACACC
CP2742_2737-F	AACATCTTCGGGTTGTGAGcTTAAGCGTGCTGAAAGCATCTAAG
CP2742_2737-R	ACAGCTTCGGCGTTGTAAAGcTTAAGCCTCTTCCGCATTTAGCTAC
CP2758_2746-F	AACATCTTCGGGTTGTGAGcTTAAGCAGCACGAAACTTGC
CP2758_2746-R	ACAGCTTCGGCGTTGTAAAGcTTAAGCAGCACTTATCTCTTCC
CP2800_2796-F	AACATCTTCGGGTTGTGAGcTTAAGCAGGGTCCTGAAGGAAC
CP2800_2796-R	ACAGCTTCGGCGTTGTAAAGcTTAAGCAGGGTCAGGGAGAAC
CP2827_2819-F	AACATCTTCGGGTTGTGAGcTTAAGCCGACGTTGATAGG
CP2827_2819-R	ACAGCTTCGGCGTTGTAAAGcTTAAGCCAACGTTCCCTTCAGG
CP2861_2856-F	AACATCTTCGGGTTGTGAGcTTAAGCTGCGTTGAGCTAAC
CP2861_2856-R	ACAGCTTCGGCGTTGTAAAGcTTAAGCTGCGCTTACACAC

^{a)} F: forward primer, R: reverse primer.

^{b)} In each primer name, the first number indicates the new 5' nucleotide for the target circular permutant, and the second number indicates the new 3' nucleotide, both in reference to the wild-type 23S rRNA nucleotide numbering scheme. Non-underlined nucleotides indicate added homology to pAM-Δ23S-AflIII linearized backbone. Underlined nucleotides indicate primer segments that anneal to CP23S template.

Table 2.2. Characterization of the growth of *E. coli* SQ171 cells expressing a pure population of ribosomes with circularly permuted 23S rRNA.

	Doubling time (min) ^{a)}		Cell density (OD ₆₀₀) at saturation ^{b)}		n ^{f)}
	30 °C	37 °C	30 °C	37 °C	
pAM552 ^{c)}	61.0 ± 3.2	53.9 ± 1.0	1.04 ± 0.06	0.93 ± 0.03	4
pAM552-AflII ^{d)}	67.4 ± 1.0	53.3 ± 2.4	1.07 ± 0.01	0.97 ± 0.00	4
CP67 ^{e)}	106.4 ± 5.4	69.6 ± 2.1	0.83 ± 0.05	0.41 ± 0.07	3
CP95	144.9 ± 35.9	82.4 ± 24.4	0.66 ± 0.31	0.51 ± 0.18	6
CP104	90.8 ± 10.3	52.7 ± 3.2	0.98 ± 0.03	0.95 ± 0.02	3
CP168	123.8 ± 27.9	57.7 ± 1.9	0.70 ± 0.22	0.88 ± 0.12	10
CP281	100.1 ± 11.0	54.6 ± 10.1	1.01 ± 0.04	0.93 ± 0.13	3
CP549	101.7 ± 18.2	46.5 ± 3.9	1.00 ± 0.02	0.98 ± 0.03	3
CP617	231.7 ± 20.5	91.5 ± 18.5	0.16 ± 0.03	0.85 ± 0.05	4
CP634	162.0 ± 34.2	212.5 ± 58.1	0.46 ± 0.19	0.50 ± 0.10	3
CP879	106.6 ± 4.7	51.4 ± 4.6	1.03 ± 0.02	0.99 ± 0.04	3
CP891	144.5 ± 41.8	60.7 ± 4.1	0.56 ± 0.43	0.76 ± 0.23	6
CP1112	89.6 ± 6.0	57.8 ± 12.2	0.96 ± 0.02	0.91 ± 0.12	3
CP1178	102.5 ± 11.0	46.2 ± 1.3	0.96 ± 0.02	0.99 ± 0.01	3
CP1498	167.5 ± 17.5	118.0 ± 17.1	0.56 ± 0.32	0.52 ± 0.19	3
CP1511	131.5 ± 4.2	76.7 ± 1.5	0.88 ± 0.01	0.88 ± 0.01	3
CP1587	98.1 ± 12.4	55.1 ± 6.6	0.93 ± 0.05	0.92 ± 0.08	3
CP1716	174.4 ± 31.9	117.8 ± 16.5	0.44 ± 0.16	0.62 ± 0.34	3
CP1733	117.3 ± 8.2	83.8 ± 2.2	0.95 ± 0.01	0.80 ± 0.01	3
CP1741	230.0 ± 14.7	269.0 ± 50.3	0.28 ± 0.00	0.66 ± 0.09	3
CP1873	108.4 ± 6.5	52.9 ± 0.8	0.94 ± 0.01	0.91 ± 0.01	3
CP2148	83.0 ± 2.9	52.4 ± 3.9	0.73 ± 0.09	0.82 ± 0.02	4
CP2800	85.9 ± 15.7	53.5 ± 9.7	1.04 ± 0.03	0.91 ± 0.12	3
CP2861	138.4 ± 10.7	93.7 ± 4.5	0.88 ± 0.00	0.83 ± 0.04	3

^{a)} Growth in 100 µL LB media supplemented with 50 µg/ml carbenicillin in 96-well plate with shaking.

^{b)} After 18 hours of growth.

^{c)} pAM552: wild type *rmb* operon.

^{d)} pAM552-AflII: *rmb* operon with the 23S rRNA mutations G2C and C2901G used to introduce the AflII restriction sites.

^{e)} CPx: *rmb* with 23S circular permutations and G2C/C2901G mutations; x indicates the 5' starting nucleotide of the circularly permuted 23S gene. n: number of individual colonies used for growth analysis.

^{f)} Biological replicates are indicated in the “n” column, which is number of separate colonies that were used for each number average and standard deviation.

Table 2.3. The results of sequencing of the oligo(A) linkers T1 and T2 in pRibo-T isolated from randomly picked POP2136 clones transformed with the linker library.

T1	T2	Number of clones
5A	10A	1
7A	9A	1
7A	10A	1
7A	11A	1
8A	10A	1
9A	9A	1
9A	11A	2
9A	12A	1
10A	8A	1
10A	10A	2
10A	11A	1
11A	9A	1
11A	12A	1
12A	8A	1
12A	12A	1

3. Improvements to a ribosome with tethered subunits for *in vivo* ribosome engineering

Our recent advancement engineering a ribosome with tethered subunits, Ribo-T, represents a paradigm shift in the ability to engineer the key catalyst in gene expression, the ribosome. Across all known life, the ribosome is composed of two separate, completely dissociable subunits. Extensive ribosome engineering *in vivo* was limited by the requirement for ribosomes to maintain life. By mutating the mRNA ribosome binding site and the corresponding site on the small subunit, specialized orthogonal small subunits are created that operate in parallel to the wild-type pool; since the cell is not dependent on these orthogonal small subunits for life, their function can be altered in extraordinary ways. However, the large subunit, which contains the key engineering targets of the peptidyl transferase center and the nascent polypeptide exit tunnel, was not orthogonal due to promiscuous exchange between the wild-type and orthogonal small subunit pools. We were the first to solve this problem by tethering the large subunit to the small subunit via two short RNA linkers to create Ribo-T. While this first version of Ribo-T represents a step-change in our ability to engineer the ribosome and gives great promise for advancing basic science and synthetic biology, several limitations need to be overcome to develop it into a versatile tool with broader impact. Here, we use knowledge-driven and evolution-based approaches to improve Ribo-T properties, including the tether and orthogonal function. We then use the improved system for incorporation of the non-canonical amino acid p-azido-phenylalanine into proteins. The new Ribo-T version 2.0 will be more versatile and will serve as a better tool for many biotechnological, engineering and basic science applications.

3.1 Introduction

Our recent advancement in engineering a ribosome with tethered subunits, Ribo-T (Fig. 3.1), represents a paradigm shift in the ability to engineer the key catalyst in gene expression, the ribosome^{41, 82}. Across all kingdoms of life, the ribosome is composed of two distinct, completely dissociable subunits. Extensive ribosome engineering *in vivo* was limited by the requirement for native ribosomes to maintain life. To overcome this challenge, the mRNA ribosome binding site (Shine-Dalgarno; SD) as well as the corresponding site on the small subunit (anti-Shine-Dalgarno; aSD) are mutated such that they do not interact significantly with the wild-type mRNA and ribosomal small subunit pools. Because the cell is not dependent on such orthogonal small subunits for life, their function can be altered in ways that were previously unattainable. However, the large subunit, which contains the key engineering targets of the peptidyl transferase center and the nascent polypeptide exit tunnel, was never truly orthogonal. In these engineered systems, there still existed promiscuous exchange between the wild-type and orthogonal small subunit pools.

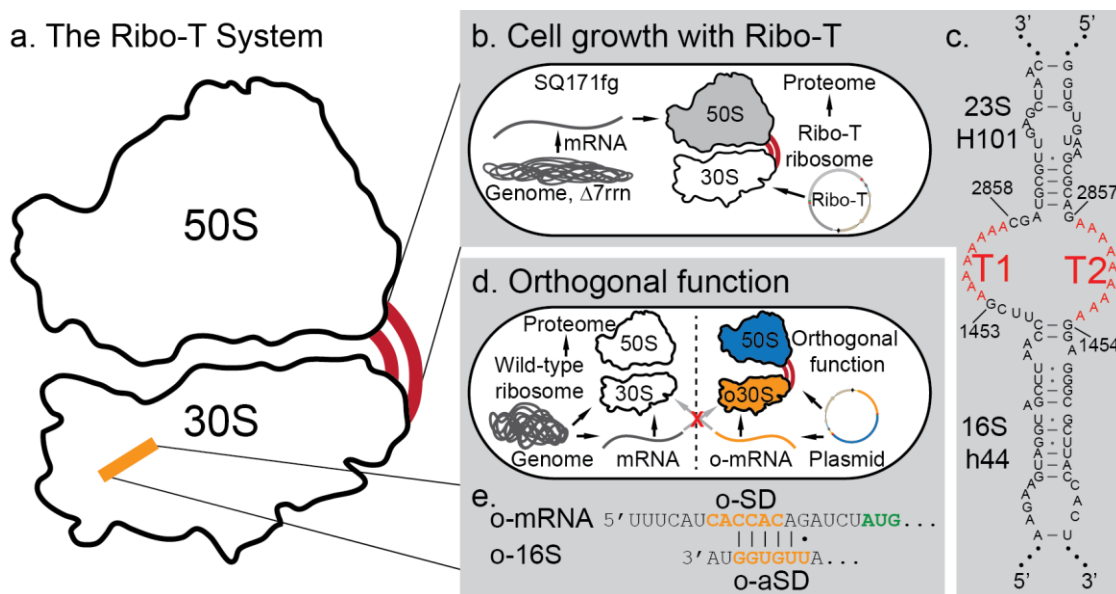


Figure 3.1. Ribo-T system improvement strategies. a. Schematic of Ribo-T showing tether (red) and orthogonal ribosome binding site (yellow). b. The tether is optimized in cells growing exclusively from the Ribo-T plasmid. c. Previously published Ribo-T tether sequence. d. Orthogonal function evolved for Ribo-T. e. Previously published orthogonal mRNA (o-mRNA) Shine-Dalgarno (SD) sequence and orthogonal 16S rRNA anti-SD sequence shown.

We addressed this problem by physically tethering the large subunit to the small subunit via two short RNA linkers to create a ribosome with tethered subunits, Ribo-T (Fig. 3.1a,c)⁴¹. Amazingly, Ribo-T with a wild-type anti-Shine-Dalgarno sequence is able to fully sustain life in the absence of wild-type untethered ribosomes (Fig. 3.1b). Furthermore, in mutating to an orthogonal small subunit (Fig. 3.1d,e), we are able to express otherwise inaccessible mutations in the 23S rRNA, endowing new functionality to the large subunit in living cells⁴¹. While the original version of Ribo-T represents a transformative leap in our ability to engineer the ribosome *in vivo* and gives great promise for advancing basic science and synthetic biology, several limitations need to be overcome to develop it into a versatile tool with broader impact.

Data illustrated that the current Ribo-T is limited at translation initiation *in vitro*⁴¹. Additionally, it is possible that the architecture of Ribo-T could impact translation in other ways. This may include: i) hindering ribosome subunit ratcheting during translation; ii) changing interactions with translation factors; and iii) fundamentally altering the ribosome biogenesis pathways. Finally, the orthogonal system is a modified version of previous works^{35, 36}, evolved in the untethered context and with different plasmid backbones and promoters than our current published poRibo-T2/o-mRNA system. Each of these limitations offers room for significant improvements to the current Ribo-T system.

3.2 Materials and Methods

3.2.1 Construction of the tether libraries

Plasmid construction and DNA manipulations were performed following standard molecular biology techniques. The library of tether sequences were introduced into the wild-type pRibo-T plasmid by inverse PCR amplification with Phusion polymerase (NEB) with primers listed in Supplementary Table 3.S1. All primers were synthesized by Integrated DNA Technologies. Amplification was followed by re-circularization with the Gibson assembly reaction (Supplementary Fig. 3.S1). Specifically, Ribo-T backbone plasmid was prepared by PCR amplification with primers 5'-GGAGGGCGCTTACCACTTTG and 5'-GGTTAAGCTACCTACTTCTTTTG using pRibo-T⁴¹ as template. Using Phusion polymerase, PCR was performed at 98 °C initial denaturing for 3 min, (98 °C 30 seconds, 55 °C 30 seconds, 72 °C 70 seconds)x25, and 72 °C final extension for 10 minutes. This amplifies the pRibo-T vector, excluding the tethers and 23S region of the plasmid.

To generate the tether libraries (Fig. 3.2b), primer pools were first prepared from primers listed in Supplementary Table 3.S1. For library 1, equimolar amounts of primers T1-A7-f through T1-A20-f were mixed to create the forward primer pool, and equimolar amounts of primers T1-T7-r through T1-T20-r were mixed to create the reverse primer pool. For library 2, equimolar amounts of primers T1-A7-f through T1-A20-f were mixed to create the forward primer pool, and equimolar amounts of primers T1-A7-r through T1-A20-r were mixed to create the reverse primer pool. Library 3 is generated using primers T1-8N-f and T2-9N-r. Library 4 is generated using primers T1-15N-f and T2-10N-r. In 4 separate PCRs under the same reaction conditions just described, respective library primers were used with template pRibo-T to generate PCR products of tether libraries flanking CP23S rRNA (Supplementary Fig. 3.S1). Following gel extraction of the Ribo-T backbone and 4 tether

libraries from 0.7% agarose gels with E.Z.N.A. gel extraction kit (Omega), 50 ng of Ribo-T backbone was recircularized in 4 separate Gibson assembly reactions with 3-fold molar excess of respective libraries. 2 μ L of each library was transformed into POP2136 cells via electroporation and incubated at 30 °C to repress expression of the p_L promoter with POP2136 constitutively expressed cI repressor. 40–80 colonies were selected from each library plate and library diversity was verified by DNA sequencing (Northwestern Sequencing Core). For each library, transformations and plating was scaled until total number of colonies exceeded 3x the theoretical library sizes. Plates were then washed and miniprepmed with the E.Z.N.A miniprep kit (Omega) to prepare the 4 plasmid libraries.

3.2.2 Replacement of the wild-type ribosome by Ribo-T v2.0

SQ171 and SQ171fg cells harboring the pCSacB plasmid were transformed with the Ribo-T v2.0 library preparations (Supplemental Fig. S1). In brief, 20 ng of plasmid was added to 50 μ L of electrocompetent cells. Cells were resuspended in 800 μ L of SOC and incubated for 1 hour at 37°C with shaking. A 250 μ L aliquot of recovering cells was transferred to 1.85 mL of SOC supplemented with 50 μ g mL⁻¹ of carbenicillin and 0.25% sucrose (final concentrations) and grown overnight at 37°C with shaking. Cells were spun down and plated on LB agar plates containing 50 μ g mL⁻¹ carbenicillin, 5% sucrose and 1 mg mL⁻¹ erythromycin.

3.2.3 Selecting mutants, evaluating growth rate and analyzing tethers

Colonies that appeared after 24–48 hour incubation of the plates at 37°C were inoculated in a Costar flat bottom 96-well plate containing 100 μL of LB supplemented with 50 $\mu\text{g mL}^{-1}$ carbenicillin and 1 mg mL^{-1} erythromycin. Growth rates were monitored at 37°C in a BioTek microplate reader. Absorbance at 600 nm was read every 10 minutes (continuous linear shaking with a 2-mm amplitude). Doubling times were calculated from the growth curve readings during logarithmic growth as determined by regression.

The fastest growing tether mutants were inoculated in 2 mL LB supplemented with 50 $\mu\text{g mL}^{-1}$ carbenicillin, 5% sucrose and 1 mg mL^{-1} erythromycin and grown for 24–48 hr. Plasmids were isolated from clones and tethers were sequenced (Northwestern Sequencing Core). Tether composition and library diversity were analyzed by sequencing with primers 5'- GCTGTCGTCAGCTCGTGTG-3' for T1 site and 5'-CTGGAGAACTGAGGGG-3' for T2 site.

3.2.4 Total RNA analysis of tethered Ribo-T v2.0.

Successful replacement of the wild type of pCSacB plasmid with the pRibo-T plasmids carrying Ribo-T v2.0 was confirmed via total RNA extraction. Total RNA was extracted from these clones using RNeasy Mini Kit (Qiagen) and analyzed by agarose gel electrophoresis (Supplemental Fig S2).

3.2.5 Selection of new orthogonal pairs

Before selection could be carried out for a highly orthogonal and active 16S/mRNA pair, the BL21(DE3) Δ upp strain was prepared by deleting the genomic copy of *upp* from a naïve BL21(DE3) strain using Datsenko-Wanner recombination⁸³ and replacement with a KanR cassette. The deletion cassette was PCR amplified from pKD4 plasmid⁸³ with primers AATCCGTCGATTTTTTTTGTGGCTGCCCTCAAAGGAGAAAGAGTTGTGTAGGCTGGAGCTGCTTC and AAAAAAAGCCGACTCTTAAAGTCGGCTTTAATTATTTTTATTCTGTCCATATGAATATCCTCCTTAG, with Phusion polymerase (NEB) and 98 °C initial denaturing for 3 min, (98 °C 30 seconds, 55 °C 30 seconds, 72 °C 2 minutes)x25, and 72 °C final extension for 10 minutes. Plasmid pCP20 was transformed into a kanamycin-resistant colony to remove the KanR cassette by the incorporated flippase sites⁸³. Transformed cells were plated on LB agar supplemented with 50 μ g ml⁻¹ carbenicillin and grown overnight at 30 °C. Colonies were picked, plated on LB agar plates, and grown overnight at 42 °C to select for loss of pCP20 plasmid. Colonies were checked for kanamycin sensitivity, and deletion was confirmed by sequencing of PCR product from colony PCR using primers TGCCAGGGTAAAGGTTAG and GACGGTTGCACCAAAC, and Multiplex PCR mix (Qiagen), flanking the deletion site.

For plasmid compatibility with the rRNA pAM552 plasmid backbone, the origin of replication on pLpp5oGFP⁴¹ was first switched from pMB1 to p15A. Plasmid origin of replication p15A was synthesized by IDT as a gBlock (Supplementary Table 3.S1), and amplified using primers GATGGCCTTTTTGCGTTTC and CTGAGAGTGCACCATACAG with Phusion polymerase (NEB) and 98 °C initial denaturing for 3 min, (98 °C 30 seconds, 55 °C 30 seconds, 72 °C 30 seconds)x25, and 72 °C final extension for 10 minutes. Plasmid pT7wtK⁴¹ was amplified with primers GGATCTGTATGGTGCCTC and TGTAGAAACGCAAAAAGGCCATC with 98 °C initial denaturing for 3 min, (98 °C 30 seconds, 55 °C 30 seconds, 72 °C 2 minutes)x25, and 72 °C final extension for 10 minutes. Following digestion with

DpnI (NEB), correct sized DNA was gel extracted from a 0.7% agarose gel with E.Z.N.A. gel purification kit (Omega). Using Gibson assembly⁸⁴, 50 ng of backbone was recircularized with 3-fold molar excess of p15A insert and transformed into DH5 α electrocompetent cells, plated on LB agar plates supplemented with 30 $\mu\text{g ml}^{-1}$ kanamycin and isolated for sequence confirmation.

Next, *cat-upp* gene was prepared from pRepCM3 plasmid⁸⁵, containing an internal TAG codon for amber suppression. The TAG codon was mutated back to CAA with inverse PCR using primers CACCCTTGTTACACCGTTTTCCATGAGCAAAACTGAAACGTTTTCATCGCTC and CTCATGGAAAACGGTGTAAAC, pRepCM3 template, and Phusion polymerase (NEB) with 98 °C initial denaturing for 3 min, (98 °C 30 seconds, 55 °C 30 seconds, 72 °C 105 seconds)x25, and 72 °C final extension for 10 minutes. PCR product was gel extracted from a 0.7% agarose gel with E.Z.N.A. gel extraction kit (Omega), and recircularized with Gibson assembly⁸⁴. Recircularized plasmid was transformed into DH5 α electrocompetent cells and plated on LB agar plates supplemented with tetracycline at 20 $\mu\text{g ml}^{-1}$.

P_{trp} promoter through the *cat-upp* was amplified from pRepCM-CAA with primers GGTGGTGATCTGTGCACTTCAAAAATCGATG and GGTGGTGCGGCCCAAGCTTCGAATCTTTATTTTCG, adding BglII and NotI sites respectively (underlined), with Phusion polymerase (NEB) with 98 °C initial denaturing for 3 min, (98 °C 30 seconds, 55 °C 30 seconds, 72 °C 1 min)x25, and 72 °C final extension for 10 minutes. Plasmid pT7wtK-p15A and column purified PCR product (E.Z.N.A. cycle pure kit from Omega) were digested with BglII and NotI (NEB) for 1 hour at 37 °C, and gel extracted with E.Z.N.A. gel extraction kit (Omega). 50 ng of pT7wtK-p15A backbone was ligated with 3-fold molar excess P_{trp}-*cat-upp* insert with T4 ligase (NEB) for 14 hours at 16 °C. Product was transformed into DH5 α electrocompetent cells and plated on LB agar plates supplemented with kanamycin at 30 $\mu\text{L ml}^{-1}$. Plasmids were isolated with E.Z.N.A. miniprep kit (Omega) and sequence confirmed. T7 promoter was then deleted using inverse PCR with phosphorylated primers GTGCACTTCAAAAATCGATG and

GGATCCGTCGACCTGCAG with Phusion polymerase (NEB) with 98 °C initial denaturing for 3 min, (98 °C 30 seconds, 55 °C 30 seconds, 72 °C 3 min)x25, and 72 °C final extension for 10 minutes. Following gel extraction with E.Z.N.A. gel extraction kit (NEB) product was ligated with T4 ligase (NEB) for 14 hours at 16 °C, and transformed into DH5 α electrocompetent cells and plated on LB agar plates supplemented with kanamycin at 30 μ L ml⁻¹. Plasmids were isolated with E.Z.N.A. miniprep kit (Omega) and sequence confirmed. This plasmid is named pPtrp-catupp-p15A.

Plasmid pPtrp-p15A (Δ catupp) was prepared from pPtrp-catupp-p15A by PCR with primers AAGAATTCGAAGCTTGG (forward primer binding at the 3' end of *cat-upp* gene, including a NotI restriction site in PCR product) and GCATCAGCGGCCGCAACGCTGCGTAGCAACAGATCTCCTCCTTATGAAAGCGAC (reverse primer binding at 5' end of gene), adding a BglII/NotI cloning site. Following column purification (E.Z.N.A. cycle pure kit, Omega), product was digested with NotI (NEB), gel extracted (E.Z.N.A gel extraction kit, Omega), and ligated with T4 ligase (NEB) for 14 hours at 16 °C. Product was transformed into DH5 α electrocompetent cells and plated on LB agar plates supplemented with kanamycin at 30 μ L ml⁻¹. Plasmids were isolated with E.Z.N.A. miniprep kit (Omega) and sequence confirmed.

Plasmid plpp5-catupp-p15A was prepared from plasmid pPtrp-catupp-p15A and synthesized gBlock (IDT) lpp5-oRBS-BglII (Supplementary Table 3.S1). First, pPtrp-catupp-p15A was amplified with primers CACTGGATATACCACCGTTG and GGAAAGCCACGTTGTGTCTC. The linear product is pPtrp-catupp-p15A excluding the Ptrp promoter. Promoter lpp5 with orthogonal ribosome binding site and BglII restriction site⁴¹ was amplified from gBlock lpp5-oRBS-BglII with primers GAGACACAACGTGGCTTTCC and CAACGGTGGTATATCCAGTG. Both PCRs were run with Phusion polymerase (NEB) with 98 °C initial denaturing for 3 min, (98 °C 30 seconds, 55 °C 30 seconds, 72 °C 90 seconds)x25, and 72 °C final extension for 10 minutes. Following gel extraction from 0.7% agarose gel with E.Z.N.A. gel extraction

kit (Omega), 50 ng of backbone was recircularized with 3-fold molar excess of lpp5-oRBS-BglII insert using Gibson assembly⁸⁴. Product was transformed into DH5 α electrocompetent cells, plated in LB plates supplemented with 30 $\mu\text{g ml}^{-1}$ kanamycin, incubated at 37 °C and plasmids isolated and sequenced.

Selection conditions for BL21(DE3) Δ upp were determined using pPtrp-catupp-p15A plasmid with the wild-type Shine-Dalgarno sequence (Supplementary Fig. 3.S5). Two colonies each of BL21(DE3) Δ upp transformed with pPtrp-catupp-p15A (*cat-upp*) or pPtrp-p15A (Δ *cat-upp*) were grown in LB supplemented with kanamycin at 30 $\mu\text{g ml}^{-1}$ at 37 °C overnight with shaking. Fresh LB-kanamycin (30 $\mu\text{g ml}^{-1}$) was inoculated 1/50 with overnight culture and grown for 3 hours at 37 °C with shaking. Cultures were normalized to 0.1 OD and 1 μL was plated on i) M9 minimal media agar plates supplemented with 0.2% casamino acids, 0.4% glucose, 30 $\mu\text{g ml}^{-1}$ kanamycin and 5-fluorouracil at concentrations 0, 0.25, 0.5, 0.75, 1, 2.5, 5, 10 and 50 $\mu\text{g ml}^{-1}$, and ii) LB-agar plates supplemented with 30 $\mu\text{g ml}^{-1}$ kanamycin and chloramphenicol at concentrations 0, 5, 10, 25, 50, 75, 100, 150 and 200 $\mu\text{g ml}^{-1}$. Plates were incubated at 37 °C for 18 hours and imaged (Supplementary Fig S5).

For selection, the Shine-Dalgarno site on plasmid plpp5-catupp was fully randomized by PCR mutagenesis using Phusion (NEB), primers GCATCAAGATCTATGGAGAAAAAATCACTGG and CGAGTCCAGATCTNNNNNNGAAAAATAACAGATATAGAATTG (IDT), and plpp5-catupp template, with 98 °C initial denaturing for 3 min, (98 °C 30 seconds, 55 °C 30 seconds, 72 °C 90 seconds)x25, and 72 °C final extension for 10 minutes. Following DpnI (NEB) digestion for 1 hour at 37 °C, PCR product was column purified with E.Z.N.A. cycle pure kit (Omega). Product was digested with BglII (NEB) for 1 hour at 37 °C, and purified by gel extraction using E.Z.N.A. gel extraction kit (Omega). Linear product was re-circularized with T4 ligase (NEB) for 14 hours at 16 °C.

Ligated product was transformed into DH5 α cells (NEB), and plated on LB-agar plates supplemented with 30 $\mu\text{g ml}^{-1}$ kanamycin and incubated overnight at 37 $^{\circ}\text{C}$. Transformation and plating was repeated until colony counts exceeded 3x library size. Plates were then washed and miniprepmed to generate a plasmid library. Two μL of purified plasmid library was transformed into electrocompetent BL21(DE3) Δupp and plated on M9 minimal media agar plates supplemented with 0.2% casamino acids, 0.4% glucose, 10 $\mu\text{g ml}^{-1}$ 5-FU, 30 $\mu\text{g ml}^{-1}$ kanamycin and 0.1 mM isopropyl- β -D-thiogalactopyranoside (IPTG). Plates were incubated for 24 hours at 37 $^{\circ}\text{C}$. Plates were washed and the pellet was washed three times with LB-Lennox supplemented with 30 $\mu\text{g ml}^{-1}$ kanamycin, and used to inoculate 500 ml LB-Lennox supplemented with 30 $\mu\text{g/ml}$ kanamycin to prepare electrocompetent cells.

In a first round of selection, the anti-Shine-Dalgarno of pAM552-LT, encoding for wild-type untethered ribosomes, was fully randomized for a library of 4,096 theoretical members. Specifically, pAM552-LT aSD was fully randomized by PCR mutagenesis using Phusion (NEB), primers GCATCAGGTAACCGTAGGGGAACCTGCGGTTGGATCANNNNNTACCTTAAAGAAGCGTAC and CCCTACGGTTACCTTGTTACG (IDT), with 98 $^{\circ}\text{C}$ initial denaturing for 3 min, (98 $^{\circ}\text{C}$ 30 seconds, 55 $^{\circ}\text{C}$ 30 seconds, 72 $^{\circ}\text{C}$ 2 minutes)x25, and 72 $^{\circ}\text{C}$ final extension for 10 minutes. PCR product was column purified with E.Z.N.A. cycle pure kit (Omega), and digested with BstEII and DpnI (NEB) for 1 hour at 37 $^{\circ}\text{C}$, and purified by gel extraction using E.Z.N.A. gel extraction kit (Omega). Linear product was recircularized with T4 ligase (NEB) for 14 hours at 16 $^{\circ}\text{C}$. Ligated product was transformed into POP2136 electrocompetent cells, and plated on LB-agar plates supplemented with 50 $\mu\text{g ml}^{-1}$ carbenicillin and incubated overnight at 30 $^{\circ}\text{C}$. Transformation and plating was repeated until colony counts exceeded 3x library size. Plates were then washed and miniprepmed to generate a plasmid library.

The library was transformed into BL21(DE3) Δ upp cells containing the negatively selected mRNA library. Cells were recovered in 1 ml SOC, and used to inoculate 50 ml LB supplemented with 30 $\mu\text{g/ml}$ kanamycin, 50 $\mu\text{g ml}^{-1}$ carbenicillin and 1 mM IPTG. Cultures were grown for 3 hours at 37 $^{\circ}\text{C}$ with shaking at 250 rpm. One ml aliquots were plated on LB agar plates supplemented with 30 $\mu\text{g/ml}$ kanamycin, 50 $\mu\text{g/ml}$ carbenicillin, 1 mM IPTG and 100 $\mu\text{g ml}^{-1}$ chloramphenicol. Surviving colonies were picked and grown in 96 deep-well format in 750 μL LB media supplemented with 50 $\mu\text{g ml}^{-1}$ carbenicillin and 30 $\mu\text{g ml}^{-1}$ kanamycin at 37 $^{\circ}\text{C}$ for 18 hours. Total plasmids were extracted with ZyppyTM-96 plasmid miniprep kit (Zymo Research).

To isolate the pAM552-LT rRNA plasmid and plpp5-catupp reporter plasmids from the total plasmid pool, we identified unique restriction sites on each plasmid that is absent from the other (KpnI present on pAM552-LT, BamHI present on plpp5-catupp). To isolate pAM552-LT, we digested the total plasmid pool with BamHI-HF restriction enzyme (NEB), transformed the digestion pool into POP2136 CaCl₂ chemically competent cells, and plated on LB agar plates supplemented with 50 $\mu\text{g ml}^{-1}$ carbenicillin and grown overnight at 30 $^{\circ}\text{C}$. To isolate plpp5-catupp, total plasmids were digested with KpnI restriction enzyme (NEB), and transformed into DH5alpha CaCl₂ chemically competent cells, and plated on LB agar plates supplemented with 30 $\mu\text{g ml}^{-1}$ kanamycin and grown overnight at 37 $^{\circ}\text{C}$.

Individual plasmids were isolated with E.Z.N.A. miniprep kit (Omega) for sequencing of the Shine-Dalgarno region of plpp5-catupp, and the anti-Shine-Dalgarno region of pAM552-LT (NU genomics core). CaCl₂ chemically competent BL21(DE3) Δ upp cells containing pAM552 plasmid were transformed with the plpp5-catupp isolated members, and plated on LB agar plates supplemented with 50 $\mu\text{g ml}^{-1}$ carbenicillin and 30 $\mu\text{g ml}^{-1}$ kanamycin and grown overnight at 37 $^{\circ}\text{C}$. Pair performance was initially evaluated by plating cells on a range of chloramphenicol. Colonies were picked into 100

μL of LB supplemented with $50 \mu\text{g ml}^{-1}$ carbenicillin and $30 \mu\text{g ml}^{-1}$ kanamycin and grown to saturation overnight at 37°C with shaking. Cultures were diluted 1/50 into fresh LB supplemented with $50 \mu\text{g ml}^{-1}$ carbenicillin, $30 \mu\text{g ml}^{-1}$ kanamycin and 1 mM IPTG and grown at 37°C with shaking for 3 hours. LB-agar plates supplemented with $50 \mu\text{g ml}^{-1}$ carbenicillin, $30 \mu\text{g ml}^{-1}$ kanamycin, 0.1 mM IPTG and chloramphenicol at 0, 0.5, 1, 2.5, 10, 20, 40, 60, 80, 100, 200, 300, 400 or $500 \mu\text{g ml}^{-1}$ were spot plated with 1 μL of induced culture and incubated at 37°C for 18 hours. Max chloramphenicol concentration with growth was noted (Supplementary Fig. 3.S6a).

Reporter plasmids from top performing pairs were pooled and transformed into fresh BL21(DE3) Δupp strain. Cells were plated on LB agar plates supplemented with $30 \mu\text{g ml}^{-1}$ kanamycin and grown overnight at 37°C . Plates were washed and the pellet was washed three times with LB-Lennox supplemented with $30 \mu\text{g ml}^{-1}$ kanamycin, and used to inoculate 500 ml LB-Lennox supplemented with $30 \mu\text{g ml}^{-1}$ kanamycin to prepare electrocompetent cells.

With version 2 tethers evolved and characterized, the improved tether sequences were cloned into poRibo-T2 plasmid⁴¹, named pORT1A. The anti-Shine-Dalgarno sequence of pORT1A was randomized with the protocol described above, and passaged through POP2136 cells at 30°C (expression from p_{LT} promoter repressed). Positive selection was repeated as previously described in the first round. Total plasmid was extracted from colonies using the ZyppyTM-96 plasmid miniprep kit (Zymo Research). Reporter and rRNA plasmids were isolated with KpnI and BamHI-HF digestion, respectively, as before.

3.2.6 Evaluation of new orthogonal pairs

Plasmid plpp5.A.cat was prepared by digesting plasmid plpp5.A.gfp with BglIII (NEB) and NotI (NEB), restriction sites flanking the *sf-gfp* coding sequence. Backbone was purified by gel extraction using E.Z.N.A. gel extraction kit (Omega). PCR was performed on template pAM552C (Mankin Lab) using primers GGTGGTTAGATCTATGGAAAAAAAAATCACCGG and GGTGGTGCGGCCGCCTTATTAGGCGGGCTAGG (BglIII and NotI restriction sites underlined) with Phusion polymerase (NEB) with 98 °C initial denaturing for 3 min, (98 °C 30 seconds, 55 °C 30 seconds, 72 °C 2 minutes)x25, and 72 °C final extension for 10 minutes.

For the superfolder green fluorescent protein (*sf-gfp*) assay, 3 colonies for each pair were picked and grown to saturation at 37 °C. Fresh LB supplemented with 30 µg/ml kanamycin, 50 µg/ml carbenicillin and 1 mM IPTG was inoculated with 1/50 saturated culture and grown at 37 °C for 18 hours on Biotek Synergy H1 plate reader with linear shaking at 2 mm. OD₆₀₀ and 485/528 excitation/emission were monitored.

For chloramphenicol acetyltransferase (*cat*) assay, 3 colonies for each pair were picked and grown to saturation at 37 °C. Fresh LB supplemented with 30 µg/ml kanamycin, 50 µg/ml carbenicillin and 1 mM IPTG was inoculated with 1/50 saturated culture and grown at 37 °C for 3 hours. 96 well plates containing 100 µL LB supplemented with 30 µg/ml kanamycin, 50 µg/ml carbenicillin and 1 mM IPTG, and 0, 0.5, 1, 2.5, 5, 10, 20, 30, 40, 50, 60, 70, 100, 150, 200 or 300 µg/ml chloramphenicol were inoculated with 1/100 induced culture. Plates were incubated for 18 hrs at 37 °C with shaking. OD₆₀₀ was read on BioTek Synergy H1 plate reader, and IC₅₀ values determined (Fig. 3.5d).

3.2.7 Non-canonical amino acid incorporation with Ribo-T

Strain construction for ncAA incorporation with orthogonal ribosome

Strain C321. ΔA ⁸⁶ contains cI repressor, which represses p_L promoter driving expression of the rRNA constructs. Therefore, the strain was prepared for used in the following experiments. Firstly, mutS⁻ genotype was mutated back to mutS wild-type (mutS⁺) by multiplex advanced genome engineering⁸⁷ and the MAGE oligo
 accccatgagtgcfaatagaaaatttcgacgcccatacgcacatgatgcagcagtatctcaggctgaaagcccagcatcccagatc
 ctgc. Mutations to mutS⁺ were screened with colony PCR and primers CATGATGCAGCAGTATCTCAG and
 5'-CTTCTGCATACAGCAGTTC and confirmed by sequencing.

To remove cI repressor, the λ -red machinery and the *bla* resistance marker, a kanamycin knockout cassette was generated from pKD4 plasmid⁸³ with primers
 GTATGTCGTTTCAGCTAAACGGTATCAGCAATGTTTATGTAAAGATGTGTAGGCTGGAGCTGCTTC and
 TTTGCCGACTACCTTGGTGATCTCGCCTTTCACGTAGTGGACAAAGTCCATATGAATATCCTCCTTAG with Phusion
 polymerase and 98 °C initial denaturing for 3 min, (98 °C 30 seconds, 55 °C 30 seconds, 72 °C 30
 seconds)x25, and 72 °C final extension for 10 minutes. Product was column purified with E.Z.N.A.
 cycle pure kit (Omega). Expression of λ -red machinery was induced with 15 minute incubation at 42
 °C, and electrocompetent cells were prepared. KanR knockout cassette was electroporated into the
 cells, plated on LB agar supplemented with 30 $\mu\text{g ml}^{-1}$ kanamycin and incubated overnight at 42 °C to
 select against heat-induced toxic expression of λ -red cassette. Kanamycin resistant colonies were
 screened for sensitivity to carbenicillin, indicating loss of *bla*. A sensitive colony was picked and
 transformed with pCP20 plasmid for removal of kanamycin marker by the incorporated flippase sites
⁸³. Transformed cells were plated on LB agar supplemented with 50 $\mu\text{g ml}^{-1}$ carbenicillin and grown
 overnight at 30 °C. Colonies were picked, plated on LB agar plates, and grown overnight at 42 °C to

select for loss of pCP20 plasmid. Colonies were checked for kanamycin sensitivity, and deletion was confirmed by sequencing of PCR product from colony PCR using primers GCCGACTCTATATCTATACCTTCATC and 5'-GCAACCGAGCGTTCTGAAC, and Multiplex PCR mix (Qiagen), flanking the deletion site. Furthermore, this strain has *upp* gene knocked out using the same methodology described in preparing the BL21(DE3) Δ *upp* strain above. This strain is named MCJ.1217.

Combined orthogonal ribosome-sf-gfp reporter system

The orthogonal *sf-gfp* cassette was amplified from plpp5.B.gfp template with primers AGAGTTGCGATCCCCTTGTATTACTGTTTATGTAAGC and AAGAGTT**GCGCGCC**AAAAAAAAGCCCGCCTTTCGGCGGGCTTGTATTTTTTCGAACTGCGGATG for forward orientation, and primers AGAGTT**GCGCGCC**CTTGTATTACTGTTTATGTAAGC and AAGAGTTGCGATCCAAAAAAAAGCCCGCCTTTCGGCGGGCTTGTATTTTTTCGAACTGCGGATG for reverse orientation using Phusion polymerase (NEB) with 98 °C initial denaturing for 3 min, (98 °C 30 seconds, 55 °C 30 seconds, 72 °C 2 min)x25, and 72 °C final extension for 10 minutes. Added BamHI restriction site is underlined, added AscI restriction site is bolded, and t500 terminator is italicized. Plasmid backbones were amplified from plasmids pAM552, pO2 or pORT3 with primers 5'-CCTGTCGTCATATCTACAAG flanking the AscI restriction site and 5'-AAGAGTTGCGATCCTGTAGAAACGAAAAAGGCCATC, adding in a BamHI restriction site, using Phusion polymerase (NEB) with 98 °C initial denaturing for 3 min, (98 °C 30 seconds, 55 °C 30 seconds, 72 °C 2 min)x25, and 72 °C final extension for 10 minutes. PCR products were individually purified by E.Z.N.A. cycle pure kit (Omega), and digested with BamHI-HF and AscI (NEB) for 1 hour at 37 °C. Digestion products were purified by gel extraction with 1% agarose gel and E.Z.N.A. gel extraction kit (Omega), and ligated in combination (Supplementary Fig S10a) with 25 ng of rRNA backbones and 25 ng of *sf-gfp* inserts assembled via ligation with T4 DNA ligase (NEB).

Two μL of the ligation products were transformed into POP2136 cells via electroporation, plated on LB-agar supplemented with $50 \mu\text{g ml}^{-1}$ carbenicillin, and grown overnight at 30°C . Plasmids were purified from colonies with E.Z.N.A. miniprep kit (Omega), and sequence-confirmed (Northwestern Sequencing Core). Plasmids constructed are named pAM.B.gfp-f, pAM.B.gfp-r, pO2B.gfp-f, pO2B.gfp-r, pORT3B.gfp-f and pORT3B.gfp-r.

Six replicates of each construct were picked and grown to saturation at 30°C in LB supplemented with $50 \mu\text{g/ml}$ carbenicillin. Fresh LB supplemented with $50 \mu\text{g/ml}$ carbenicillin, was inoculated with 1/50 volume saturated culture and grown at 30°C for 4 hours, then 42°C for 12 hours in the Biotek Synergy H1 plate reader with linear shaking at 2 mm. OD_{600} and fluorescence (485 nm/528 nm excitation/emission) was monitored.

Incorporation of p-azido-phenylalanine into sfGFP using orthogonal Ribo-T

The integrated ribosome-*sf-gfp* plasmids with the *sf-gfp* gene in the reverse direction relative to rRNA operons were used as the backbone, and amplified with primers 5'-GACCACATGGTTCTGCAC and 5'-CGCTGAATTTGTGACCGTTC with the same PCR conditions as above. Plasmids pDT7sfGFP1TAGTT2 (1TAG) and pDT7sfFP5TAGTT2 (5TAG)⁸⁸ were used as templates with primers 5'-CGGTCACAAATTCAGCGTG and 5'-TTCGTGCAGAACCATGTG with the same PCR conditions as above. PCR products were digested with DpnI (NEB), gel extracted as before, and Gibson assembled⁸⁴ with 50 ng backbone and 3-fold molar excess insert. Two μL of the assembled products were transformed into POP2136 cells via electroporation, plated on LB-agar supplemented with $50 \mu\text{g ml}^{-1}$ carbenicillin, and grown overnight at 30°C . Plasmids were purified from colonies with E.Z.N.A. miniprep kit (Omega), and sequence-confirmed (Northwestern Sequencing Core).

Plasmid pEVOL-pAzF, a gift from Peter Schultz (Addgene plasmid # 31186)⁸⁹, and the sequence-verified plasmid of each ribosome-*sf-gfp* construct were co-transformed into MCJ.1217 cells and plated on LB agar plates supplemented with 50 $\mu\text{g ml}^{-1}$ carbenicillin and 34 $\mu\text{g ml}^{-1}$ chloramphenicol. An initial screen of 6 replicates were picked and tested as described below for *sf-gfp* expression and pAzF incorporation. Of the 6 replicates tested, we observed a bimodal on/off phenotype for *sf-gfp* expression, presumably due to burden of the orthogonal translation systems present. Colonies that exhibited successful *sf-gfp* expression were isolated and 3 replicates of each construct were picked and grown to saturation at 37°C in LB supplemented with 50 $\mu\text{g ml}^{-1}$ carbenicillin and 34 $\mu\text{g ml}^{-1}$ chloramphenicol. Fresh LB supplemented with 50 $\mu\text{g ml}^{-1}$ carbenicillin, 34 $\mu\text{g ml}^{-1}$ chloramphenicol, 0.2% w/v arabinose, 1 mM IPTG, and 1 mM *p*-azido-L -phenylalanine was inoculated with 1/50 volume saturated culture and grown at 37 °C for 18 hours in the Biotek Synergy H1 plate reader with linear shaking at 2 mm. OD₆₀₀ and fluorescence (485 nm/528 nm excitation/emission) was monitored.

3.3 Tether optimization improves growth with Ribo-T

We first seek to improve Ribo-T function by optimizing the tether for length and sequence. The current Ribo-T tether connects the 3' end of 16S helix 44 (h44) to the 5' end of 23S helix 101 (H101) with tether 1 (T1), and the 3' end of H101 to the 5' end of h44 (T2), with remnants of the apex loop and an added 9A/8A for T1/T2, respectively (Fig. 3.2a). We designed and built four libraries towards improving Ribo-T functionality (Fig. 3.2b, Supplementary Fig. 3.S1). Libraries 1 and 2 explore tether length in a paired and unpaired format, respectively, without the apex loop remnants left in our original library design⁴¹. Specifically, library 1 explores tether length with potential base pairing using a 7A-20A tether paired with a 7U-20U tether without apex loop remnants, for a total library size of 196 members. Library 2 explores a dual polyA tether without apex loop remnants ranging from 7A-20A for a total library size of 196 members. Libraries 3 and 4 explore tether sequence with fixed length of the published pRibo-T tether⁴¹. Library 3 keeps the apex loop remnants of the original Ribo-T sequence for an 8N/9N randomized library of 1.7×10^{10} members. To optimize the paired helix-to-helix tether structure without the loop remnants, we created library 4 which fully randomizes the h44-tether-H101 structure for a 15N/10N randomized library of 1.1×10^{15} members.

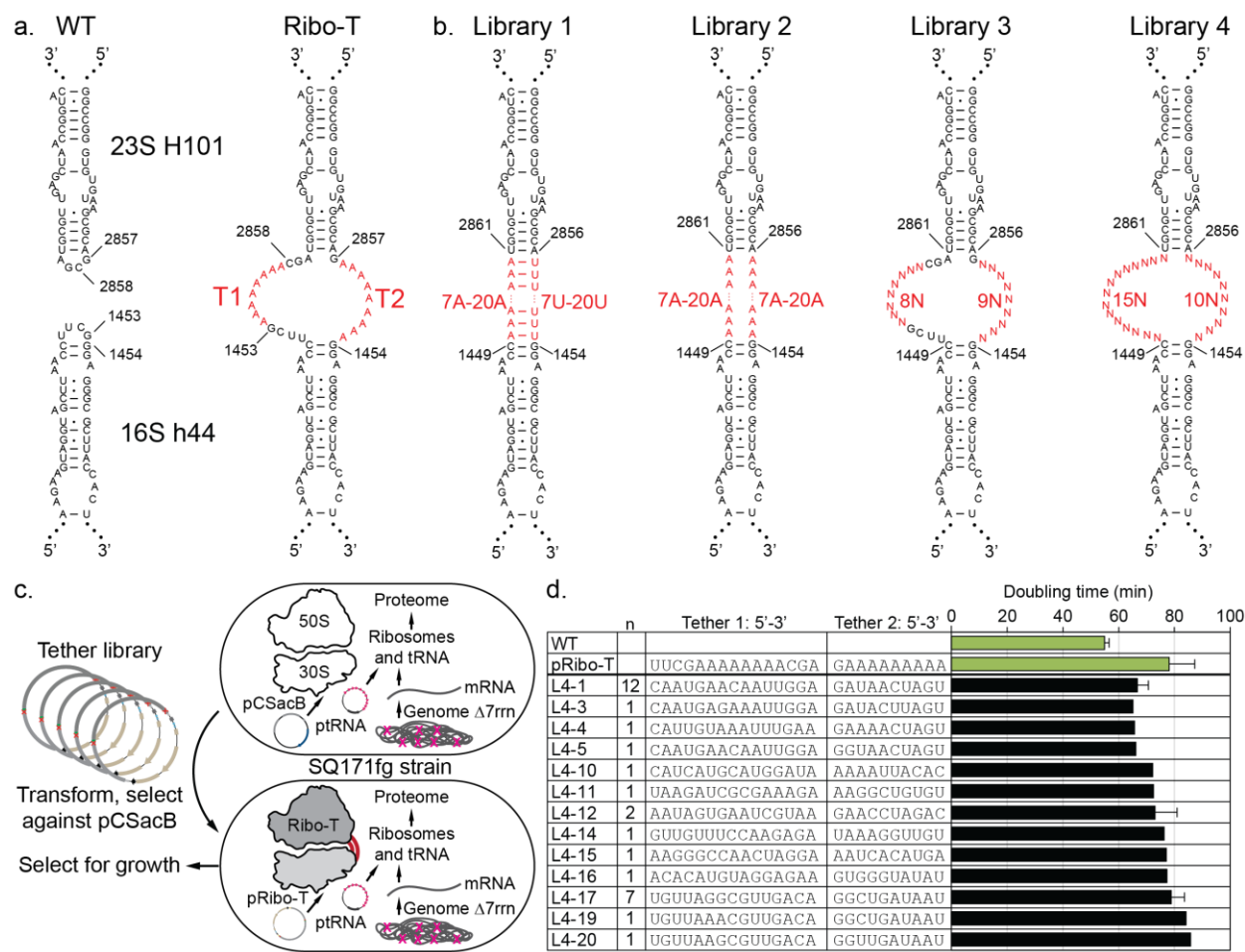


Figure 3.2. Optimizing tether sequence improves performance. a. Wild-type 23S rRNA Helix 101 and 16S rRNA helix 44 are connected to create Ribo-T with 9A for 5' tether, T1, and 8A for 3' tether, T2. b. Library 1: paired 5' tether T1 poly A from 7-20 nucleotides, with 3' tether T2 poly T from 7-20 nucleotides. Library 2: unpaired polyA on both T1 and T2, ranging in 7-20 nucleotides long. Library 3: randomized T1 (8N) and T2 (9N) keeping residues of opened H101 and h44 apex loops. Library 4: randomized apex-to-apex T1 (15N) and T2 (10N) of tether. c. Selection scheme for improved tethers. Strains lacking genomic copies of rRNA operons ($\Delta 7rrn$) are transformed with plasmid-based Ribo-T tether libraries, and the wild-type pCSacB plasmid is removed. d. Doubling time rank and tether sequences of selected library 4 colonies.

The libraries were individually transformed into the SQ171fg strain, and from all libraries, colonies grew in the presence of sucrose indicating the loss of the pCSacB plasmid and support by the tethered ribosome plasmid (Fig. 3.2c). Total RNA gels of a sampling of colonies from each library show the expected dominant Ribo-T size RNA, confirming no significant wild-type ribosome contamination or tether cleavage (Supplementary Fig. 3.S2). Individual colonies were picked from each library, tethers were sequenced, and doubling times were determined (Supplementary Fig. 3.S3). Library 4 had the most members with improved doubling times, and was thus chosen for further analysis.

Colonies (31 total) were picked from library 4 plates, biasing towards larger colonies. Plasmids were extracted for tether sequencing, and doubling times were determined (Fig. 3.2d). The most prevalent tether sequence with $n=12$ exhibited an improved doubling time compared to the original Ribo-T. We call this tether sequence Ribo-T-v2 (Fig. 3.3a). In both liquid culture growth (Fig. 3.3b) and plate growth assays (Fig. 3.3c), cells supported fully by pRibo-T-v2 outperform pRibo-T in both SQ171 and SQ171fg strains. Specifically, in the SQ171fg strain, the pRibo-T-v2 plasmid improves growth rate by 24% and max OD_{600} by 12% as compared to the pRibo-T plasmid. Notably, the benefits are more pronounced in the original SQ171 strain lacking the fast-growing phenotype mutations of SQ171fg strain; growth rates improve by 86%, and max OD_{600} by 70% compared to pRibo-T. Gel electrophoresis of total RNA extracted from cells supported by Ribo-T-v2 plasmids show the expected dominant Ribo-T sized RNA, and the loss of individual 16S and 23S rRNA bands (Fig. 3.3d).

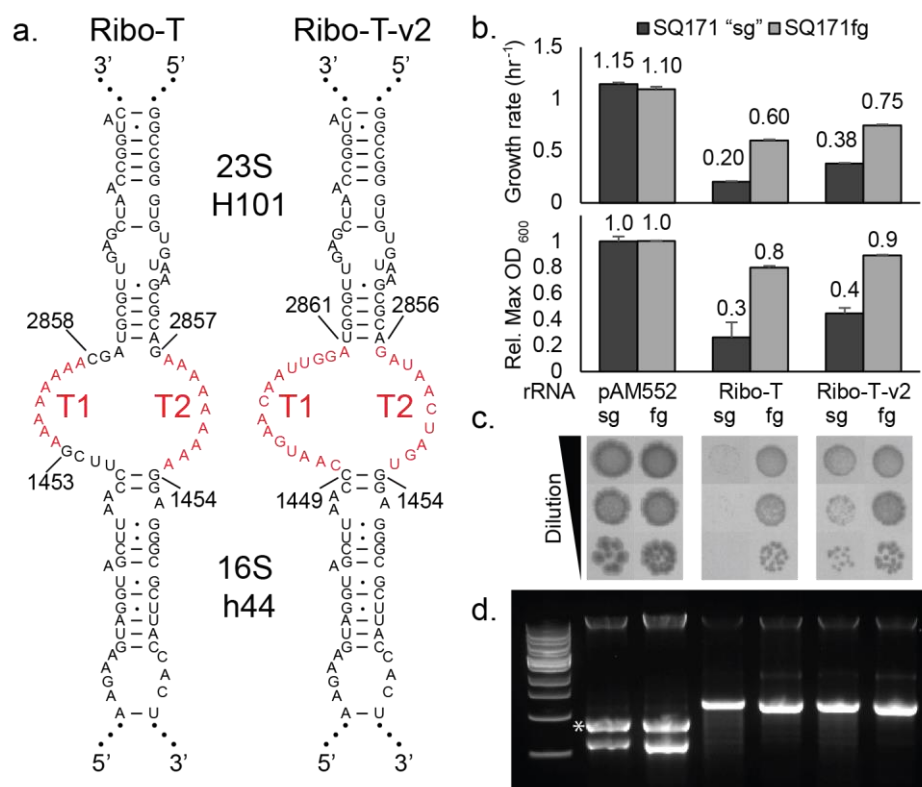


Figure 3.3. Optimizing tether sequence improves performance. a. Ribo-T: previously published tether sequence. Ribo-T-v2: fastest growing and most frequent selected tether sequence. b. Growth rate and max OD₆₀₀ of SQ171 slow growing (sg) and SQ171 fast growing (fg) cells growing with pAM552 (wild-type *rnb* operon), pRibo-T and pRibo-T-v2. c. Spot plated SQ171 and SQ171fg cells growing with pAM552, pRibo-T and pRibo-T-v2 imaged after 48 hours at 37 °C. d. Total RNA extraction from SQ171 and SQ171fg cells growing with pAM552, pRibo-T and pRibo-T-v2.

3.4 Improved orthogonal function

The published orthogonal Ribo-T system⁴¹ utilizes a modified version of previously evolved orthogonal SD/a-SD pairs^{35, 36} which is not optimized for the tethered context or the specific plasmid system used. The selection of highly functional orthogonal 16S-mRNA pairs is achieved through the fusion of two genes enabling both negative and positive selections. The *upp* gene produces uracil phosphoribosyltransferase (UPRT), which causes cell death in the presence of the small molecule 5-fluorouracil (5-FU), which is added to the media for the negative selection. For the positive selection, chloramphenicol acetyltransferase (CAT), encoded by the *cat* gene, conferring resistance to the antibiotic chloramphenicol (Cm). This gene fusion is called *cat-upp* (Supplementary Fig. 3.S4), and was cloned into plasmid vectors under control of medium P_{trp} promoter⁸⁵ and strong lpp5 promoter⁷². The native *E. coli upp* gene was knocked out of BL21(DE3) to generate BL21(DE3) Δ upp. Selection conditions for BL21(DE3) Δ upp were determined using pP_{trp}-catupp-p15A plasmid with the wild-type Shine-Dalgarno sequence (Supplementary Fig. 3.S5). For a strong selection with a high range above background, 10 $\mu\text{g ml}^{-1}$ 5-FU was chosen for the negative selection, and 100 $\mu\text{g ml}^{-1}$ chloramphenicol was chosen for the positive selection. 5-FU concentrations of 1 and 5 $\mu\text{g ml}^{-1}$ were also tried, but did not yield highly orthogonal pairs (data not shown).

The selection process is illustrated in Fig. 3.4a. Firstly, the Shine-Dalgarno sequence of the lpp5 promoter construct plpp5-catupp-p15A was randomized by PCR mutagenesis. These plasmids were subsequently transformed into BL21(DE3) Δ upp cells and plated on M9 minimal media agar plates supplemented with 10 $\mu\text{g/ml}$ 5-FU. Surviving cells contain mRNA that is either not efficiently initiated by endogenous ribosomes, or a non-functional plasmid/transcript. To select active orthogonal pairs, a first round of positive selection was performed wherein the anti-Shine-Dalgarno (aSD) sequence of plasmid-based untethered ribosomes (pAM552-LT vector, Supplementary Fig.

3.S4) was randomized and transformed into the negative selected cells, and plated on LB-agar plates in the presence of 100 $\mu\text{g}/\text{ml}$ chloramphenicol. Surviving colonies were picked, and plasmids were isolated and sequenced. Initial characterization of pair activity was performed using a chloramphenicol resistance assay and the *cat-upp* reporter plasmids. To measure pair orthogonality from the wild-type ribosome pool, each orthogonal mRNA construct was isolated and co-transformed into fresh BL21(DE3) Δupp with the pAM552 plasmid containing the wild-type *rmb* rRNA operon. Cells were plated on a range of chloramphenicol concentrations (0, 0.5, 1, 2.5, 5, 10, 20, 40, 60, 80, 100, 200, 300, 400 and 500 $\mu\text{g ml}^{-1}$), and maximum growth concentrations noted (Supplementary Fig. 3.S6).

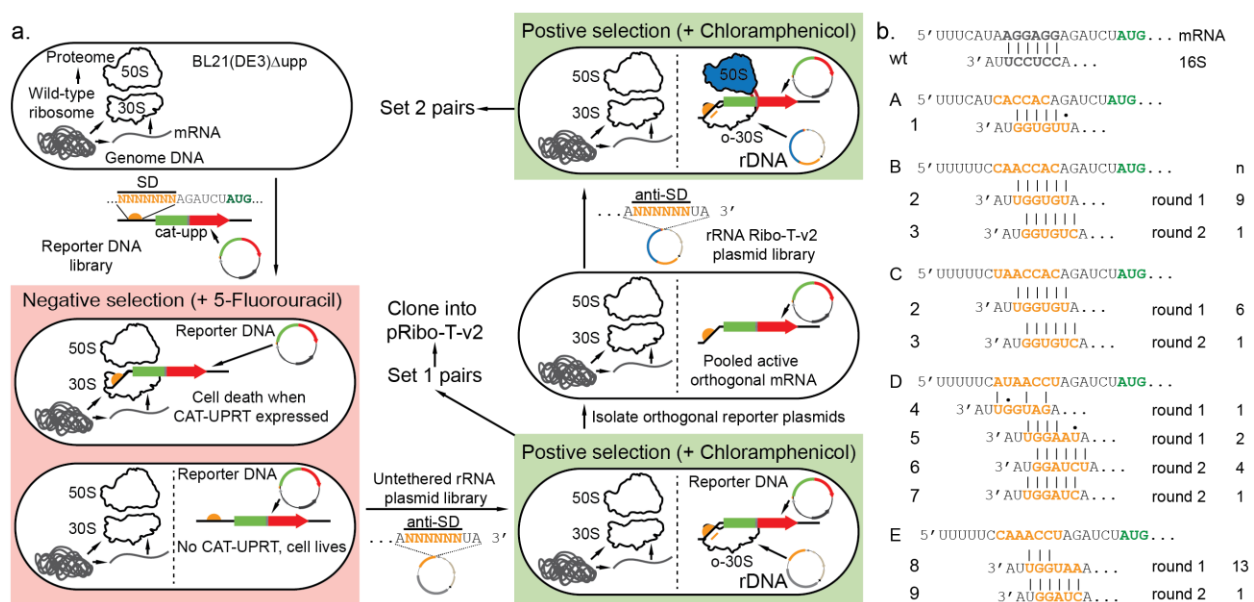


Figure 3.4. Improved orthogonal pairs. a. Selection scheme to optimize orthogonal Shine-Dalgarno (SD) and anti-Shine-Dalgarno (aSD) pairs in untethered and tethered context. b. Top evolved orthogonal mRNA and 16S with predicted pairing. Selection round is noted by “round 1” or “round 2” to the right of each pair. “n” denotes number of isolated members with that sequence from the selection.

A second round of positive selection was performed where top orthogonal active mRNA were isolated, pooled and transformed into the BL21(DE3) Δ upp strain. The aSD sequence on pRibo-T-v2 plasmid was randomized, transformed into BL21(DE3) Δ upp containing top performing orthogonal mRNA, and plated on LB-agar plates supplemented with 100 μ g/ml chloramphenicol. Surviving colonies were picked, and plasmids were isolated and sequenced. Top performing pairs are shown in Figure 3.4b, and were aligned using the RBS calculator ^{90, 91}. Orthogonal Ribo-T constructs with improved v2 tethers are named pORTx.y, where “x” is a number indicating the aSD sequence, and “y” is a letter indicating the corresponding cognate SD sequence. Corresponding rRNA plasmids with untethered ribosomes are named pOx.y.

3.3.1 Evaluation of evolved orthogonal pairs

When evaluating orthogonal pair performance, we consider two key metrics: i) the overall activity of the pair and ii) the orthogonality to wild-type ribosomes. A percent orthogonality is defined:

$$\% \text{ orthogonality} = \frac{A_{\text{pair}} - A_{\text{mRNA}}}{A_{\text{pair}}} * 100$$

Where A_{pair} is the activity of the orthogonal pair (green fluorescence protein fluorescence divided by OD₆₀₀ for the *sf-gfp* assay, and IC₅₀ for the *cat* assay), and A_{mRNA} is the activity of just the orthogonal mRNA expressed without the cognate orthogonal ribosome. The percent orthogonality is shown below each pair in the activity plots in Figure 3.5. With this metric, a higher percentage value is desired, indicating a lower background expression of o-mRNA as compared to the expression with the cognate orthogonal rRNA.

For evaluation of selected orthogonal pairs, SD variants were cloned into plpp5-gfp and plpp5-cat vectors containing super folder green fluorescent protein (*sf-gfp*) and chloramphenicol acetyltransferase (*cat*), respectively. Anti-SD variants were freshly cloned into pRibo-T-v2 plasmid. Plasmids were fully sequenced, and pairs transformed into a naïve BL21(DE3) Δ upp strain for testing. Activity of *sf-gfp* is shown as final fluorescence normalized by the final OD₆₀₀ reading (Fig. 3.5a). Activity of *cat* is given as chloramphenicol IC₅₀ values (Fig. 3.5b). Pair activity is improved in both *sf-gfp* and *cat* assays over the original published oRibo-T system⁴¹ (noted as v1), and the published orthogonal pair cloned with the optimized tether sequences (noted as 1.A). Best performing pairs in BL21(DE3) Δ upp strain are pORT2.B and pORT3.B with o-mRNA B when considering both assays, and metrics of pair activity and orthogonality (Fig. 3.5a and 3.5b).

For plasmids pORT2 and pORT3 paired with plpp5.B.gfp, pair activity increased 154% and 208% over pORT1, respectively. Percent orthogonality also increased 8% and 9%, respectively. For plasmids pORT2 and pORT3 paired with plpp5.B.cat, pair activity increased 77% and 121% over pORT1, respectively. Percent orthogonality increased 19% and 23% over pORT1, respectively. While the plpp5.C.gfp message had higher functionality than plpp5.B.gfp with pORT2 and pORT3, background for plpp5.C.cat was higher, reducing orthogonality (Fig. 3.5a,b).

Orthogonal pairs were also cloned into the naïve untethered rRNA construct pAM552-LT and tested in *sf-gfp* and *cat* assays. Untethered orthogonal function increases from 426% to 1981% (Supplementary Fig. 3.S7a), but with non-significant increases in percent orthogonality since the original system is more active than the tethered system.

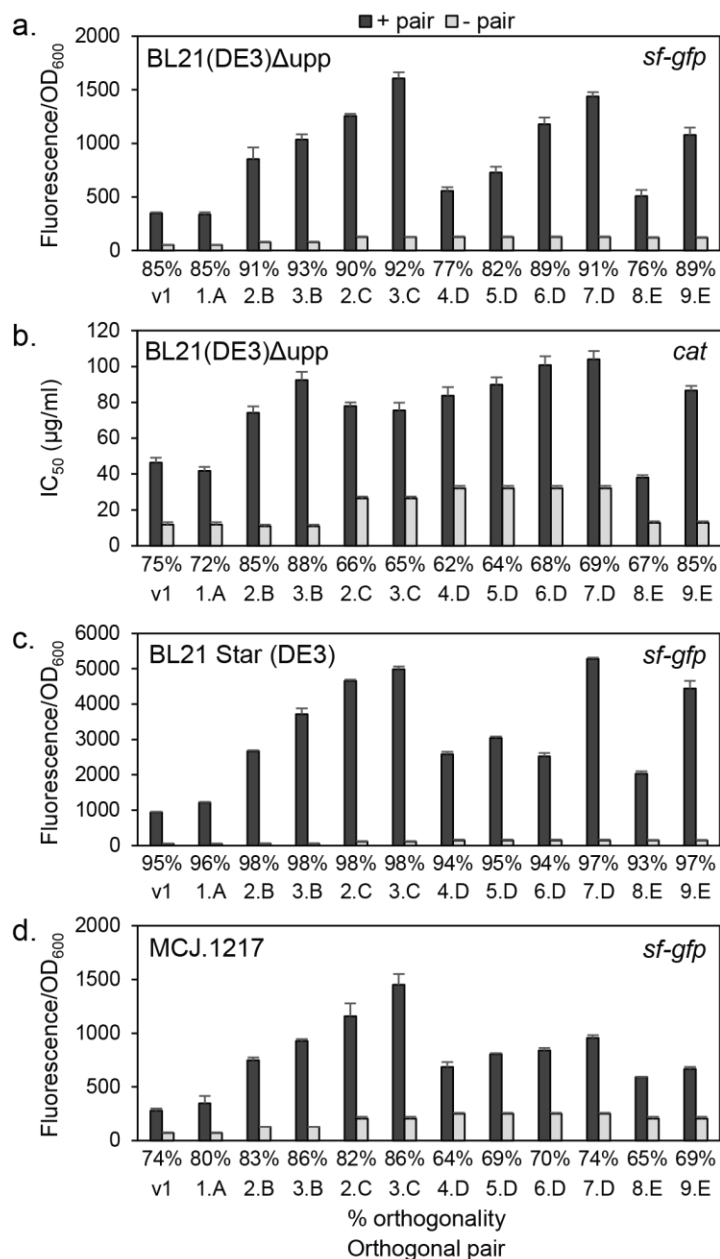


Figure 3.5. Improved orthogonal pair function in Ribo-T-v2. Original orthogonal Ribo-T system denoted by “v1”. a. Orthogonal expression of super folder green fluorescent protein (*sf-gfp*) in BL21(DE3) Δ upp. + pair: both o-rRNA and o-mRNA, - pair: just o-mRNA. % orthogonality shown below column labels. b. Orthogonal expression of chloramphenicol acetyltransferase (*cat*) in BL21(DE3) Δ upp. c. Orthogonal expression of *sf-gfp* in BL21 Star (DE3) strain. d. Orthogonal expression of *sf-gfp* in C321. Δ A derived strain MCJ.1217.

Pair activity in other strains of E. coli

To ensure system functionality in a wide range of strains, top plasmid pairs for the *sf-gfp* reporter set were transformed into BL21 Star (DE3) (Invitrogen) and C321-based strain⁸⁶ (MCJ.1217), and assayed for orthogonal *sf-gfp* activity (Fig. 3.5c and 3.5d respectively). General trends hold with 2.B, 3.B, 2.C and 3.C sets performing better than the original pair with improved orthogonality. Similarly for untethered orthogonal ribosomes, improved pairs perform with similar trends to BL21(DE3) Δ upp in strains BL21 Star (DE3) and C321. Δ A.mutS⁺. Δ λ red. Δ upp (Supplementary Fig. 3.S7b and S7c).

Synergistic effect of evolved tether and orthogonal pairs

To parse out the effects of improved tethers and orthogonal pairs on the improved performance, select orthogonal aSD sequences were cloned into the poRibo-T2 plasmid⁴¹ with original published tether sequences. For *sf-gfp* (Supplementary Fig. 3.S8a), v2 tether and improved orthogonal pairs work synergistically and improve orthogonal function over the v1 tethers up to 55%. The *cat* assay did not show significant difference between v1 and v2 tethers (Supplementary Fig. 3.S8b), presumably because of the less sensitive assay range compared to the *sf-gfp* fluorescence assay.

3.5 Non-canonical amino acid incorporation by a ribosome with tethered subunits

As a first application of the improved orthogonal ribosomes oRibo-T v2.0, we sought to use pORT3 for expanding the genetic code via non-canonical amino acid (ncAA) incorporation. Participating in orthogonal translation of ncAA-containing proteins requires oRibo-T to work cooperatively alongside other orthogonal translation machinery in the cell (orthogonal tRNA and aaRS pair), which has never before been shown. Incorporation of ncAAs into polypeptides have yielded proteins with new side-chain chemistries, with applications ranging from recombinant protein products to insights in fundamental science^{5,21}. For this study, we tested the ability of orthogonal Ribo-T v2 pORT3, in conjunction with a previously reported variant of the *M. jannaschii* TyrRS⁸⁹ (henceforth referred to as pAzFRS) and corresponding tRNA, to site-specifically incorporate *p*-azido-L-phenylalanine (pAzF) into superfolder green fluorescent protein.

To minimize plasmid requirements for non-canonical amino acid incorporation, we combined the ribosomal rRNA and the reporter plasmids into one. Directional orientation of the two expression cassettes from a single plasmid can have a significant impact on system performance⁹²⁻⁹⁴. To determine optimal placement, we constructed combined variants of top orthogonal rRNA/reporter pairs into a single plasmid. Reporter construct *yf-gfp* with orthogonal Shine-Dalgarno 'B' (Fig. 3.4b) under the *lpp5* promoter was cloned into plasmids pAM552, pO2 and pORT3, in the forward and reverse directions (Supplementary Fig. 3.10a). Expression output and strain fitness was determined in POP2136 cells. The cassettes oriented in opposite directions (pO2.B.gfp-r and pORT3.B.gfp-r) had optimal expression and cell fitness characteristics compared to the same orientation (Supplementary Fig. 3.10b).

E. coli strain MCJ.1217, with 321 TAG amber stop codons recoded to TAA, and RF1 knocked out, was used to test a combined orthogonal rRNA-*sf-gfp* plasmid with the pEVOL-pAzF plasmid encoding the mutant *M. jannaschii* TyrRS⁸⁹ and suppressor tRNA pair for incorporation of pAzF. In the opposite direction, the wild-type *sf-gfp* gene was replaced with variants containing 1 or 5 TAG codons at D190 (1 TAG) or D36, K101, E132, D190 and E213 (5 TAG) (Fig. 3.6a, Supplementary Fig. 3.S10c). Plasmids pORT3B.gfp1TAG or pORT3B.gfp5TAG with pAzF added to the growth media gave robust expression of *sf-gfp* containing 1 or 5 TAG above background (Fig. 3.6b). We observe similar expression with the untethered orthogonal ribosome system with plasmids pO2B.gfp1TAG and pO2B.gfp5TAG (Supplementary Fig. S10d). These combined plasmids provide a flexible system for expression of TAG containing proteins in conjunction with orthogonal non-canonical amino acid incorporation systems. Importantly, the integration of a ncAA system with the oRibo-Tv2 system enables *in vivo* 23S rRNA evolution with ncAA orthogonal translation system development.

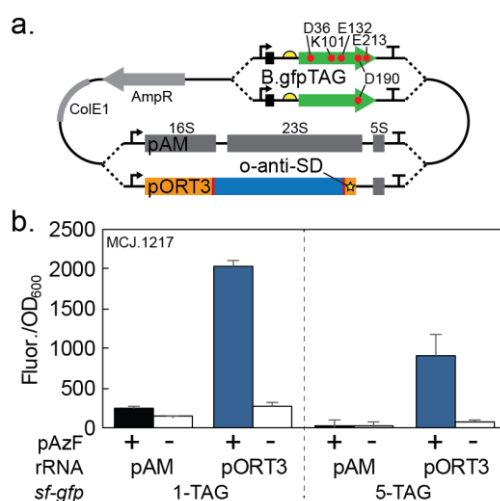


Figure 3.6. Incorporation of non-canonical amino acid p-azidophenylalanine (pAzF) by orthogonal Ribo-T. a. Combined rRNA and *sf-gfp* plasmid with *sf-gfp* gene is replaced with a 1TAG or 5TAG version to create pORT3B.gfp1TAG and pORT3B.gfp5TAG. Wild-type *rrnB* operon was cloned as negative control for background orthogonal expression (pAM.B.gfp1TAG and pAM.B.gfp5TAG). b. Expression of *sf-gfp* with 1TAG or 5TAG in C321.ΔA derived strain MCJ.1217, in the presence of pAzF (+) or without pAzF (-).

3.6 Discussion

In this work, we report significant improvements to the Ribo-T system. Ribo-T-v2 tethers provide a significant improvement to the tethered ribosome performance at the h44/H101 junction. A robustness for tether sequence at the h44/H101 junction was displayed based on members from all 4 libraries being able to support cell growth. This demonstrates a surprising versatility to the Ribo-T design, suggesting that perhaps other tether sites could be explored to further improve Ribo-T performance. One concern is that the 23S rRNA circular permutation at H101 has a doubling time increase simply from this mutation alone (93.7 +/- 4.5 minute doubling time compared to wild-type ribosome 53.9 +/- 1.0 minute doubling time). This could be a fundamental limit to this design architecture, as we were not able to push past this doubling time with this tether site and our libraries. We are therefore interested in exploring other tether sites using less-encumbered 23S rRNA circular permutations found in our previous study⁴¹.

Significant improvements to the orthogonal system were made as well, providing more active and orthogonal pairs compared to the original system. Our system expands the utility of orthogonal gene expression by both orthogonal untethered and tethered ribosomes, theoretically in any bacterial strain, since construct expression does not rely on non-native T7 polymerase as in previous systems. With these range of pair options, a quick screen can be used to find a highly active and orthogonal pair in the desired strain. Furthermore, we demonstrated the ability of the Ribo-T system to incorporate the non-canonical amino acid pAzF into green fluorescent protein containing 1 and 5 TAG internal amber stop codons.

The new Ribo-T version 2.0 will be more versatile and will serve as a better tool for many biotechnological, engineering and basic science applications. Finally, by combining oRibo-T with existing orthogonal translation systems developed for synthetic biology, we showcase its applicability and potential for future efforts in engineering the translation machinery for both engineering and fundamental science applications.

3.7 Acknowledgements, contributions and publishing information

The authors would like to thank Prof. Peter G. Schultz for providing the pEVOL plasmid. We thank Paul D. Carlson for helpful discussions and comments on this manuscript.

This manuscript is being prepared for publication:

Carlson, E.D., d'Aquino, A.E., Kim, D.S., Fulk, E.M., Szal, T., Vazquez-Laslop, N., Mankin, A.S. and Michael C. Jewett (2016) Improvements to a ribosome with tethered subunits for *in vivo* ribosome engineering. *In preparation*.

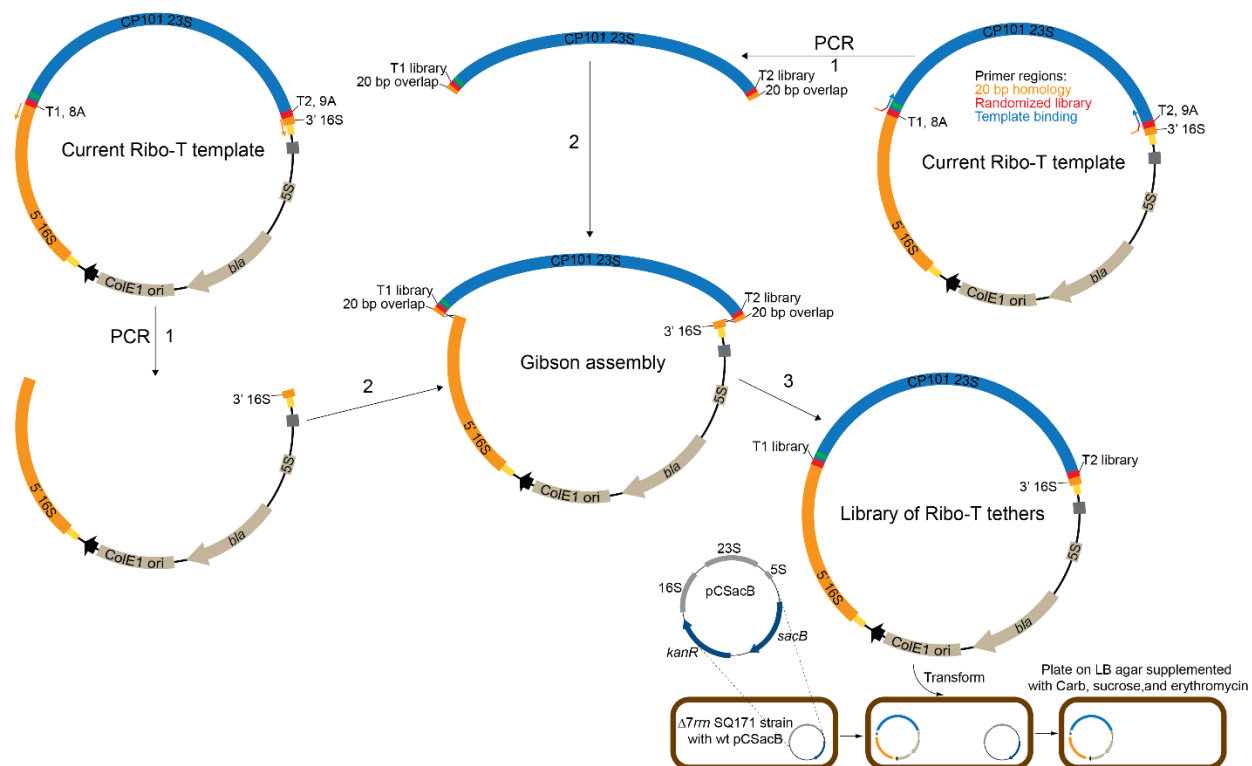
EDC, MCJ, NVL and ASM conceived of the study. EDC and MCJ wrote the manuscript. EDC, AED, EMF and DSK performed experiments and analyzed data.

Patent applications:

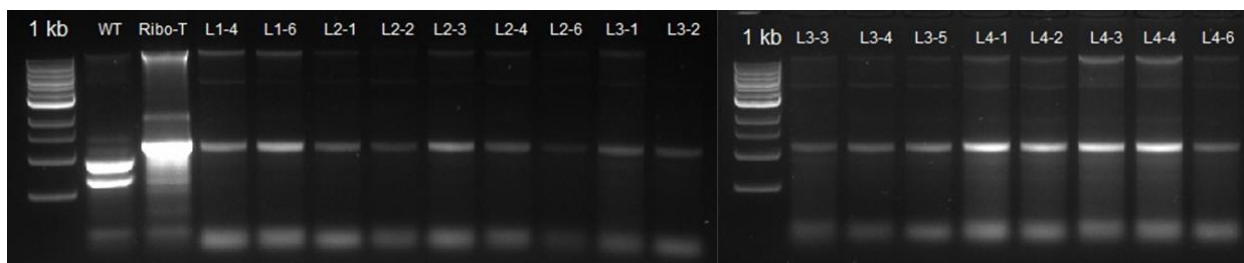
Carlson, E.D., Mankin, A.S. & Jewett, M.C. Improvements to a ribosome with tethered subunits. (2016) US provisional 62/331,784

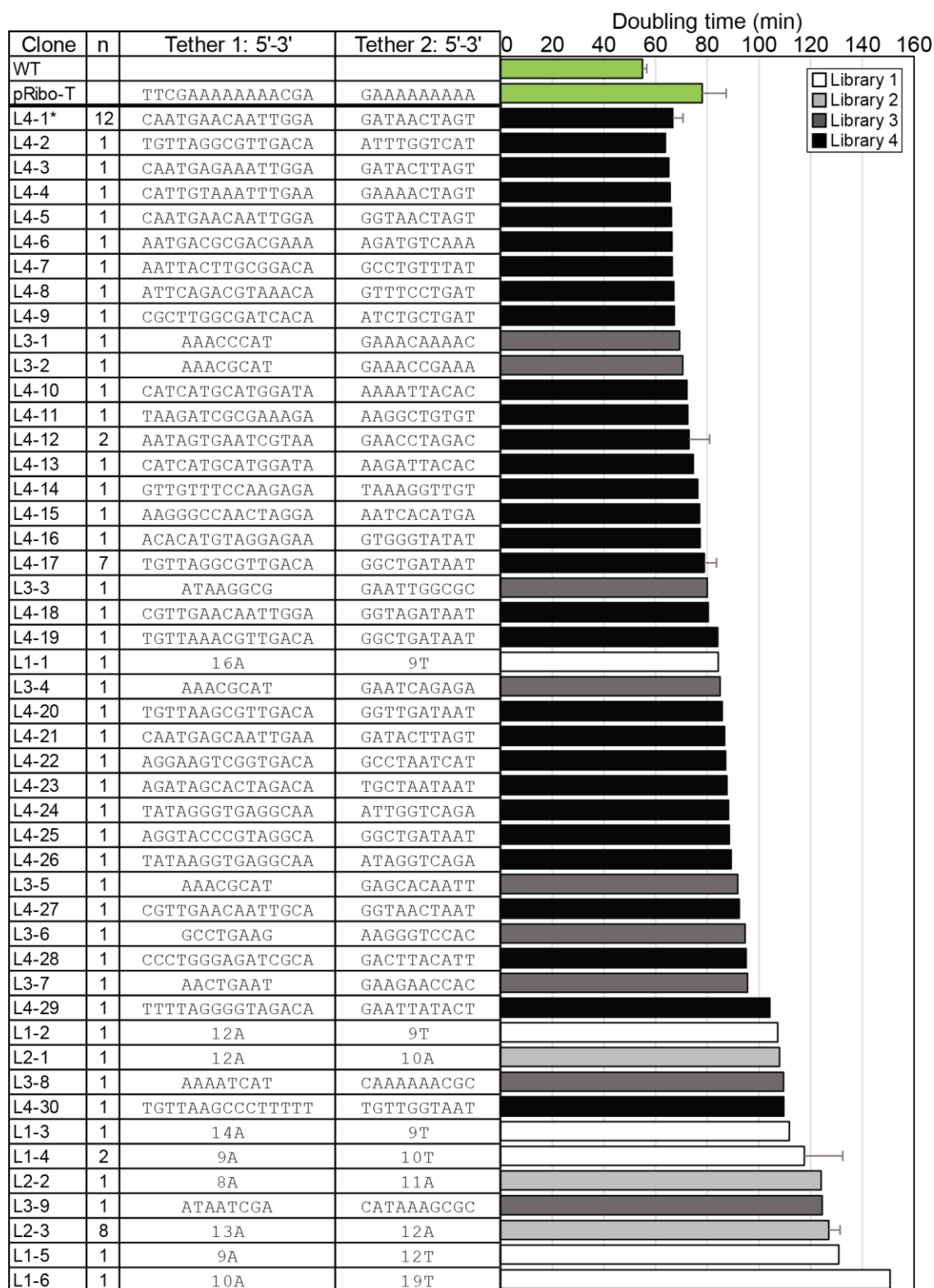
Carlson, E.D., Kim, D.S., & Jewett, M.C. Tethered ribosomes for unnatural amino acid incorporation (2016) US provisional 62/362,923

3.8 Supplementary figures and tables

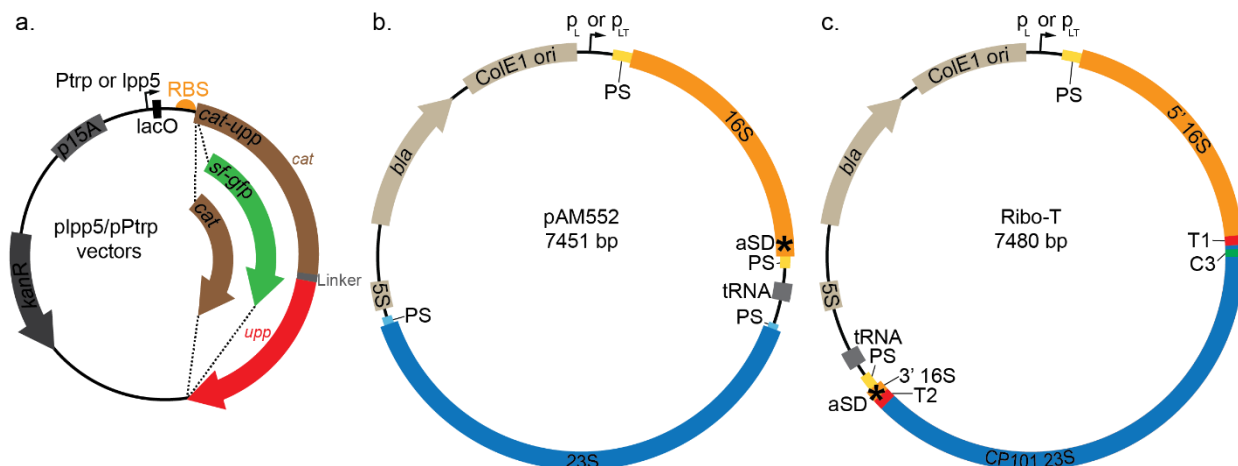


Supplementary Fig. 3.S1. Library construction and selection strategy for tether optimization.

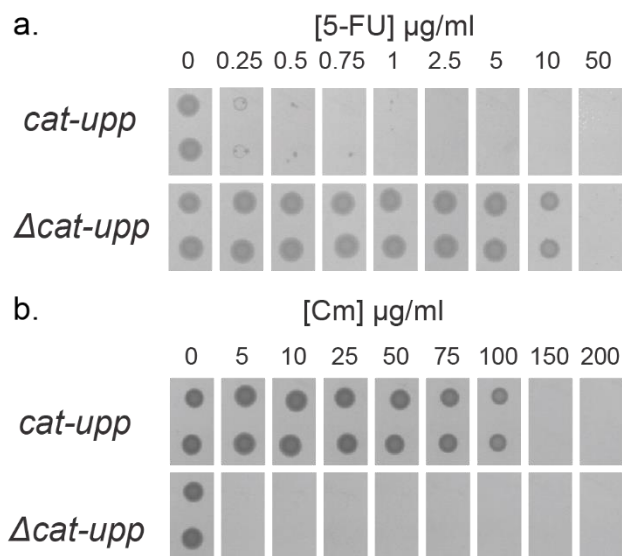
Supplementary Fig. 3.S2. Total RNA gel of selected library members. WT: wildtype ribosomes extracted from SQ171fg cells with pAM552 plasmid. Ribo-T: Ribo-T ($v1$)^{fl} ribosomes extracted from SQ171fg cells with pRibo-T plasmid.



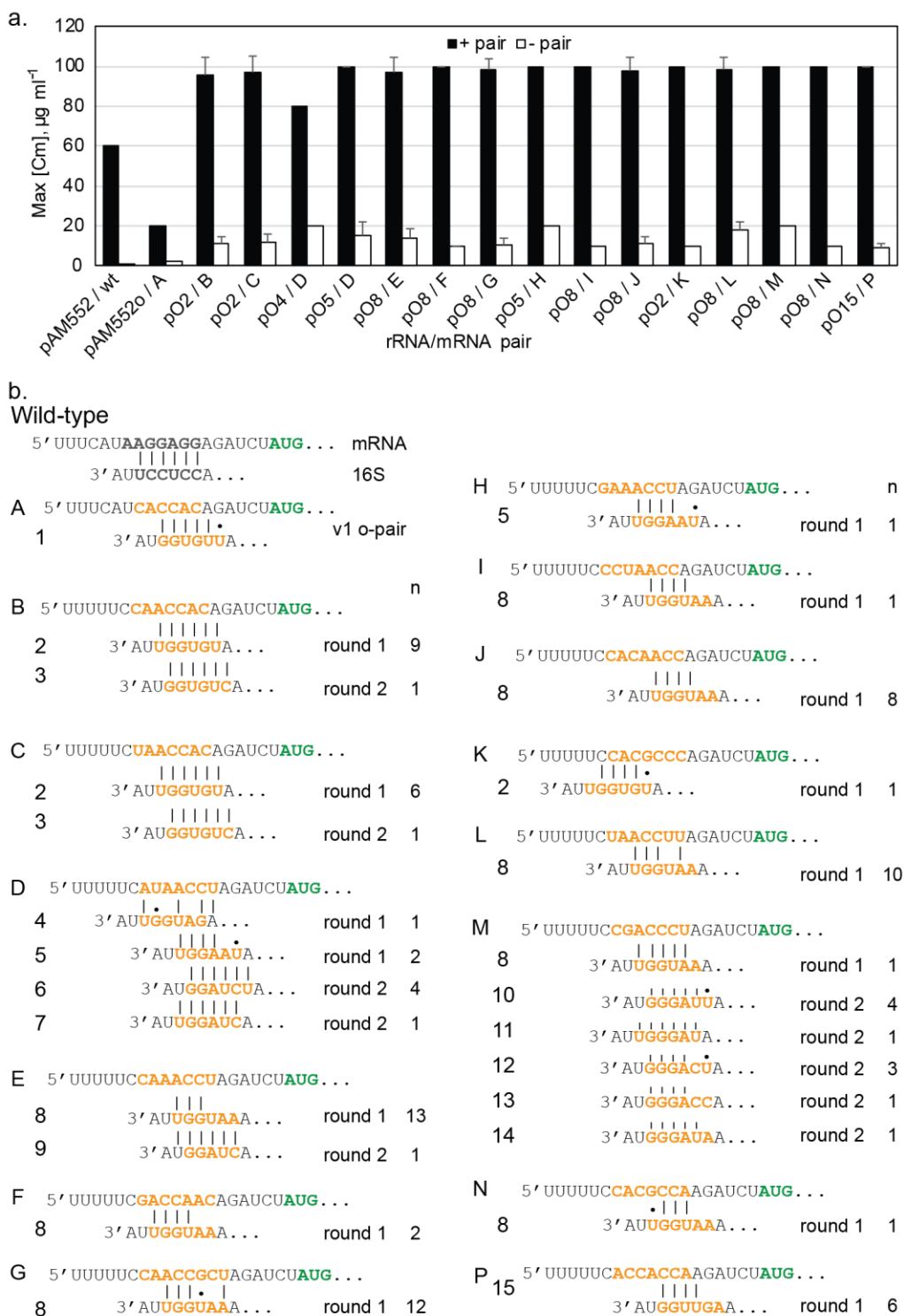
Supplementary Fig. 3.S3. Ribo-T supported cell growth in SQ171fg strain. Tether sequence and doubling time of selected clones shown.



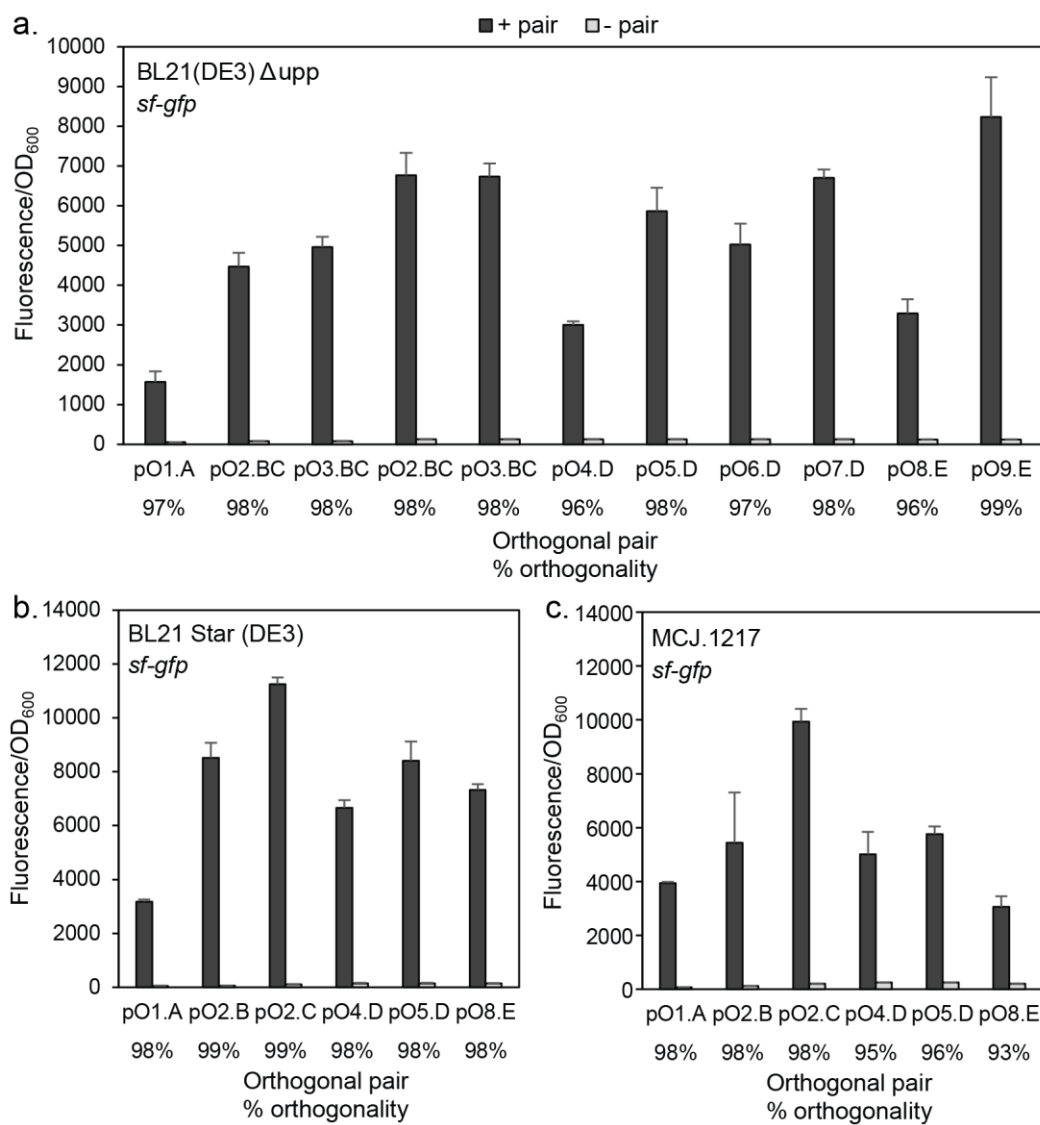
Supplementary Fig. 3.S4. Reporter plasmid and ribosome plasmid maps. a. Reporter plasmid with Pptrp or lpp5 promoter, and chloramphenicol acetyltransferase-uracil phosphoribosyltransferase (*cat-upp*), super folder green fluorescent protein (*sf-gfp*), or *cat* gene. Plasmid contains kanamycin resistance and p15A origin of replication. b. Plasmid coding for untethered ribosomal RNA (rRNA) from *rmb* operon, with either p_L promoter or p_{LT} promoter for orthogonal expression. Plasmid contains ampicillin resistance gene lactamase, and ColE1 origin of replication. Processing stems (PS) and anti-Shine-Dalgarno (aSD) sites indicated. c. Plasmid coding for tethered ribosome Ribo-T. 5' tether 1 (T1) and 3' tether 2 (T2), and 23S circular permutation connecting piece C3 noted.



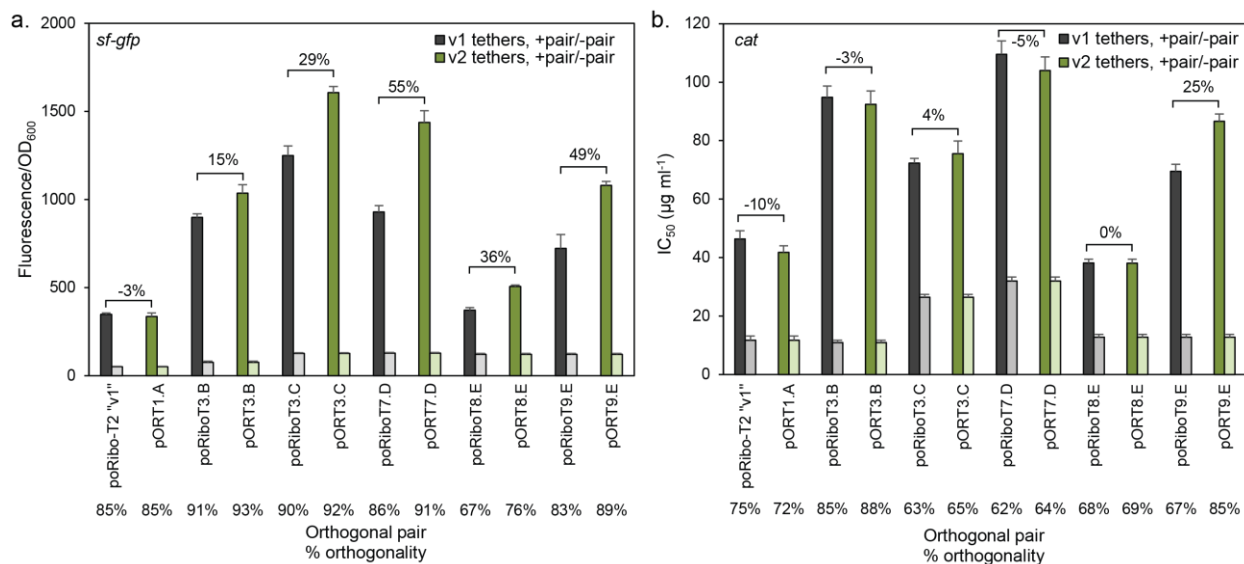
Supplementary Fig. 3.S5. Combined positive and negative selection scheme for evolving new orthogonal Shine-Dalgarno/anti-Shine-Dalgarno pairs. a. BL21(DE3) Δupp cells with pPptrp-*catupp*-p15A and *cat-upp* expressed die in the presence of 5-Fluorouracil. b. BL21(DE3) Δupp cells with pPptrp-*catupp*-p15A and *cat-upp* expressed gain resistance to the antibiotic chloramphenicol.



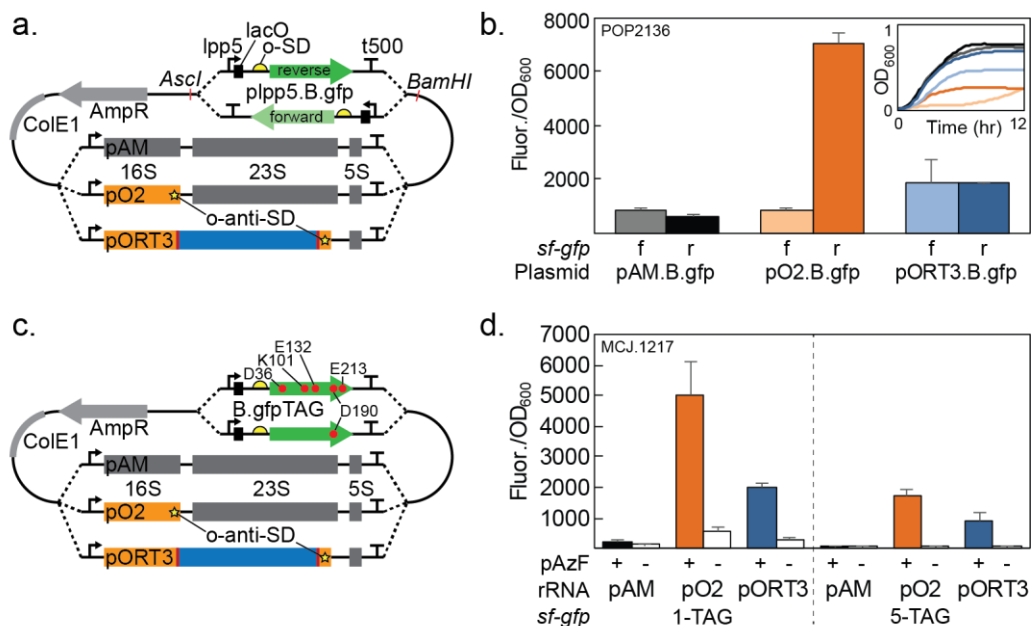
Supplementary Fig. 3.S6. Evolved orthogonal pairs. a. Activity testing following first second rounds of positive selection. b. Selected Shine-Dalgarno (SD) and anti-SD sequences. Round of selection and number of colonies (n) noted for each pair sequence. Orthogonal mRNA SD sequence is labeled with letters, and orthogonal 16S aSD sequence is labeled with numbers. Pair 1A is the previously published orthogonal pair noted as “v1 o-pair”⁴¹.



Supplementary Fig. 3.S7. Orthogonal pair activity in untethered ribosomes in BL21(DE3) Δ upp strain (a), BL21 Star (DE3) (b) and recoded TAG-less strain MCJ.1217 (c).



Supplementary Fig. 3.S8. Comparison between original published tether and v2 tethers with a. *sf-gfp* and b. *cat* reporters in BL21(DE3) Δ upp strain.



Supplementary Fig. 3.S10. Incorporation of non-canonical amino acid p-azidophenylalanine (pAzF) by orthogonal ribosomes. a. Combined rRNA and sfGFP reporter plasmid system. The orthogonal reporter sfGFP is inserted in the forward (light green) and reverse (dark green) direction relative to the *rna* operon. b. Expression of orthogonal *sf-gfp* from combined plasmid in POP2136. Fluorescence is normalized by OD₆₀₀ and is the average of at least 3 independent colonies with error bars showing standard deviation. c. Combined rRNA and *sf-gfp* plasmid with reverse orientation. For amber suppression, *sf-gfp* gene is replaced with a 1TAG or 5TAG version as noted. d. Expression of *sf-gfp* with 1TAG or 5TAG in MCJ.1217, in the presence of pAzF (+) or without pAzF (-).

Supplementary Table 3.S1. Primers used for the construction of Ribo-T tether libraries and gBlocks used in cloning steps.

Primer name	Sequence, 5'-3'
RiboTbb-f	GGAGGGCGCTTACCACCTTTG
RiboTbb-r	GGTTAAGCTACCTACTTCTTTTG
T1-A7-f	AAGAAGTAGGTAGCTTAACCAAAAAATGCGTTGAGCTAAC
T1-A8-f	AAGAAGTAGGTAGCTTAACCAAAAAATGCGTTGAGCTAAC
T1-A9-f	AAGAAGTAGGTAGCTTAACCAAAAAATGCGTTGAGCTAAC
T1-A10-f	AAGAAGTAGGTAGCTTAACCAAAAAATGCGTTGAGCTAAC
T1-A11-f	AAGAAGTAGGTAGCTTAACCAAAAAATGCGTTGAGCTAAC
T1-A12-f	AAGAAGTAGGTAGCTTAACCAAAAAATGCGTTGAGCTAAC
T1-A13-f	AAGAAGTAGGTAGCTTAACCAAAAAATGCGTTGAGCTAAC
T1-A14-f	AAGAAGTAGGTAGCTTAACCAAAAAATGCGTTGAGCTAAC
T1-A15-f	AAGAAGTAGGTAGCTTAACCAAAAAATGCGTTGAGCTAAC
T1-A16-f	AAGAAGTAGGTAGCTTAACCAAAAAATGCGTTGAGCTAAC
T1-A17-f	AAGAAGTAGGTAGCTTAACCAAAAAATGCGTTGAGCTAAC
T1-A18-f	AAGAAGTAGGTAGCTTAACCAAAAAATGCGTTGAGCTAAC
T1-A19-f	AAGAAGTAGGTAGCTTAACCAAAAAATGCGTTGAGCTAAC
T1-A20-f	AAGAAGTAGGTAGCTTAACCAAAAAATGCGTTGAGCTAAC
T2-T7-r	CAAAGTGGTAAGCGCCCTCCAAAAATGCGTTACACAC
T2-T8-r	CAAAGTGGTAAGCGCCCTCCAAAAATGCGTTACACAC
T2-T9-r	CAAAGTGGTAAGCGCCCTCCAAAAATGCGTTACACAC
T2-T10-r	CAAAGTGGTAAGCGCCCTCCAAAAATGCGTTACACAC
T2-T11-r	CAAAGTGGTAAGCGCCCTCCAAAAATGCGTTACACAC
T2-T12-r	CAAAGTGGTAAGCGCCCTCCAAAAATGCGTTACACAC
T2-T13-r	CAAAGTGGTAAGCGCCCTCCAAAAATGCGTTACACAC
T2-T14-r	CAAAGTGGTAAGCGCCCTCCAAAAATGCGTTACACAC
T2-T15-r	CAAAGTGGTAAGCGCCCTCCAAAAATGCGTTACACAC
T2-T16-r	CAAAGTGGTAAGCGCCCTCCAAAAATGCGTTACACAC
T2-T17-r	CAAAGTGGTAAGCGCCCTCCAAAAATGCGTTACACAC
T2-T18-r	CAAAGTGGTAAGCGCCCTCCAAAAATGCGTTACACAC
T2-T19-r	CAAAGTGGTAAGCGCCCTCCAAAAATGCGTTACACAC
T2-T20-r	CAAAGTGGTAAGCGCCCTCCAAAAATGCGTTACACAC
T2-A7-r	CAAAGTGGTAAGCGCCCTCCTTTTTTTTTCGCTTACACAC
T2-A8-r	CAAAGTGGTAAGCGCCCTCCTTTTTTTTTCGCTTACACAC
T2-A9-r	CAAAGTGGTAAGCGCCCTCCTTTTTTTTTCGCTTACACAC
T2-A10-r	CAAAGTGGTAAGCGCCCTCCTTTTTTTTTCGCTTACACAC
T2-A11-r	CAAAGTGGTAAGCGCCCTCCTTTTTTTTTCGCTTACACAC
T2-A12-r	CAAAGTGGTAAGCGCCCTCCTTTTTTTTTCGCTTACACAC
T2-A13-r	CAAAGTGGTAAGCGCCCTCCTTTTTTTTTCGCTTACACAC
T2-A14-r	CAAAGTGGTAAGCGCCCTCCTTTTTTTTTCGCTTACACAC
T2-A15-r	CAAAGTGGTAAGCGCCCTCCTTTTTTTTTCGCTTACACAC
T2-A16-r	CAAAGTGGTAAGCGCCCTCCTTTTTTTTTCGCTTACACAC

Primer name	Sequence, 5'-3'
T2-A17-r	CAAAGTGGTAAGCGCCCTCCTTTTTTTTTTTTTTTTTTTTGCGCTTACACAC
T2-A18-r	CAAAGTGGTAAGCGCCCTCCTTTTTTTTTTTTTTTTTTTTGCGCTTACACAC
T2-A19-r	CAAAGTGGTAAGCGCCCTCCTTTTTTTTTTTTTTTTTTTTGCGCTTACACAC
T2-A20-r	CAAAGTGGTAAGCGCCCTCCTTTTTTTTTTTTTTTTTTTTGCGCTTACACAC
T1-8N-f	AAGAAGTAGGTAGCTTAACCTTCGNNNNNNNNNCGATGCGTTGAGCTAAC
T2-9N-r	CAAAGTGGTAAGCGCCCTCCGNNNNNNNNNTGCGCTTACACAC
T1-15N-f	AAGAAGTAGGTAGCTTAACCNNNNNNNNNNNNNNTGCGTTGAGCTAAC
T2-10N-r	CAAAGTGGTAAGCGCCCTCCNNNNNNNNNNNTGCGCTTACACAC
p15A gBlock	GATGGCCTTTTTGCGTTTTCTACAGAGCGTCAGACCCCTTAATAAGATGATCTTCTTGAGATCGT TTTTGGTCTGCGCGTAATCTCTTGCTCTGAAAACGAAAAAACCGCCTTGCAGGGCGGTTTTTCGA AGGTTCTCTGAGCTACCAACTCTTTGAACCGAGGTAAGTGGCTTGGAGGAGCGCAGTCACCAAA ACTTGTCTTTTTAGTTTTAGCCTTAACCGGCGCATGACTTCAAGACTAACTCCTCTAAATCAATT ACCAGTGGCTGCTGCCAGTGGTGCTTTTGCATGTCTTTCCGGGTGGACTCAAGACGATAGTTA CCGGATAAGGCGCAGCGGTCCGACTGAACGGGGGTTTCGTGCATACAGTCCAGCTTGGAGCGAA CTGCCTACCCGGAAGTGAAGTGTGAGGCGTGAATGAGACAAACGCGGCCATAACAGCGGAATGA CACCGGTAAACCGAAAGGCAGGAACAGGAGAGCGCACGAGGGAGCCGCCAGGGGGAAACGCCTG GTATCTTTATAGTCTGTCTGGGTTTCGCCACCCTGATTTGAGCGTCAGATTTCTGTGATGCTTG TCAGGGGGGGCGGAGCCTATGGAAAACGGCTTTGCCGCGGCCCTCTCGGATCTGTATGGTGCAC TCTCAG
lpp5-oRBS	GAGACACAACGTGGCTTTCATCAAAAAAATATTGACAACATAAAAAACTTTGTGTTATACTTG TGGAATTGTGAGCGGATAACAATTCTATATCTGTTATTTTTTACACCACAGATCTATGGAGAA AAAAATCACTGGATATACCACCGTTG

4. Conclusions and future outlook

While I am very proud of the work we as a team have accomplished, there are still many significant routes for improving the Ribo-T system. Firstly, the improved orthogonal system, while much more active and orthogonal compared to our first publication⁴¹, shows a lower activity compared to untethered systems, and a non-zero cross-talk with the wild-type ribosome and mRNA pool. Specifically, background expression level when just the orthogonal mRNA is expressed without the cognate orthogonal rRNA is non-zero, suggesting that our negative selection steps need to be improved. A limit to our work here was use of the *cat-upp* selection scheme³⁵, which is difficult to work with. Besides requiring genomic knockout of the *upp* gene in each strain, the selection must be performed in minimal media; rich media contains high levels of uracil, greatly reducing strain sensitivity to the uracil analog 5-fluorouracil used for the negative selection. We found this limits the strains the selection can be performed in, and the strength of the negative selection. Target strains such as recoded C321.ΔA, which are less fit compared to wild-type *E. coli*, were too sick to perform the negative selection with the *cat-upp* system.

An alternative negative selection uses a mutant phenylalanine aminoacyl-tRNA synthetase with relaxed substrate specificity, *pheS*. If *pheS* is expressed in the presence of the added small molecule 4-chloro-DL-phenylalanine (Cl-Phe), the cell dies. The negative selection provided by combined positive/negative selection system *cat-pheS* is significantly more robust and versatile⁹⁵, and does not require growth on minimal media or genomic modifications. Repeating orthogonal pair selection with multiple rounds of negative selection using the *cat-pheS* gene could help decrease the background cross-talk expression.

While we significantly improved Ribo-T functionality via tether randomization and selection, we were not able to improve SQ171 or SQ171fg growth with Ribo-T back to wild-type levels (Fig. 3.3b,c). This not unexpected given the current Ribo-T tether site architecture. Tether site determines both the circular permutation of the 23S rRNA, and the splitting point of the 16S rRNA. The 23S rRNA circular permutation can interfere with ribosome biogenesis assembly processes and functionality⁴³, and we observed a wide range of growth phenotypes in our CP23S screen (Table 2.2). Untethered ribosomes with 23S circularly permuted at H101 supporting cell growth in SQ171 has a doubling time 1.7x greater than wild-type ribosomes. Therefore, the circular permutation of the 23S rRNA at H101 may be one of the fundamentally limiting factors in the current Ribo-T architecture. From our work⁴¹, we have a variety of different viable circular permutations (Table 2.2) that could provide alternative tether sites using less-inhibitory CP23S variants. Towards this goal, several new candidate tether sites were designed for further exploration (Fig. 4.1).

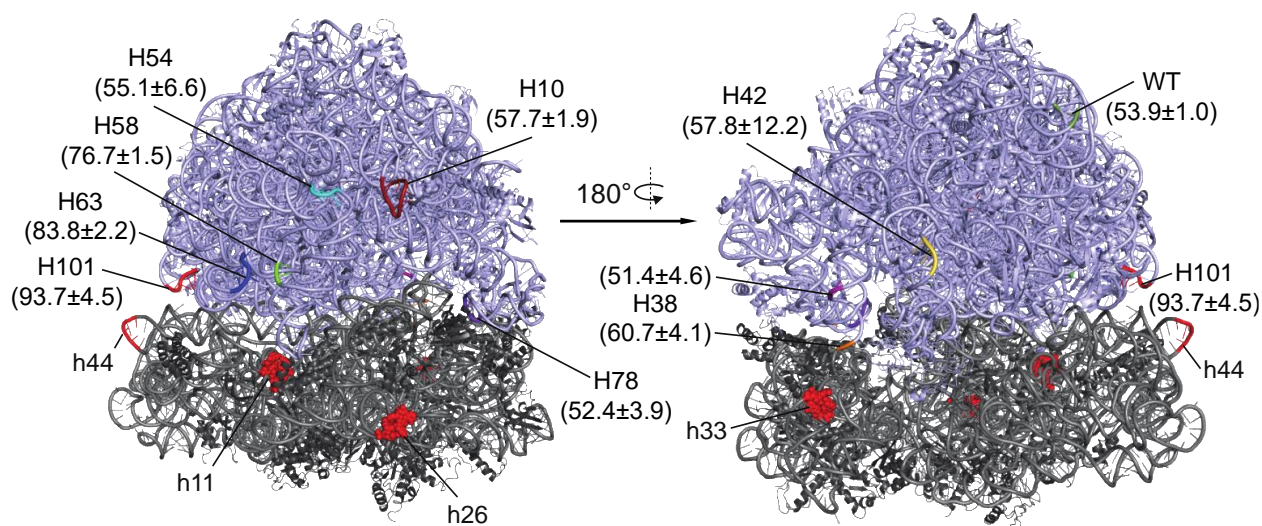


Figure 4.1. Possible tether sites, with CP23S mutation doubling time \pm standard deviation (min) indicated for 23S circular permutations. New 16S connection points in red spheres. Structure PDB 3R8S and 4GD1.

The strains described in Appendix B would provide an important set of tools for fundamental study of the ribosome and engineering efforts alike. With the CRISPR-Cas9 integration scheme designed and planned, these strains are ready-to-finish. Furthermore, integration of orthogonal ribosomes onto the genome in recoded C321.ΔA strains would enable continuous MAGE-enabled evolution. This requires optimization of integration site and promoter strength driving orthogonal expression.

An important sister technology to the Ribo-T system is the integrated synthesis assembly and translation (iSAT) system and ribosome synthesis and evolution (RISE) method developed in the Jewett lab^{30-32, 96}. For example, in the effort to incorporate exotic side chain or modified backbone monomers, a major challenge is the ability to specifically charge the ncAA to a suppressor tRNA for incorporation by a modified ribosome, which would need to be evolved as well. However, the co-evolution of both an orthogonal aaRS and the ribosome would be practically impossible. With iSAT/RISE, chemically or flexizyme-charged suppressor tRNAs can be supplied to the cell-free reaction and the ribosome evolved towards the new substrates *in vitro*. The mutations can be ported to the Ribo-T system for *in vivo* expression to evolve an aaRS capable of specifically charging the suppressor tRNA with the new monomer *in vivo*. Furthermore, EF-Tu variants can be readily evolved *in vivo* to effectively bind and deliver the charged suppressor tRNA to the ribosome as needed⁸⁸. This sequential co-evolution requires both the *in vitro* and *in vivo* platforms and will be an important synergy moving forward.

With all these enticing opportunities, I am excited to see what the community does with the Ribo-T system. I am grateful to have been a part of it.

References

1. Ambrogelly, A., Palioura, S., and Soll, D. (2007) Natural expansion of the genetic code, *Nat Chem Biol* 3, 29-35.
2. Mann, M., and Jensen, O. N. (2003) Proteomic analysis of post-translational modifications, *Nature biotechnology* 21, 255-261.
3. Jefferis, R. (2005) Glycosylation of Recombinant Antibody Therapeutics, *Biotechnology Progress* 21, 11-16.
4. Yang, J.-D., Lu, C., Stasny, B., Henley, J., Guinto, W., Gonzalez, C., Gleason, J., Fung, M., Collopy, B., Benjamino, M., Gangi, J., Hanson, M., and Ille, E. (2007) Fed-batch bioreactor process scale-up from 3-L to 2,500-L scale for monoclonal antibody production from cell culture, *Biotechnology and Bioengineering* 98, 141-154.
5. Liu, C. C., and Schultz, P. G. (2010) Adding new chemistries to the genetic code, *Annu Rev Biochem* 79, 413-444.
6. Fujino, T., Goto, Y., Suga, H., and Murakami, H. (2016) Ribosomal Synthesis of Peptides with Multiple β -Amino Acids, *Journal of the American Chemical Society* 138, 1962-1969.
7. Katoh, T., Tajima, K., and Suga, H. (2017) Consecutive Elongation of D-Amino Acids in Translation, *Cell Chemical Biology* 24, 46-54.
8. Dedkova, L. M., Fahmi, N. E., Golovine, S. Y., and Hecht, S. M. (2006) Construction of modified ribosomes for incorporation of D-amino acids into proteins, *Biochemistry* 45, 15541-15551.
9. Cheloha, R. W., Sullivan, J. A., Wang, T., Sand, J. M., Sidney, J., Sette, A., Cook, M. E., Suresh, M., and Gellman, S. H. (2015) Consequences of periodic α -to- β 3 residue replacement for immunological recognition of peptide epitopes, *ACS chemical biology* 10, 844.
10. Webb, A. I., Dunstone, M. A., Williamson, N. A., Price, J. D., de Kauwe, A., Chen, W., Oakley, A., Perlmutter, P., McCluskey, J., and Aguilar, M.-I. (2005) T cell determinants incorporating β -amino acid residues are protease resistant and remain immunogenic in vivo, *The Journal of Immunology* 175, 3810-3818.
11. Kimmerlin, T., and Seebach, D. (2005) '100 years of peptide synthesis': ligation methods for peptide and protein synthesis with applications to β -peptide assemblies*, *The Journal of Peptide Research* 65, 229-260.
12. Albericio, F. (2004) Developments in peptide and amide synthesis, *Current Opinion in Chemical Biology* 8, 211-221.
13. Guichard, G., and Seebach, D. (1997) Solid-phase synthesis of β -oligopeptides, *CHIMIA International Journal for Chemistry* 51, 315-318.
14. van Hest, J. C. M., and Tirrell, D. A. (1998) Efficient introduction of alkene functionality into proteins in vivo, *FEBS Letters* 428, 68-70.
15. Des Soye, B. J., Patel, J. R., Isaacs, F. J., and Jewett, M. C. (2015) Repurposing the translation apparatus for synthetic biology, *Current opinion in chemical biology* 28, 83-90.
16. Lang, K., and Chin, J. W. (2014) Cellular incorporation of unnatural amino acids and bioorthogonal labeling of proteins, *Chemical reviews* 114, 4764-4806.
17. Hoesl, M. G., and Budisa, N. (2012) Recent advances in genetic code engineering in Escherichia coli, *Current opinion in biotechnology* 23, 751-757.

18. Eisenhauer, B. M., and Hecht, S. M. (2002) Site-Specific Incorporation of (Aminoxy)acetic Acid into Proteins†, *Biochemistry* 41, 11472-11478.
19. Taki, M., Hohsaka, T., Murakami, H., Taira, K., and Sisido, M. (2002) Position-Specific Incorporation of a Fluorophore–Quencher Pair into a Single Streptavidin through Orthogonal Four-Base Codon/Anticodon Pairs, *Journal of the American Chemical Society* 124, 14586-14590.
20. Fahmi, N. E., Dedkova, L., Wang, B., Golovine, S., and Hecht, S. M. (2007) Site-specific incorporation of glycosylated serine and tyrosine derivatives into proteins, *J Am Chem Soc* 129, 3586-3597.
21. Neumann, H., Hancock, S. M., Buning, R., Routh, A., Chapman, L., Somers, J., Owen-Hughes, T., van Noort, J., Rhodes, D., and Chin, J. W. (2009) A method for genetically installing site-specific acetylation in recombinant histones defines the effects of H3 K56 acetylation, *Molecular cell* 36, 153-163.
22. Kanamori, T., Nishikawa, S.-I., Shin, I., Schultz, P. G., and Endo, T. (1997) Probing the environment along the protein import pathways in yeast mitochondria by site-specific photocrosslinking, *Proceedings of the National Academy of Sciences* 94, 485-490.
23. Mori, H., and Ito, K. (2006) Different modes of SecY–SecA interactions revealed by site-directed in vivo photo-cross-linking, *Proceedings of the National Academy of Sciences* 103, 16159-16164.
24. Ye, S., Zaitseva, E., Caltabiano, G., Schertler, G. F. X., Sakmar, T. P., Deupi, X., and Vogel, R. (2010) Tracking G-protein-coupled receptor activation using genetically encoded infrared probes, *Nature* 464, 1386-1389.
25. Grünewald, J., Hunt, G. S., Dong, L., Niessen, F., Wen, B. G., Tsao, M.-L., Perera, R., Kang, M., Laffitte, B. A., Azarian, S., Ruf, W., Nasoff, M., Lerner, R. A., Schultz, P. G., and Smider, V. V. (2009) Mechanistic studies of the immunochemical termination of self-tolerance with unnatural amino acids, *Proceedings of the National Academy of Sciences* 106, 4337-4342.
26. Maini, R., Nguyen, D. T., Chen, S., Dedkova, L. M., Chowdhury, S. R., Alcalá-Torano, R., and Hecht, S. M. (2013) Incorporation of β -amino acids into dihydrofolate reductase by ribosomes having modifications in the peptidyltransferase center, *Bioorganic & medicinal chemistry* 21, 1088-1096.
27. Dedkova, L. M., Fahmi, N. E., Paul, R., Del Rosario, M., Zhang, L., Chen, S., Feder, G., and Hecht, S. M. (2011) β -Puromycin selection of modified ribosomes for in vitro incorporation of β -amino acids, *Biochemistry* 51, 401-415.
28. Maini, R., Chowdhury, S. R., Dedkova, L. M., Roy, B., Daskalova, S. M., Paul, R., Chen, S., and Hecht, S. M. (2015) Protein synthesis with ribosomes selected for the incorporation of β -amino Acids, *Biochemistry* 54, 3694.
29. Kaczanowska, M., and Rydén-Aulin, M. (2007) Ribosome Biogenesis and the Translation Process in *Escherichia coli*, *Microbiology and Molecular Biology Reviews* 71, 477-494.
30. Jewett, M. C., Fritz, B. R., Timmerman, L. E., and Church, G. M. (2013) In vitro integration of ribosomal RNA synthesis, ribosome assembly, and translation, *Molecular systems biology* 9, 678.
31. Liu, Y., Fritz, B. R., Anderson, M. J., Schoborg, J. A., and Jewett, M. C. (2014) Characterizing and alleviating substrate limitations for improved in vitro ribosome construction, *ACS synthetic biology* 4, 454-462.
32. Fritz, B. R., and Jewett, M. C. (2014) The impact of transcriptional tuning on in vitro integrated rRNA transcription and ribosome construction, *Nucleic acids research* 42, 6774-6785.
33. Shimizu, Y., Inoue, A., Tomari, Y., Suzuki, T., Yokogawa, T., Nishikawa, K., and Ueda, T. (2001) Cell-free translation reconstituted with purified components, *Nature biotechnology* 19, 751-755.

34. Ohashi, H., Shimizu, Y., Ying, B.-W., and Ueda, T. (2007) Efficient protein selection based on ribosome display system with purified components, *Biochemical and biophysical research communications* 352, 270-276.
35. Rackham, O., and Chin, J. W. (2005) A network of orthogonal ribosome*mRNA pairs, *Nat Chem Biol* 1, 159-166.
36. An, W., and Chin, J. W. (2009) Synthesis of orthogonal transcription-translation networks, *Proceedings of the National Academy of Sciences* 106, 8477-8482.
37. Neumann, H., Wang, K., Davis, L., Garcia-Alai, M., and Chin, J. W. (2010) Encoding multiple unnatural amino acids via evolution of a quadruplet-decoding ribosome, *Nature* 464, 441-444.
38. Hui, A., and de Boer, H. A. (1987) Specialized ribosome system: preferential translation of a single mRNA species by a subpopulation of mutated ribosomes in Escherichia coli, *Proc Natl Acad Sci U S A* 84, 4762-4766.
39. Wang, K., Neumann, H., Peak-Chew, S. Y., and Chin, J. W. (2007) Evolved orthogonal ribosomes enhance the efficiency of synthetic genetic code expansion, *Nat Biotech* 25, 770-777.
40. Byer, R. L. (2013) In *Nature Podcast* (Stoddart, C., Ed.), <http://www.nature.com/nature/podcast/index-2013-10-03.html>.
41. Orelle, C., Carlson, E. D., Szal, T., Florin, T., Jewett, M. C., and Mankin, A. S. (2015) Protein synthesis by ribosomes with tethered subunits, *Nature* 524, 119-124.
42. Peralta, E. A., Soong, K., England, R. J., Colby, E. R., Wu, Z., Montazeri, B., McGuinness, C., McNeur, J., Leedle, K. J., Walz, D., Sozer, E. B., Cowan, B., Schwartz, B., Travish, G., and Byer, R. L. (2013) Demonstration of electron acceleration in a laser-driven dielectric microstructure, *Nature* 503, 91.
43. Kitahara, K., and Suzuki, T. (2009) The ordered transcription of RNA domains is not essential for ribosome biogenesis in Escherichia coli, *Mol Cell* 34, 760-766.
44. Shepotinovskaya, I. V., and Uhlenbeck, O. C. (2008) Catalytic Diversity of Extended Hammerhead Ribozymes†, *Biochemistry* 47, 7034-7042.
45. Been, M. D., and Wickham, G. S. (1997) Self-cleaving ribozymes of hepatitis delta virus RNA, *The FEBS Journal* 247, 741-753.
46. Erlacher, M. D., Lang, K., Shankaran, N., Wotzel, B., Hüttenhofer, A., Micura, R., Mankin, A. S., and Polacek, N. (2005) Chemical engineering of the peptidyl transferase center reveals an important role of the 2'-hydroxyl group of A2451, *Nucleic acids research* 33, 1618-1627.
47. Asai, T., Zaporozhets, D., Squires, C., and Squires, C. L. (1999) An Escherichia coli strain with all chromosomal rRNA operons inactivated: Complete exchange of rRNA genes between bacteria, *Proceedings of the National Academy of Sciences* 96, 1971-1976.
48. Wolf, Y. I., and Koonin, E. V. (2007) On the origin of the translation system and the genetic code in the RNA world by means of natural selection, exaptation, and subfunctionalization, *Biology Direct* 2, 14.
49. Noller, H. F. (2012) Evolution of Protein Synthesis from an RNA World, *Cold Spring Harbor Perspectives in Biology* 4.
50. Karbstein, K. Quality control mechanisms during ribosome maturation, *Trends in Cell Biology* 23, 242-250.
51. Isaacs, F. J., Dwyer, D. J., Ding, C., Pervouchine, D. D., Cantor, C. R., and Collins, J. J. (2004) Engineered riboregulators enable post-transcriptional control of gene expression, *Nat Biotechnol* 22, 841-847.

52. Gibson, D. G., Young, L., Chuang, R. Y., Venter, J. C., Hutchison, C. A., 3rd, and Smith, H. O. (2009) Enzymatic assembly of DNA molecules up to several hundred kilobases, *Nat Methods* 6, 343-345.
53. Douthwaite, S., Powers, T., Lee, J. Y., and Noller, H. F. (1989) Defining the Structural Requirements for a Helix in 23 S Ribosomal RNA that Confers Erythromycin Resistance, *Journal of Molecular Biology* 209, 655-665.
54. Rottmann, N., Kleuvers, B., Atmadja, J., and Wagner, R. (1988) Mutants with base changes at the 3'-end of the 16S RNA from Escherichia coli. Construction, expression and functional analysis, *Eur J Biochem* 177, 81-90.
55. Nakatogawa, H., and Ito, K. (2002) The Ribosomal Exit Tunnel Functions as a Discriminating Gate, *Cell* 108, 629-636.
56. Cannone, J. J., Subramanian, S., Schnare, M. N., Collett, J. R., D'Souza, L. M., Du, Y., Feng, B., Lin, N., Madabusi, L. V., and Müller, K. M. (2002) The comparative RNA web (CRW) site: an online database of comparative sequence and structure information for ribosomal, intron, and other RNAs, *BMC bioinformatics* 3, 2.
57. Dunkle, J. A., Wang, L., Feldman, M. B., Pulk, A., Chen, V. B., Kapral, G. J., Noeske, J., Richardson, J. S., Blanchard, S. C., and Cate, J. H. D. (2011) Structures of the bacterial ribosome in classical and hybrid states of tRNA binding, *Science* 332, 981-984.
58. Gerbi, S. (1996) Expansion segments: regions of variable size that interrupt the universal core secondary structure of ribosomal RNA, *Ribosomal RNA structure, evolution, processing, and function in protein biosynthesis* 71, 87.
59. Dorywalska, M., Blanchard, S. C., Gonzalez, R. L., Kim, H. D., Chu, S., and Puglisi, J. D. (2005) Site-specific labeling of the ribosome for single-molecule spectroscopy, *Nucleic acids research* 33, 182-189.
60. Yusupov, M. M., Yusupova, G. Z., Baucom, A., Lieberman, K., Earnest, T. N., Cate, J., and Noller, H. F. (2001) Crystal structure of the ribosome at 5.5 Å resolution, *science* 292, 883-896.
61. Voorhees, R. M., Weixlbaumer, A., Loakes, D., Kelley, A. C., and Ramakrishnan, V. (2009) Insights into substrate stabilization from snapshots of the peptidyl transferase center of the intact 70S ribosome, *Nature structural & molecular biology* 16, 528-533.
62. Marshall, R. A., Dorywalska, M., and Puglisi, J. D. (2008) Irreversible chemical steps control intersubunit dynamics during translation, *Proceedings of the National Academy of Sciences* 105, 15364-15369.
63. Frank, J., and Agrawal, R. K. (2000) A ratchet-like inter-subunit reorganization of the ribosome during translocation, *Nature* 406, 318-322.
64. Horan, L. H., and Noller, H. F. (2007) Intersubunit movement is required for ribosomal translocation, *Proceedings of the National Academy of Sciences* 104, 4881-4885.
65. Kannan, K., Vázquez-Laslop, N., and Mankin, A. S. (2012) Selective protein synthesis by ribosomes with a drug-obstructed exit tunnel, *Cell* 151, 508-520.
66. Merryman, C., and Noller, H. F. (1998) Footprinting and modification-interference analysis of binding sites on RNA, *RNA: protein interactions, a practical approach*. Oxford University Press, Oxford, United Kingdom, 237-253.
67. Pédelacq, J.-D., Cabantous, S., Tran, T., Terwilliger, T. C., and Waldo, G. S. (2006) Engineering and characterization of a superfolder green fluorescent protein, *Nature biotechnology* 24, 79-88.
68. Bundy, B. C., and Swartz, J. R. (2010) Site-specific incorporation of p-propargyloxyphenylalanine in a cell-free environment for direct protein-protein click conjugation, *Bioconjugate chemistry* 21, 255-263.

69. Vazquez-Laslop, N., Thum, C., and Mankin, A. S. (2008) Molecular Mechanism of Drug-Dependent Ribosome Stalling, *Molecular Cell* 30, 190-202.
70. Orelle, C., Szal, T., Klepacki, D., Shaw, K. J., Vazquez-Laslop, N., and Mankin, A. S. (2013) Identifying the targets of aminoacyl-tRNA synthetase inhibitors by primer extension inhibition, *Nucleic acids research*, gkt526.
71. Vázquez-Laslop, N., Ramu, H., Klepacki, D., Kannan, K., and Mankin, A. S. (2010) The key function of a conserved and modified rRNA residue in the ribosomal response to the nascent peptide, *The EMBO journal* 29, 3108-3117.
72. Inouye, S., and Inouye, M. (1985) Up-promoter mutations in the lpp gene of Escherichia coli, *Nucleic Acids Research* 13, 3101-3110.
73. Schägger, H., and Von Jagow, G. (1987) Tricine-sodium dodecyl sulfate-polyacrylamide gel electrophoresis for the separation of proteins in the range from 1 to 100 kDa, *Analytical biochemistry* 166, 368-379.
74. Thomason, L. C., Costantino, N., and Court, D. L. (2007) E. coli genome manipulation by P1 transduction, *Current protocols in molecular biology*, 1.17. 11-11.17. 18.
75. Mankin, A. S. (1997) Pactamycin resistance mutations in functional sites of 16 S rRNA, *Journal of molecular biology* 274, 8-15.
76. Bhushan, S., Hoffmann, T., Seidelt, B., Frauenfeld, J., Mielke, T., Berninghausen, O., Wilson, D. N., and Beckmann, R. (2011) SecM-stalled ribosomes adopt an altered geometry at the peptidyl transferase center, *PLoS Biol* 9, e1000581.
77. Thompson, J., Kim, D. F., O'Connor, M., Lieberman, K. R., Bayfield, M. A., Gregory, S. T., Green, R., Noller, H. F., and Dahlberg, A. E. (2001) Analysis of mutations at residues A2451 and G2447 of 23S rRNA in the peptidyltransferase active site of the 50S ribosomal subunit, *Proc Natl Acad Sci U S A* 98.
78. Sato, N. S., Hirabayashi, N., Agmon, I., Yonath, A., and Suzuki, T. (2006) Comprehensive genetic selection revealed essential bases in the peptidyl-transferase center, *Proceedings of the National Academy of Sciences* 103, 15386-15391.
79. Arenz, S., Ramu, H., Gupta, P., Berninghausen, O., Beckmann, R., Vázquez-Laslop, N., Mankin, A. S., and Wilson, D. N. (2014) Molecular basis for erythromycin-dependent ribosome stalling during translation of the ErmBL leader peptide, *Nature communications* 5.
80. Nissen, P., Hansen, J., Ban, N., Moore, P. B., and Steitz, T. A. (2000) The structural basis of ribosome activity in peptide bond synthesis, *Science* 289.
81. Moll, I., Hirokawa, G., Kiel, M. C., Kaji, A., and Bläsi, U. (2004) Translation initiation with 70S ribosomes: an alternative pathway for leaderless mRNAs, *Nucleic acids research* 32, 3354-3363.
82. Carlson, E. D. (2015) Creating Ribo-T: (Design, Build, Test)n, *ACS synthetic biology* 4, 1173-1175.
83. Datsenko, K. A., and Wanner, B. L. (2000) One-step inactivation of chromosomal genes in Escherichia coli K-12 using PCR products, *Proceedings of the National Academy of Sciences* 97, 6640-6645.
84. Gibson, D. G., Young, L., Chuang, R.-Y., Venter, J. C., Hutchison, C. A., and Smith, H. O. (2009) Enzymatic assembly of DNA molecules up to several hundred kilobases, *Nat Meth* 6, 343-345.
85. Melançon, C. E., and Schultz, P. G. (2009) One Plasmid Selection System for the Rapid Evolution of Aminoacyl-tRNA Synthetases, *Bioorganic & medicinal chemistry letters* 19, 3845-3847.

86. Lajoie, M. J., Rovner, A. J., Goodman, D. B., Aerni, H.-R., Haimovich, A. D., Kuznetsov, G., Mercer, J. A., Wang, H. H., Carr, P. A., Mosberg, J. A., Rohland, N., Schultz, P. G., Jacobson, J. M., Rinehart, J., Church, G. M., and Isaacs, F. J. (2013) Genomically Recoded Organisms Expand Biological Functions, *Science* *342*, 357-360.
87. Wang, H. H., Isaacs, F. J., Carr, P. A., Sun, Z. Z., Xu, G., Forest, C. R., and Church, G. M. (2009) Programming cells by multiplex genome engineering and accelerated evolution, *Nature* *460*, 894-898.
88. Gan, R., Perez, J. G., Carlson, E. D., Ntai, I., Isaacs, F. J., Kelleher, N. L., and Jewett, M. C. (2017) Translation system engineering in *Escherichia coli* enhances non-canonical amino acid incorporation into proteins, *Biotechnology and Bioengineering* *114*, 1074-1086.
89. Chin, J. W., Santoro, S. W., Martin, A. B., King, D. S., Wang, L., and Schultz, P. G. (2002) Addition of p-Azido-l-phenylalanine to the Genetic Code of *Escherichia coli*, *Journal of the American Chemical Society* *124*, 9026-9027.
90. Salis, H. M., Mirsky, E. A., and Voigt, C. A. (2009) Automated design of synthetic ribosome binding sites to control protein expression, *Nat Biotech* *27*, 946-950.
91. Espah Borujeni, A., Channarasappa, A. S., and Salis, H. M. (2014) Translation rate is controlled by coupled trade-offs between site accessibility, selective RNA unfolding and sliding at upstream standby sites, *Nucleic Acids Research* *42*, 2646-2659.
92. Chong, S., Chen, C., Ge, H., and Xie, X. S. Mechanism of Transcriptional Bursting in Bacteria, *Cell* *158*, 314-326.
93. Shearwin, K. E., Callen, B. P., and Egan, J. B. Transcriptional interference-a crash course, *Trends in Genetics* *21*, 339-345.
94. Yeung, E., Dy, A. J., Martin, K. B., Ng, A. H., Del Vecchio, D., Beck, J. L., Collins, J. J., and Murray, R. M. (2016) The Effect of Compositional Context on Synthetic Gene Networks, *bioRxiv*, 083329.
95. Thyer, R., Filipovska, A., and Rackham, O. (2013) Engineered rRNA Enhances the Efficiency of Selenocysteine Incorporation during Translation, *Journal of the American Chemical Society* *135*, 2-5.
96. Fritz, B. R. (2014) In Vitro Synthesis and Evolution of *Escherichia coli* Ribosomes, Northwestern University.
97. Fried, S. D., Schmied, W. H., Uttamapinant, C., and Chin, J. W. (2015) Ribosome subunit stapling for orthogonal translation in *E. coli*, *Angewandte Chemie International Edition* *54*, 12791-12794.
98. Steinbeck, J. (1952) *East of Eden*, Penguin books.
99. Mali, P., Esvelt, K. M., and Church, G. M. (2013) Cas9 as a versatile tool for engineering biology, *Nature methods* *10*, 957-963.
100. Doudna, J. A., and Charpentier, E. (2014) The new frontier of genome engineering with CRISPR-Cas9, *Science* *346*, 1258096.
101. Li, Y., Lin, Z., Huang, C., Zhang, Y., Wang, Z., Tang, Y.-j., Chen, T., and Zhao, X. (2015) Metabolic engineering of *Escherichia coli* using CRISPR-Cas9 mediated genome editing, *Metabolic engineering* *31*, 13-21.
102. Jiang, Y., Chen, B., Duan, C., Sun, B., Yang, J., and Yang, S. (2015) Multigene editing in the *Escherichia coli* genome via the CRISPR-Cas9 system, *Applied and environmental microbiology* *81*, 2506-2514.
103. Bassalo, M. C., Garst, A. D., Halweg-Edwards, A. L., Grau, W. C., Domaille, D. W., Mutalik, V. K., Arkin, A. P., and Gill, R. T. (2016) Rapid and efficient one-step metabolic pathway integration in *E. coli*, *ACS synthetic biology* *5*, 561-568.

104. Haurwitz, R. E., Jinek, M., Wiedenheft, B., Zhou, K., and Doudna, J. A. (2010) Sequence- and structure-specific RNA processing by a CRISPR endonuclease, *Science* *329*, 1355-1358.
105. Urbano, L. (2013) Simple DNA Writer.
106. Maeda, M., Shimada, T., and Ishihama, A. (2015) Strength and regulation of seven rRNA promoters in *Escherichia coli*, *PLoS one* *10*, e0144697.

Appendices

A. Comparison to a stapled ribosome

A.1 Introduction

A short time after our publication of Ribo-T⁴¹, a parallel work was published by the Chin lab at the MRC⁹⁷. This work describes the construction of a ribosome with “stapled” subunits, connecting 23S rRNA helix 101 with 16S rRNA helix 44 as in our Ribo-T design. The stapled ribosome uses a flexible hinge-like region from a *Tetrahymena* group 1 self-splicing intron (Fig. A.1d). The stapled ribosome is cloned with an orthogonal anti-Shine-Dalgarno site for orthogonal expression. Fried *et al.* demonstrate detection of a 23S/16S fusion molecule via Northern blot against the orthogonal aSD sequence on the 3' end of the molecule (Figure 3A⁹⁷), and subsequent orthogonal expression and translation of a reporter gene with an orthogonal stapled ribosome containing dominant lethal mutations G2252A or G2553C could be expressed in living cells. However, the work did not show cell growth supported completely by a stapled ribosome. By comparing tether sequences across different single subunit ribosomes, we hoped to accumulate and assemble design rules for the engineering of active tethered ribosomes. Thus, we first sought to verify that the stapled ribosome tether was able to stably support cell growth in strains lacking wild-type untethered ribosomes, and subsequently characterize cell health, growth and orthogonality.

A.2 Materials and methods

A.2.1 A stapled ribosome with a wild-type anti-Shine-Dalgarno site

We cloned the stapled tether sequences into the pRibo-T plasmid with A2058G Erythromycin resistance mutation using our standard tether cloning pipeline described in Section 3.2, using primers 5'-GGAGGGCGCTTACCACTTTG and 5'-GGTTAAGCTACCTACTTCTTTTG to amplify the backbone plasmid pRibo-T-A2058G. From the same template, the tethers were replaced with staple sequences using primers **AAGAAGTAGGTAGCTTAACC**GGGGTCAACAGCCGTTCAGTGCGTTGAGCTAACCGTA and **CAAGTGGTAAGCGCCCTCC**AGGACCATGTCCGTCAGTGCGCTTACACACC. Underlined sequence indicates stapled tether sequences, and bold sequence indicates added homology with the generated backbone plasmid. Plasmids were re-circularized with Gibson assembly⁵², and transformed into POP2136 strain for plasmid isolation and sequencing. Sequence confirmed plasmids (all containing A2058G mutation) coding for untethered ribosomes (Fig. A.1a), Ribo-T (Fig. A.1b), Ribo-Tv2 (Fig. A.1c), and Stapled ribosome (Fig. A.1d) were transformed into SQ171fg/pCSacB electrocompetent cells, and recovered for 1 hour at 37 °C in SOC. Cells were then incubated at 37 °C in SOC supplemented with 50 µg/ml carbenicillin and 0.25% sucrose until cultures were cloudy (overnight for wt, Ribo-T and Ribo-Tv2, 3 days for stapled ribosome). Cells were plated on LB agar plates supplemented with 50 µg/ml carbenicillin, 5% sucrose, and 1 mg/ml erythromycin and incubated at 37 °C. Cells appeared on the wt untethered, Ribo-T and Ribo-T-v2 plates between 24-48 hours. After 3 days at 37 °C, colonies appeared on the stapled ribosome plate. Colonies were picked for total RNA extraction and gel electrophoresis as described before.

A.2.2 A stapled ribosome with orthogonal anti-Shine-Dalgarno site

Using methods described above, the stapled tether sequence⁹⁷ was cloned into pORT1 (poRibo-T2⁴¹) to create pORT1-Stapled. Next, the anti-SD sequence used by Fried *et al.*⁹⁷ was cloned into plasmid pORT1-Stapled to create plasmid O-ribo(h44H101). Briefly, the backbone was amplified from pORT1-Stapled using primers 5'-CGGTATTCTCCAGATCTCT and 5'-TACCTTAAAGAAGCGTAC. Orthogonal anti-SD sequence was added using pORT1-Stapled template, and primers **AGAGATCTGGAGGAATACCG**CAGGCGAAGGCGGCCCTGGA and **GTACGCTTCTTTAAGGTA**ATCCCATGATCCAACCGCAGGTTTC. Underlined sequence indicates orthogonal anti-SD sequence, and bolded indicates added homology for recircularization with Gibson assembly⁵². This construct puts the orthogonal stapled ribosome from Fried *et al.* onto the same plasmid backbone as our system for direct comparison. The cognate orthogonal SD sequence from Fried *et al.* was cloned into the plpp5.A.gfp and plpp5.A.cat plasmids using phosphorylated primers TTGCGGAGGGATGTGAAAAAATAACAGATATAG and either ATGAGCAAAGGTGAAGAAC (for *sf-gfp*) or ATGGAAAAAAAATCACC (for *cat*) with recircularization by blunt-end ligation as described in Section 3.2.5. These plasmids are named Fried.gfp and Fried.cat. Constructs were transformed into BL21(DE3) Δ upp electrocompetent cells, and plated on LB agar plates supplemented with 30 μ g ml⁻¹ kanamycin and 50 μ g ml⁻¹ carbenicillin, and tested following protocols in Section 3.2.6.

A.3 Results and discussion

A.3.1 Testing a stapled ribosome in the cell growth assay

Testing of untethered, Ribo-T and Ribo-Tv2 in SQ171fg strain matches our previous observations in Chapter 3 (Fig. 3.5, Supplementary Fig. 3.S7). In total RNA gels, untethered ribosomes show the expected 23S and 16S prominent bands (Fig. A.1e). Ribo-T and Ribo-Tv2 cells show the expected clean 23S/16S dominant band in each colony analyzed, indicating stable tethering of subunits *in vivo*, with sufficient activity to support cell growth. However, while we could see cell growth after 3 days at 37 °C, the total RNA gel of the 3 stapled ribosome colonies analyzed display significant cleavage product (Fig. A.1e). This indicates that the stapled ribosome tethers are readily cleaved *in vivo* and cannot cleanly support cell growth.

This observation is consistent with reported data by Fried *et al.* Figure 3A⁹⁷ shows a Northern blot against the orthogonal aSD sequence on the ribosome with stapled subunits, which sits at the very 3' end of the construct after tether 2. In this setup, detection by Northern blot would detect the full 23S/16S band as in Figure 3A⁹⁷, and a small ~90 nt band if the tether is cleaved. This small band would presumably be run off the gel and thus not detected.

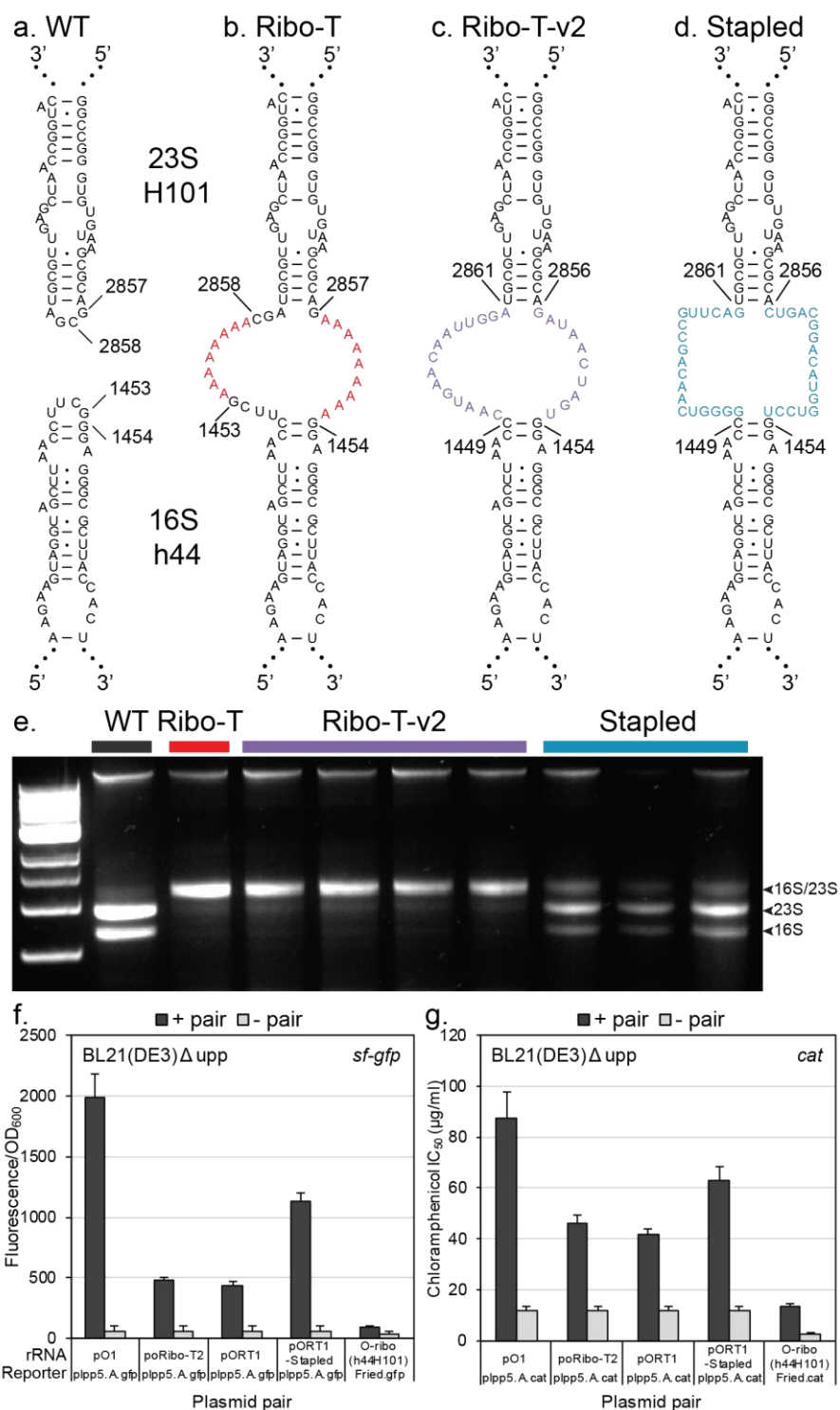


Figure A.1. Testing a ribosome with stapled subunits. a. Wild-type 23S H101 and 16S h44. b. Ribo-T system⁴⁷. c. Ribo-T-v2 system. d. A ribosome with stapled subunits⁹⁷. e. 1% agarose gel of total RNA extracted from SQ171fg strain⁴⁷ supported by pAM552 (WT), pRibo-T plasmid, pRibo-T-v2 plasmid, and stapled ribosome plasmid. f. Orthogonal *sf-gfp* expression in BL21(DE3)Δupp strain. g. Orthogonal *cat* expression in BL21(DE3)Δupp strain.

A.3.2 Testing a stapled ribosome in the orthogonal assay

Orthogonal stapled constructs were tested alongside the original oRibo-T system pairs⁴¹ with both superfolder green fluorescent protein (*sf-gfp*) and chloramphenicol acetyltransferase protein (*cat*). Firstly, given the variability in orthogonal expression observed from the plasmid context, it is not surprising that the O-ribo(h44H101)/Fried.gfp and O-ribo(h44H101)/Fried.cat conditions (Fig. A.1f,g) are so low. However, they do show significant expression of *sf-gfp* and *cat* over the just o-reporter condition.

As expected, untethered orthogonal ribosomes pO1 have highest expression in both *sf-gfp* and *cat* assays. Expression by the original poRibo-T2 and pORTA (with improved tethers) show similar expression compared to the previously observed results. However, the pORT1-Stapled construct showed 157% higher expression over the pORTA construct in the *sf-gfp* assay (Fig. A.1f), and 50% in the *cat* assay (Fig. A.1g). This is likely due to our observed stapled tether cleavage (Fig. A.1e). In this context, the orthogonal 16S would be split into two molecules. Split 16S constructs such as this can still form functional subunits⁴³, and thus give higher orthogonal expression since they would operate more similarly to the untethered state.

A.4 Conclusions

In our hands and plasmid backbones, the ribosome with stapled subunits is unable to support cell growth in the SQ171fg strain⁴¹. SQ171fg with a ribosome with stapled subunits is significantly less fit compared to our Ribo-T and Ribo-Tv2 strains as indicated by increased required incubation times from 24-28 hours at 37 °C to nearly 3 days until colonies appear. While we observe some accumulation of 23S/16S sized RNA, the majority of RNA is in the cleaved 23S and 16S size range. While the stapled ribosome tethers cloned into our plasmid backbone and orthogonal system (pORT1-Stapled) outperform our tethered constructs, we believe this is due to cleaved tethers leading to a subpopulation of free orthogonal 30S subunits. Therefore, we are confident in the robustness of our Ribo-T system in respect to the stability of the tethers *in vivo* to enable reliable *in vivo* ribosome engineering.

A.5 Acknowledgements

This work was carried out with Anne D'Aquino.

B. Designer strains for ribosome engineering

“But the Hebrew word, the word timshel—‘Thou mayest’— that gives a choice. It might be the most important word in the world. That says the way is open.”—John Steinbeck, East of Eden⁹⁸

B.1 Introduction

The orthogonal Ribo-T system provides a transformative ability to engineer ribosomes in a living cell, and can be used to evolve new functionalities and expand our understanding of the *E. coli* ribosome (Fig. B.1b). However, these insights are qualified with being uncovered in the context of a tethered ribosome, and not in the untethered wild-type context. The lower-activity of the current h44-H101 tether architecture, even with the improved tether sequences, could limit more challenging engineering targets. To solve this, a swapped system could be employed wherein Ribo-T is responsible for proteome production and cell growth, and an orthogonal untethered ribosome (o70S) can be used for engineering (Fig. B.1d,f,h). This system can be realized by careful plasmid engineering using the SQ171fg strain (Fig. B.1d). However, plasmid limitations quickly become an issue, especially with our aim to use the orthogonal ribosomes with non-canonical amino acid incorporations systems, which require multiple plasmids and specialized strains beyond SQ171fg. In this work, we designed a workflow to build enabling ribosome engineering strains organisms using CRISPR-Cas9 genome editing technology. This pipeline includes strains such as a “clean” Squires strain (Fig. B.1e,f), and a strain with Ribo-T operons completely replacing the genomic wild-type operons for streamlined swapped systems (Fig. B.1g,h).

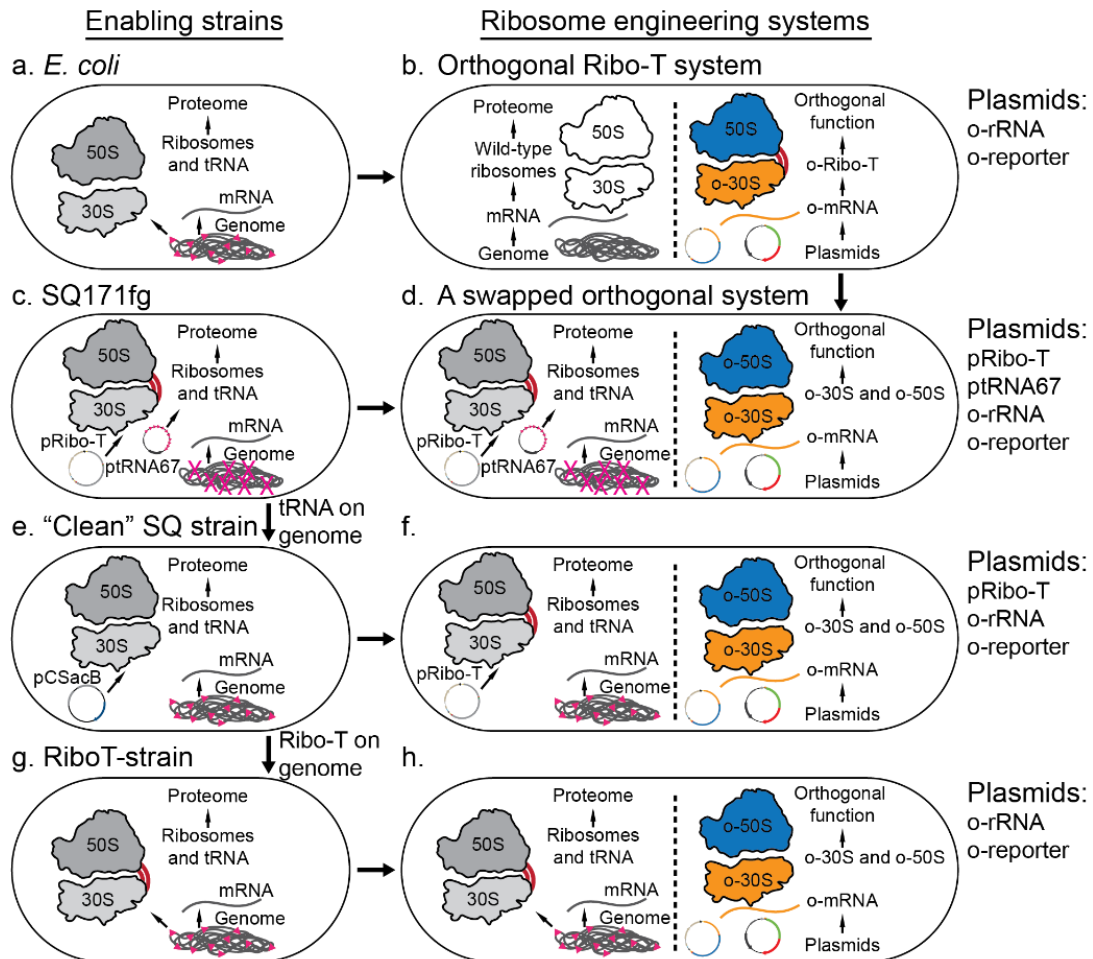


Figure B.1. Ribo-T strains for ribosome engineering. b. Current orthogonal system with wild-type untethered ribosomes producing the proteome for cell viability, and an orthogonal plasmid-based Ribo-T for engineering. d. In a swapped system, Ribo-T rRNA is transcribed from a plasmid-based operon, and translates the proteome, while an orthogonal untethered ribosome is used for engineering.

The SQ171 strain⁴⁷ has all 7 ribosomal operons deleted from the genome, so all rRNA is transcribed from a plasmid-based operon (Fig. B.1c). This is a vital tool for studying ribosomal mutations by simple plasmid exchange with the pCSacB counter-selectable maintenance plasmid. This strain was developed by full ribosomal operon knockouts with Datsenko/Wanner recombination⁸³, fully deleting the promoter region, 16S rRNA, 23S rRNA, 5S rRNA, terminator, and rRNA operon-based tRNA genes. As such, SQ171-based strains require an rRNA operon plasmid, and a tRNA plasmid (ptRNA67) as shown in Figure 5.1e. A “clean” Squires strain in which only the 16S, 23S and 5S rRNA are deleted, leaving the promoter region and operon-based tRNA genes intact (Fig. B.1f) would alleviate plasmid barriers and increase strain flexibility for ribosome engineering (Fig. B.1c). Furthermore, a RiboT-strain in which genomic untethered *rnm* operons are surgically replaced by Ribo-T-v2 leaving the tRNA in place (Fig. B.1g) would provide a plasmid-free blank slate strain for use in untethered orthogonal ribosome systems (Fig. B.1h).

Our attempts to use Datsenko/Wanner recombineering⁸³ to integrate Ribo-T into the genome failed owing to inefficiencies with larger cassette integrations, and high homology with the Ribo-T-KanR cassette and the 7 genomic copies of *rnm* operons. Therefore, we turned to the highly-site specific CRISPR-Cas9 system. CRISPR-Cas9 genome engineering^{99, 100} is a power platform to readily engineering genomes of a wide array of organisms, including bacteria¹⁰¹⁻¹⁰³.

B.2 Materials and methods

Following standard guide RNA (gRNA) design rules, two unique 20 bp target sequences next to a required NGG protospacer adjacent motif (PAM) sequence at the 3' end of the target sequence (5'-N₂₀NGG). Target N₂₀ sites were searched against the rest of the genome, to confirm uniqueness. Designed target 5'-N₂₀NGG sequences are shown in Table B.1. CRISPR-Cas9 genome editing is achieved using the system of Jiang *et al*¹⁰², but with a chloramphenicol resistance marker replacing the spectinomycin resistance marker on pTarget plasmid for compatibility with pTRNA67 plasmid in the SQ171 strains (Fig. B.3b). Each 5' and 3' gRNA cassette was synthesized as a gBlock (IDT) with a pJ23119 promoter, 5'-N₂₀NGG site, gRNA scaffold sequence, 6T terminator sequence, and proper added homology for 3 piece Gibson assembly with the pTarget-Cm backbone, the 5' gRNA cut cassette and the 3' gRNA cut cassette. While the Csy4 protein can process multiple gRNA from a single transcript¹⁰⁴, another plasmid is required; this is undesirable, as it limits modification flexibility in plasmid-limited strains like SQ171. Primers and gBlocks are shown in Table B.2.

Homologous repair fixing cassettes (Fig. B.3d-e) were constructed with overlap assembly PCR using primers and templates shown in Table B.3. A unique primer binding site, TAGCTGACATGACGTCTAATC, was added into the *rnm* operon fixing cassette as a convenient screening site and water-marking sequence (Fig. B.3c,e). This sequence reads '*timshe!*' coded in DNA¹⁰⁵. For a first proof of principle demonstration, pTarget-*rnmA* dual cutting plasmid and pTarget-S1 (target sequence and fixing piece scheme shown in Figure B.2) were assembled and sequence verified. S1 fixing piece (Fig. 5.3d) was assembled and cloned into the pTarget-S1 vector. Clean SQ strain (Fig. B.3c) and Ribo-T-v2 (Fig. B.3e) fixing pieces were assembled and purified for the *rnmA* operon (Fig. B.3a).



Figure B.2. S1 fast growing C549T mutation with CRISPR-Cas9. S1 gene (blue highlighted) and target gRNA sequence (green highlighted) with CGG PAM sequence (red box) shown. Homologous repair cassette introduces C549T mutation and mutated PAM sequence to AAC for colony PCR screening.

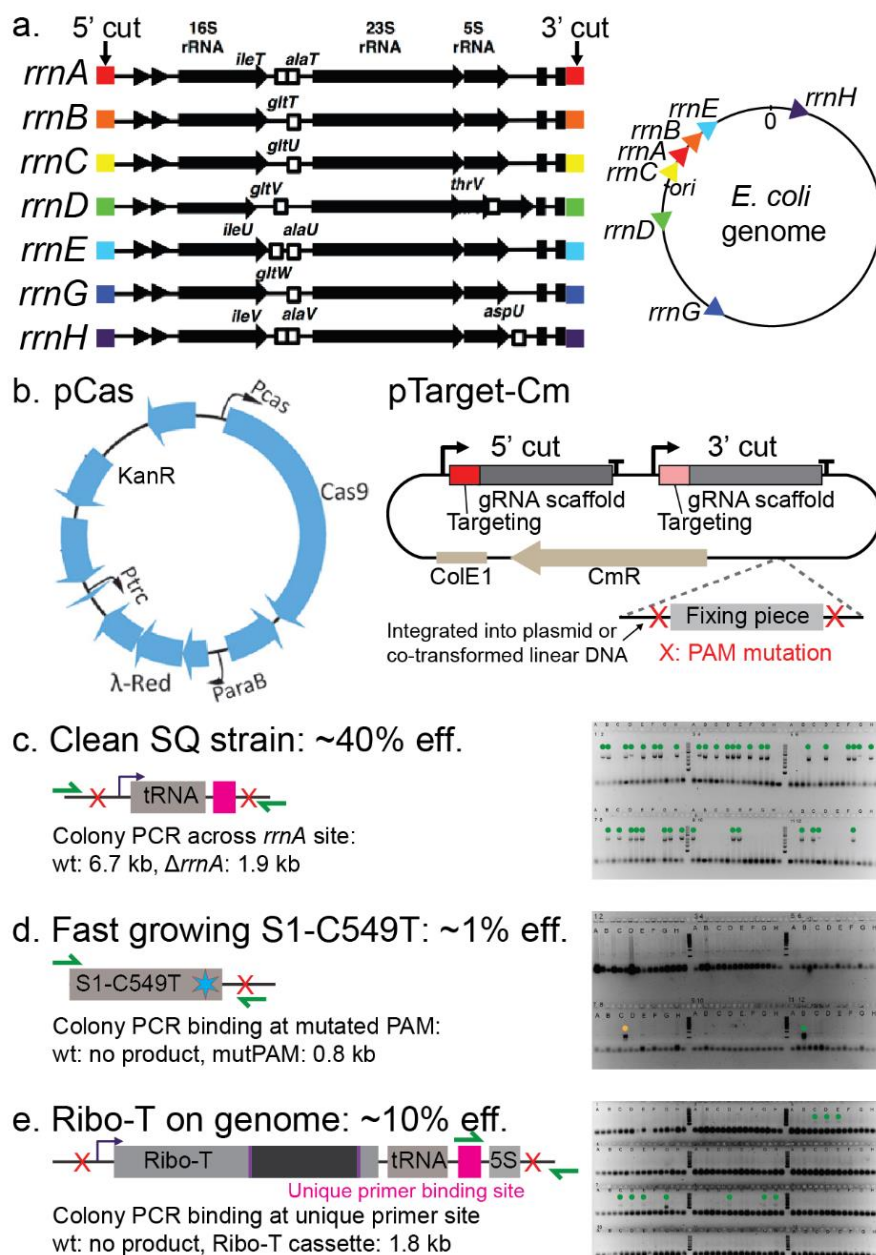
Genome editing was performed per Jiang *et al*¹⁰². Briefly, MG1655 electrocompetent cells were transformed with pCas plasmid, and used to prepare electrocompetent cells in LB media supplemented with 50 $\mu\text{g ml}^{-1}$ kanamycin and 10 mM arabinose for λ red induction. Plasmid pTarget-*rrnA* and double stranded linear fixing pieces, or just pTarget-S1, were transformed into induced MG1655/pCas cells. MG1655/pCas/pTarget-*rrnA* cells were plated on LB agar plates supplemented with 30 $\mu\text{g ml}^{-1}$ kanamycin and 34 $\mu\text{g ml}^{-1}$ chloramphenicol, and cultured at 30 °C overnight. MG1655/pCas/pTarget-S1 cells were plated on LB agar plates supplemented with 34 $\mu\text{g ml}^{-1}$ chloramphenicol at 37 °C overnight (pCas plasmid will be lost due to temperature-sensitive origin of replication), since the fast-growing mutation is cold-sensitive. Colonies were screened with colony PCR using the primers indicated in Table 5.1 and run on 1% agarose gels (Fig. B.3c-e). Positive hits are amplified with colony PCR and sequenced (ACGT inc.).

B.3 Results and discussion

Towards the clean SQ strain (Fig. B.1e), incorporation efficiencies of the tRNA-*rrnA* cassette are ~40% (Fig. B.3c). For the fast growing S1-C549T cassette, two positive colony PCR hits were observed (Fig. B.3d, yellow and green dot). Both were sequenced, revealing one sample with the mutated PAM sequence and the C549T fast-growing mutation (green dot), and one with a mutated PAM sequence but wild-type C549 (yellow dot). This gives an efficiency of 1%, so in future efforts to make this mutation, multiple plates may have to be screened. Finally, incorporation of the entire RiboT-v2 cassette (Fig. B.3e) was achieved at ~10% efficiency.

B.4 Future works

With genome engineering capabilities demonstrated, strains can now be built. Construction target strains are shown in Table B.4. Importantly, the SQ171fg mutation effects can now be elucidated. Deletion of the *ybeX* gene alone in SQ171 naïve strain does not give the fast-growing phenotype. With the pTarget-S1 plasmid, SQ171 naïve S1 *rpsA* gene can be mutated to C549T to confirm if this confers the fast-growing phenotype.



B.5 Primers, gBlocks and tables

Table B.1. Designed target sequences for genome engineering of *rrn* operons.

Operon	5' target sequence N ₂₀ -NGG	3' target sequence N ₂₀ -NGG
A	AAGCTGATTATGAAGATGTCAGG	AAGATTAAGCGGCACATCAC TGG
B	ACTGTTACAAGTGCTGCCAGAGG	AGGACAACCCGTTCTTATTC TGG
C	TCTCAGCCAGAACATACGAAAGG	TGCTATCGACAACGGTATGCAGG
D	ATTACGCGCTGACCGATTTGTGG	TCAGGATCGAGCGCCGACGT TGG
E	GACTGGACGACGTTGTTGCATGG	AACTCCACCCACGTTCAACCTGG
G	CTGAAACTGCTGAGCGAGAACGG	GTGATACTCGTCGCCGCATT TGG
H	AGATATGCAGGCAGCGGTTGCGG	ATTATGGCTATCCCTGCATT TGG

Table B.2. gBlocks and primers for construct assemblies. Synthesized gRNA gBlocks EDC793 and EDC794 and annotated (homology-Promoter-target sequence-gRNA scaffold-terminator-homology), with same feature mapping in EDC877-EDC888. All DNA is synthesized as single stranded DNA, unless otherwise noted as a double stranded DNA gBlock.

Primer/gBlock name	Primer/gBlock sequence
EDC799_bb-f	TTCATGTGCAGCTCCATCAG
EDC800_bb-r	GCATATGCGGTGTGAAATAC
EDC793_gRNA-rna-5 (gBlock)	GTATTTTCACACCGCATATGC TGGATCC TTGACAGCTAGCTCAGTCCTAGGTATAAATACTAGT AAGCTGATTATGAAGATGTCGTTTTAGAGCTAGAAATAGCAAGTTAAAATAAGGCTAGTCCG TTATCAACTTGAAAAGTGGCACCGAGTCGGTGTCTTTTT GAATTCTCTAGAGTCGACCTG CAGAAGCTTAGATCTTTGACA
EDC794_gRNA-rna-3 (gBlock)	GAATTCTCTAGAGTCGACCTGCAGAAGCTTAGATCT TTGACAGCTAGCTCAGTCCTAGGTAT AATACTAGTAGGACAACCCGTTCTTATTCGTTTTAGAGCTAGAAATAGCAAGTTAAAATAAG GCTAGTCCGTTATCAACTTGAAAAGTGGCACCGAGTCGGTGTCTTTTTTCTACCCAGCTTC GACGTGCTCGAG TTTCATGTGCAGCTCCATCAG
EDC877_gRNA-B-5' (gBlock)	GTATTTTCACACCGCATATGC TGGATCCTTGACAGCTAGCTCAGTCCTAGGTATAAATACTAGT ACTGTTACAAGTGCTGCCAGTTTTAGAGCTAGAAATAGCAAGTTAAAATAAGGCTAGTCCG TTATCAACTTGAAAAGTGGCACCGAGTCGGTGTCTTTTTTTGAATTCTCTAGAGTCGACCTG CAGAAGCTTAGATCTTTGACA
EDC878_gRNA-B-3' (gBlock)	GAATTCTCTAGAGTCGACCTGCAGAAGCTTAGATCTTTGACAGCTAGCTCAGTCCTAGGTAT AATACTAGTAGGACAACCCGTTCTTATTCGTTTTAGAGCTAGAAATAGCAAGTTAAAATAAG GCTAGTCCGTTATCAACTTGAAAAGTGGCACCGAGTCGGTGTCTTTTTTCTACCCAGCTTC GACGTGCTCGAGTTTCATGTGCAGCTCCATCAG
EDC879_gRNA-C-5' (gBlock)	GTATTTTCACACCGCATATGC TGGATCCTTGACAGCTAGCTCAGTCCTAGGTATAAATACTAGT TCTCAGCCAGAACATACGAAGTTTTAGAGCTAGAAATAGCAAGTTAAAATAAGGCTAGTCCG TTATCAACTTGAAAAGTGGCACCGAGTCGGTGTCTTTTTTTGAATTCTCTAGAGTCGACCTG CAGAAGCTTAGATCTTTGACA
EDC880_gRNA-C-3' (gBlock)	GAATTCTCTAGAGTCGACCTGCAGAAGCTTAGATCTTTGACAGCTAGCTCAGTCCTAGGTAT AATACTAGTTGCTATCGACAACGGTATGCGTTTTAGAGCTAGAAATAGCAAGTTAAAATAAG GCTAGTCCGTTATCAACTTGAAAAGTGGCACCGAGTCGGTGTCTTTTTTCTACCCAGCTTC GACGTGCTCGAGTTTCATGTGCAGCTCCATCAG
EDC881_gRNA-D-5' (gBlock)	GTATTTTCACACCGCATATGC TGGATCCTTGACAGCTAGCTCAGTCCTAGGTATAAATACTAGT ATTACGCGTGACCGATTTGGTTTTAGAGCTAGAAATAGCAAGTTAAAATAAGGCTAGTCCG TTATCAACTTGAAAAGTGGCACCGAGTCGGTGTCTTTTTTTGAATTCTCTAGAGTCGACCTG CAGAAGCTTAGATCTTTGACA
EDC882_gRNA-D-3' (gBlock)	GAATTCTCTAGAGTCGACCTGCAGAAGCTTAGATCTTTGACAGCTAGCTCAGTCCTAGGTAT AATACTAGTTGCTATCGACAACGGTATGCGTTTTAGAGCTAGAAATAGCAAGTTAAAATAAG GCTAGTCCGTTATCAACTTGAAAAGTGGCACCGAGTCGGTGTCTTTTTTCTACCCAGCTTC GACGTGCTCGAGTTTCATGTGCAGCTCCATCAG

Primer/gBlock name	Primer/gBlock sequence
EDC883_gRNA-E-5' (gBlock)	GTATTTACACCCGCATATGCTGGATCCTTGACAGCTAGCTCAGTCCCTAGGTATAATACTAGT GACTGGACGACGTTGTTGCGAGTTTTAGAGCTAGAAATAGCAAGTTAAAAAAGGCTAGTCCG TTATCAACTTGAAAAAGTGGCACCCGAGTCGGTGCTTTTTTTGAATTCTCTAGAGTCGACCTG CAGAAGCTTAGATCTTTGACA
EDC884_gRNA-E-3' (gBlock)	GAATTCTCTAGAGTCGACCTGCAGAAGCTTAGATCTTTGACAGCTAGCTCAGTCCCTAGGTAT AATACTAGTAACTCCACCCACGTTCAACCGTTTTAGAGCTAGAAATAGCAAGTTAAAAAAG GCTAGTCCGTTATCAACTTGAAAAAGTGGCACCCGAGTCGGTGCTTTTTTTCTACCCAGCTTC GACGTGCTCGAGTTCATGTGCAGCTCCATCAG
EDC885_gRNA-G-5' (gBlock)	GTATTTACACCCGCATATGCTGGATCCTTGACAGCTAGCTCAGTCCCTAGGTATAATACTAGT CTGAAACTGCTGAGCGAGAGTTTTAGAGCTAGAAATAGCAAGTTAAAAAAGGCTAGTCCG TTATCAACTTGAAAAAGTGGCACCCGAGTCGGTGCTTTTTTTGAATTCTCTAGAGTCGACCTG CAGAAGCTTAGATCTTTGACA
EDC886_gRNA-G-3' (gBlock)	GAATTCTCTAGAGTCGACCTGCAGAAGCTTAGATCTTTGACAGCTAGCTCAGTCCCTAGGTAT AATACTAGTGTGATACTCGTCGCCGATTGTTTTAGAGCTAGAAATAGCAAGTTAAAAAAG GCTAGTCCGTTATCAACTTGAAAAAGTGGCACCCGAGTCGGTGCTTTTTTTCTACCCAGCTTC GACGTGCTCGAGTTCATGTGCAGCTCCATCAG
EDC887_gRNA-H-5' (gBlock)	GTATTTACACCCGCATATGCTGGATCCTTGACAGCTAGCTCAGTCCCTAGGTATAATACTAGT AGATATGCAGGCAGCGGTTGGTTTTAGAGCTAGAAATAGCAAGTTAAAAAAGGCTAGTCCG TTATCAACTTGAAAAAGTGGCACCCGAGTCGGTGCTTTTTTTGAATTCTCTAGAGTCGACCTG CAGAAGCTTAGATCTTTGACA
EDC888_gRNA-H-3' (gBlock)	GAATTCTCTAGAGTCGACCTGCAGAAGCTTAGATCTTTGACAGCTAGCTCAGTCCCTAGGTAT AATACTAGTATATGGCTATCCCTGCATTGTTTTAGAGCTAGAAATAGCAAGTTAAAAAAG GCTAGTCCGTTATCAACTTGAAAAAGTGGCACCCGAGTCGGTGCTTTTTTTCTACCCAGCTTC GACGTGCTCGAGTTCATGTGCAGCTCCATCAG
EDC774_rnA-f	GGTGAAACGGATACGCGCAAAG
EDC775_rnA-r	CTTGATGTCGCATTACTGG
EDC776_rnB-f	CCTGGTTGTTAGAACATGAAGC
EDC777_rnB-r	GGTTCATAGCTGCTTTCCTGATG
EDC778_rnC-f	CTTAGTATGCCACCAGGAAGTG
EDC779_rnC-r	ATGAATGGCTGGCAAGGATG
EDC780_rnD-f	CATCAGACATACTTACCTCAG
EDC781_rnD-r	CCTAAATCAGAGCGTACGAG
EDC782_rnE-f	AACGTTTGCGCAACGCTC
EDC783_rnE-r	CTGACACTTCACGTTTGC
EDC784_rnG-f	CTGAAACGTGCAATTCAGC
EDC785_rnG-r	TCCGATGCTTTTGTGCGGTC
EDC786_rnH-f	ACCTATTACGCCTGAAGCAG
EDC787_rnH-r	CTGAGGTGATTATGGGCTTC
EDC801_rn-16S-r	GCCATGATCAAACCTCTTC
EDC802_riboT-f	AAATTGAAGAGTTTGATCATG
EDC803_riboT-r	CGTCTCTTAAGGTAAGGAGG
EDC804_postRT-f	GGATCACCTCCTTACCTTAAAG
EDC805_del23S-r	GATTAGACGTCATGTCAGCTACACAACCCGAAGATGTTTC
EDC806_del23S-f	TAGCTGACATGACGTCTAATCCCTTACAACGCCGAAG
EDC807_timshel-f	TAGCTGACATGACGTCTAATC
EDC808_rnA-f	TACCTGGCTTCGGAAGTGC
EDC809_rnB-f	CGGTGCAAGAACGTTATC
EDC810_rnC-f	CCATTTTCGGCCATTAACG
EDC811_rnD-f	TGTGGGACCCAGACTAC
EDC812_rnE-f	GATAGGCTGGATCTGATG
EDC813_rnG-f	CCGTAATACGGTTCGTC
EDC814_rnH-f	TGGTGGTAGTAACCAACC
EDC815_rnA-r	GATTAAGCATACGCACC
EDC816_rnB-r	TACTGTCGCGATAGCCAAAAC
EDC817_rnC-r	AACAGCTGCATGAACG
EDC818_rnD-r	TCTCTTCCCTCATCTGAC
EDC819_rnE-r	GGTTTAGTACCCACCAATG
EDC820_rnG-r	CAGCGATCCGAAACAC

Primer/gBlock name	Primer/gBlock sequence
EDC821_rmH-r	TTTGGCTTCCAGCAGC
EDC822_pre16S-r	GAGACATCAGATGTGAGTTGACCACACAGATTGTCTG
EDC823_post16S-f	TCAACTCACATCTGATGTCTCGCTCACACAGATTGTCTG
EDC824_post5SnotD-f	TAGCTGACATGACGTCTAATCAGAGTAGGGAACTGCCAG
EDC825_post23S-D (gBlock)	TAGCTGACATGACGTCTAATCCAAATTTAGCGTGCTGATATGGCTCAGTTGGTAGAGCGCAC CCTTGGTAAGGGTGAGGTCCCAGTTCGACTCTGGGTATCAGCACCCTTTTAGGTTAAAG TTCGGCAGATTAGAAAAGAAATCAAATAAAAACAAAAGGCTCAGTCGGAAGACTGGGCCTTT GTTTTATCTGTTGTTTGTGCGGTGAACACTCTCCCGAGTAGGACAAATCCGCCGGGAGCGGAT TTGAACGTTGCGAAGCAACGGCCCGGAGGGTGGCGGGCAGGACGCCCGCCATAAACTGCCAG ACATCAAATCAAGCGAAAGGCCATCCGAAAGGATGGCCTTTTGCTTTTGAAGTAACATTC AATTAATGGATTACCTGCGATAAAAATGCCCTCGTACGCTCTGATTTAGGATGCGCAAAAA TTCATCAGGTGCAGCTTGCTCCACTATTTCCCCACGATCCATAAAAAATTACCCGGTCAGCGA CGGTTGCGTCAAACCCCATCTCATGTGTTACACACAACATGTCATACCCGACTGCGCCAGC CCAATCATCGTATCCAGCACCTCTTTCCACATCTCAGGATCGAGCGCCGACGTTGGCTCATC AAACAACATAATTTTCGGCTTCATACACAGCGAACGCGCAATGGCAACGCGTTGCTGCTGAC CACCTGAAATCTGTCCGGGAAACTTATGCGCATGTTCCGCAATTCTCACCCGCTCTAGGTAA TGCACCGCCAGATCTTCAGCCTCTTTCTTAGGCATCTTGCGTACCCAAAATCGGTGCCAGGGT ACAGTTCTGTAACCGGTGAGTATGAGGGAAGAGA
EDC847_A-5PAM-r	TGACATCTTCATAATCAGCTTGATC
EDC848_A-5PAM-f	GATCAAGCTGATTATGAAGATGTCAAACGGTGAAACGGATACGCGCAAAG
EDC849_A-3PAM-r	AGTGATGTGCCGCTTAATCTTG
EDC850_A-3PAM-f	CAAGATTAAGCGGCACATCACTAATACTACAGCAATAACATGCCTGTC
EDC851_B-5PAM-r	TCTGGCAGCACTTGTAACAG
EDC852_B-5PAM-f	CTGTTACAAGTGCTGCCAGAAAGAACCCGGCTGGTGGATTG
EDC853_B-3PAM-r	AGAATAAGAACGGGTTGTC
EDC854_B-3PAM-f	GACAACCCGTTCTTATTCTAAGTGAAGGAAGTAATGTACTTTTTTC
EDC855_C-5PAM-r	TTTCGTATGTTCTGGCTGAG
EDC856_C-5PAM-f	CTCAGCCAGAACATACGAAACCTTTTTCTGTGCAGCTAACTG
EDC857_C-3PAM-r	TGCATACCGTTGTGATAGC
EDC858_C-3PAM-f	GCTATCGACAACGGTATGCAAACCGCCTTTTTTACGCGCCAGC
EDC859_D-5PAM-r	ACAAATCGGTCAGCGCGTAATG
EDC860_D-5PAM-f	CATTACGCGCTGACCGATTTGTCCAAAAAGATCGCGGTATGG
EDC861_D-3PAM-r	AACGTCGGCGCTCGATC
EDC862_D-3PAM-f	GATCGAGCGCCGACGTTAACTCATCAAACAACATAATTTTCGGCTTC
EDC863_E-5PAM-r	ATGCAACAACGTCGTCC
EDC864_E-5PAM-f	GGACGACGTTGTTGCATCCTAAATCCCCTGGATTTGAC
EDC865_E-3PAM-r	AGGTTGAACGTGGGTG
EDC866_E-3PAM-f	CACCCACGTTCAACCTAACATTTCTTTTTTCCAGCAAAAC
EDC867_G-5PAM-r	GTTCTCGCTCAGCAGTTTC
EDC868_G-5PAM-f	GAAACTGCTGAGCGAGAACAATTACGATCCGGTCTATGG
EDC869_G-3PAM-r	AAATGCGGCGACGAG
EDC870_G-3PAM-f	CTCGTCGCCGATTTAAGCGATTGTGGGGGCTCTTC
EDC871_H-5PAM-r	GCAACCGCTGCCTGCATATC
EDC872_H-5PAM-f	GATATGCAGGCAGCGGTTGCAACGAACGTGGGAACAAAAG
EDC873_H-3PAM-r	AAATGCAGGGATAGCCATAATATG
EDC874_H-3PAM-f	CATATTATGGCTATCCCTGCATTTCTTTAGGTACTTTCCGCTCTG

Table B.3. Primer combinations and templates. Ribo-T cassettes assembled with overall assembly PCR with pieces 1-2-3-4-5-6, and tRNA cassettes 1-7-8-9-6. Numbers 808-874 correspond to primers EDC808-EDC874.

Piece*	amplified <i>rrn</i> template→	A		B		C		D		E		G		H	
1	5' PAM	808	847	809	851	810	855	811	859	812	863	813	867	814	871
2	PAM to prom RT	848	801	852	801	856	801	860	801	864	801	868	801	872	801
4	tRNA piece	804	805	804	805	804	805	804	805	804	805	804	805	804	805
5	tRNA to PAM RT	806	849	806	853	806	857	806	861	806	865	806	869	806	873
6	3' PAM mut	850	815	854	816	858	817	862	818	866	819	870	820	874	821
7	PAM 5'	848	822	852	822	856	822	860	822	864	822	868	822	872	822
8	Inter SQ	823	805	823	805	823	805	823	805	823	805	823	805	823	805
9#	3' to PAM	824	849	824	853	824	857			824	865	824	869	824	873

*Piece 3 for all cassettes: Ribo-Tv2-A2058 template amplified with EDC802 and EDC803

#Piece 9D: EDC825 gBlock template amplified with EDC807 and EDC861

Table B.4. Strain and corresponding planned genome modifications.

Strain	Genome integration
MG1655	Ribo-T-v2 and Δrrn cassettes
C321. ΔA^{86}	Ribo-T-v2
MG1655 C321. ΔA^{86} SQ171 naïve	S1 fast growing mutation
SQ110	Replace <i>rrnE</i> operon with Ribo-T-v2

Recipes

"With enough butter, anything is good."—Julia Child

Pumpkin bread

From: Mormor

Cream:

2 sticks butter

2 cups sugar

Blend in 4 eggs

Add alternating:

1 can (15 oz) pumpkin

With mixed dry ingredients:

3½ cups flour

2 tsp baking soda

2 tsp cinnamon

½ tsp ground cloves

½ tsp ginger

1 tsp nutmeg

1 tsp salt

Stir in:

1¼ cup chocolate chips

¾ cup chopped walnuts

Put in oiled loaf pan (or bundt!). Bake 45-50 min until toothpick is clean

Glaze when cool:

3 cup powdered sugar

½ tsp nutmeg

½ tsp cinnamon

~2-3 Tbs milk until a thick glaze forms

Sprinkle with toasted shelled pumpkin seeds or walnuts.

Banana bread

From: Martha Stewart & Hugh Jackman <3

Cream:

1 stick butter, softened

1 cup sugar

Beat in:

2 eggs

Mix dry together, then beat in:

1½ cups flour

1 tsp baking soda

1 tsp salt

Beat in:

1 cup mashed #ripe bananas (~3)

½ cup sour cream #fullfat

1 tsp vanilla

Stir in:

½ cup chopped walnuts

1 cup chocolate chips

Grease 9x5x3 loaf pan (or a bundt!). Bake 350 °F for ~1 hour 10 min until tooth pick is clean.

Chocolate drop cookies

Judy Carlson

Melt over double boiler or in microwave:

1 cup butterscotch chips

2 cups chocolate chips

Add:

2 cups fried chow mein noodles

1 cup peanuts

1 ½ cup mini marshmallows

Drop on wax paper with teaspoons

Carrot Cake

From: Judy Carlson

Combine in a large bowl, stir with whisk:

1½ cup flour
 1⅓ cup sugar
 ½ cup sweetened flaked coconut
 ⅓ cup chopped pecan
 2 tsp baking soda
 1 tsp salt
 2 tsp cinnamon

Mix together:

2 Tbs canola oil
 2 large eggs
 2 cups grated carrots
 1½ cups canned crushed pineapple (20 oz can),
 drained

Stir into flour mixture

Put batter into cake pan coated with cooking spray. Bake 350 °F for 35 min or wooden toothpick comes out clean. Frost when cool.

Frosting:

2 Tbs. butter, softened
 8 oz cream cheese
 3 cups powdered sugar
 2 tsp vanilla

Pumpkin Carrot Cake

Found on the internet (<https://goo.gl/Z6zsjY>) by Ashty Karim (#birthdayfave)

Combine:

2 cups flour
 ¼ cup cornmeal
 2 cups sugar
 1 tsp salt
 3 tsp baking soda
 1 tsp baking powder
 2 tsp cinnamon

In separate large bowl, beat until smooth:

3 eggs
 ½ cup oil
 2 tsp vanilla extract

Add dry ingredients to egg mixture.

Fold in:

1 cup crushed pineapple
 1 cup canned pumpkin
 2 cups grated carrot
 ½ cup chopped walnuts
 1½ flaked coconut

Pour into greased 9x13 pan, bake at 350 °F until brown on top and a toothpick comes out clean (~50-60 min).

Frosting:

Beat until smooth:
 4 Tbs butter
 16 oz cream cheese
 2 Tbs lemon juice
 Gradually beat in 3 cups powdered sugar until light and fluffy.

Flourless Peanut Butter Chocolate Chip Cookies

<https://goo.gl/sn3Ho1>

Stir until well mixed:

2 cups non-natural creamy peanut butter
1½ cup light brown sugar
⅓ cup white sugar

Add:

2 eggs
4 tsp vanilla extract
1 tsp baking soda
½ tsp salt
1¼ cups chocolate chips

Round 2 Tbs balls, don't flatten. Bake for 9-12 min at 350 °F.

Special K bars

From: Mormor

Boil until dissolved:

1 cup white sugar
1 cup lite karo syrup

Take off heat, stir in:

1½ cup smooth peanut butter
2 tsp vanilla

Stir in:

~6 cups Special K cereal (not too dry)

Put in lightly greased 9x13 pan. Spread 2 cups butterscotch chips and 1 cup chocolate chips on top, put in warm oven for a few minutes to melt. Smooth top with back of spoon.

Pumpkin Cheesecake Brownies

Modified from Irvin Lin (<https://goo.gl/eHZWmA>)

Cheesecake Batter:

15 oz can pumpkin (plus any half cans you have kicking around in the fridge...the more the better...)

Cook pumpkin in a skillet for ~10 min, stirring constantly, until about half the volume.

Stir in:

1½ teaspoon ground cinnamon
½ teaspoon ground ginger
¼ teaspoon nutmeg
¼ teaspoon sea salt

Set aside to cool slightly.

12 oz cream cheese, refrigerator cold
1 cup sugar
2 Tbs all purpose flour
2 tsp vanilla extract
2 eggs

Beat cream cheese until fluffy. Add cooled pumpkin and blend. Add sugar, flour and vanilla. Add eggs.

Make a dark chocolate boxed brownie batter as the box instructs.

Oil a 9x13 pan, pour in brownie batter. Spoon cheesecake mixture on top and spread out over brownie batter.

Bake at 325 °F for ~35 min, or until cheesecake is puffed up and set when jiggled.

Cocktails

"Life itself is the proper binge."—Julia Child

Lavender margaritas

Erik Carlson

In a pitcher filled $\frac{3}{4}$ with ice:

2 cups tequila
 $\frac{1}{2}$ cup triple sec
1 cup lavender simple syrup
 $1\frac{1}{2}$ cup lime juice

Stir well. Coarse salt on the rim, pour over ice.

Lavender simple syrup

2 cup water
6 Tbs lavender flowers
2 cups sugar

Boil until sugar is dissolved. Reduce heat, simmer for 10 min. Turn off heat, let sit for an hour to cool. Strain.

The Beyoncé

Created on September 4th by Erik, Paul & Danica Carlson

2 oz lavender infused gin
 $\frac{1}{2}$ oz triple sec
 $\frac{1}{2}$ oz lemon juice
 $\frac{1}{2}$ oz lavender simple syrup

Shake with ice, strain into martini glass. Garnish with blueberries and a lemon peel swirl.

Lavender infused gin

Combine, sit for 2 days, strain:
1.75 L gin
2 Tbs lavender

Hooch

Recreated from Homeslice Chicago by Erik, Paul & Danica Carlson.

Muddled mint, ~3 leaves per part to taste
2 parts rum
1 part lemon juice
1 part St. Germaine

Pour over sprig of mint in ice-filled glass.

The Jinkx Monsoon

Created by Danica Carlson

Over ice in a highball glass:
2 oz amaretto
4 oz ginger beer
Top off with club soda
1 Luxardo maraschino cherry
Gently stir